USGS
science for a changing world

Prepared in cooperation with the City of Cedar Rapids

Conceptual and Numerical Groundwater Flow Model of the Cedar River Alluvial Aquifer System with Simulation of Drought Stress on Groundwater Availability near Cedar Rapids, Iowa, for 2011 through 2013

Scientific Investigations Report 2021–5065

U.S. Department of the Interior
U.S. Geological Survey

Cover: Photograph showing Cedar River diversion ditch near horizontal collector well 1 (pictured) constructed during the drought of 2012 to increase infiltration to the alluvial aquifer. Photograph by Stephen J. Kalkhoff, U.S. Geological Survey, 2016.

Conceptual and Numerical Groundwater Flow Model of the Cedar River Alluvial Aquifer System with Simulation of Drought Stress on Groundwater Availability near Cedar Rapids, Iowa, for 2011 through 2013

By Adel E. Haj, Wonsook S. Ha, Lance R. Gruhn, Emilia L. Bristow, Amy M. Gahala, Joshua F. Valder, Carole D. Johnson, Eric A. White, and Shelby P. Sterner

Prepared in cooperation with the City of Cedar Rapids

Scientific Investigations Report 2021–5065

U.S. Department of the Interior
U.S. Geological Survey

U.S. Geological Survey, Reston, Virginia: 2021

For more information on the USGS—the Federal source for science about the Earth, its natural and living resources, natural hazards, and the environment—visit https://www.usgs.gov or call 1–888–ASK–USGS.

For an overview of USGS information products, including maps, imagery, and publications, visit https://store.usgs.gov/.

Any use of trade, firm, or product names is for descriptive purposes only and does not imply endorsement by the U.S. Government.

Although this information product, for the most part, is in the public domain, it also may contain copyrighted materials as noted in the text. Permission to reproduce copyrighted items must be secured from the copyright owner.

Suggested citation:
Haj, A.E., Ha, W.S., Gruhn, L.R., Bristow, E.L., Gahala, A.M., Valder, J.F., Johnson, C.D., White, E.A., and Sterner, S.P., 2021, Conceptual and numerical groundwater flow model of the Cedar River alluvial aquifer system with simulation of drought stress on groundwater availability near Cedar Rapids, Iowa, for 2011 through 2013: U.S. Geological Survey Scientific Investigations Report 2021–5065, 59 p., https://doi.org/10.3133/sir20215065.

Associated data for this publication:
Deszcz-Pan, M., Smith, D.V., Smith, B.D., Haj, A.E., and Johnson, M.R., 2018, Airborne electromagnetic and magnetic survey data and inverted resistivity models, Cedar Rapids, Iowa, May 2017: U.S. Geological Survey data release, https://doi.org/10.5066/P9BS882S.

Ha, W.S., and Haj, A.E., 2021, MODFLOW-NWT model used to simulate groundwater levels in the Cedar River alluvial aquifer near Cedar Rapids, Iowa: U.S. Geological Survey data release, https://doi.org/10.5066/P96CF4L5.

Johnson, C.D., Bristow, E.L., White, E.A., Gruhn, L.R., Pappas, K.L., Phillips, S.N., and Lane, J.W., Jr., 2020, Geophysical data collected in the Cedar River floodplain, Cedar Rapids, Iowa, 2015–2017: U.S. Geological Survey data release, https://doi.org/10.5066/P9YXJDHX.

U.S. Geological Survey, 2018, USGS water data for the Nation: U.S. Geological Survey National Water Information System database, https://doi.org/10.5066/F7P55KJN.

ISSN 2328-0328 (online)

Acknowledgments

This report was prepared in cooperation with the City of Cedar Rapids and the authors thank the City of Cedar Rapids-Utilities Department staff for their support and for providing valuable information for this study.

Several U.S. Geological Survey personnel, including Jared Weber, Mike Linhart, and Greg Littin, assisted with the collection, processing, and analysis of geological, hydrogeological, and geophysical data. Additionally, Kyle Davis provided insightful guidance for approaches to groundwater model construction.

Contents

Figures

Tables

Conversion Factors

International System of Units to U.S. customary units

Multiply	By	To obtain
	Length	
centimeter (cm)	0.3937	inch (in.)
millimeter (mm)	0.03937	inch (in.)
meter (m)	3.281	foot (ft)
meter (m)	1.094	yard (yd)
kilometer (km)	0.6214	mile (mi)
	Area	
square meter (m^2)	0.0002471	acre
square kilometer (km^2)	247.1	acre
square kilometer (km^2)	0.3861	square mile (mi^2)
	Flow rate	
meter per second (m/s)	3.281	foot per second (ft/s)
meter per minute (m/min)	3.281	foot per minute (ft/min)
meter per day (m/d)	3.281	foot per day (ft/d)
cubic meter per day (m^3/d)	264.2	gallon per day (gal/d)
	Transmissivity	
meter squared per day (m^2/d)	10.76	foot squared per day (ft^2/d)

U.S. customary units to International System of Units

Multiply	By	To obtain
	Length	
inch (in.)	2.54	centimeter (cm)
	Flow rate	
million gallons per day (Mgal/d)	0.04381	cubic meter per second (m^3/s)

Temperature in degrees Celsius (°C) may be converted to degrees Fahrenheit (°F) as follows:

$$°F = (1.8 \times °C) + 32.$$

Vertical coordinate information is referenced to the North American Vertical Datum of 1988 (NAVD 88).

Horizontal coordinate information is referenced to the North American Datum of 1983 (NAD 83).

Elevation, as used in this report, refers to distance above the vertical datum.

Supplemental Information

The standard unit for transmissivity is cubic meter per day per square meter times meter of aquifer thickness [(m^3/d)/m^2]m. In this report, the mathematically reduced form, meter squared per day (m^2/d), is used for convenience. Seismic frequency was measured in hertz and kilohertz. Electrical conductivity was measured in millisiemens per meter.

Abbreviations

AEM	airborne-electromagnetic
CRP	continuous resistivity profiling
CSP	continuous seismic profiling
DRN	Drain (Package)
EMI	electromagnetic induction
ERT	electrical resistivity tomography
EVT	Evapotranspiration (Package)
GIS	geographic information system
GPS	global positioning system
HCW	horizontal collector well
HVSR	horizontal-to-vertical spectral ratio
IEM	Iowa Environmental Mesonet
NMR	nuclear magnetic resonance
NSE	Nash-Sutcliffe efficiency
PBIAS	percentage bias
PEST	Parameter ESTimation [software]
PET	potential evapotranspiration
R^2	coefficient of determination
RCH	Recharge (Package)
RIV	River (Package)
RSR	root mean square error to observation standard deviation ratio
T_2 decay	transverse decay
T_r	recovery time
USGS	U.S. Geological Survey
WEL	Wells (Package)
±	plus or minus

Conceptual and Numerical Groundwater Flow Model of the Cedar River Alluvial Aquifer System with Simulation of Drought Stress on Groundwater Availability near Cedar Rapids, Iowa, for 2011 through 2013

By Adel E. Haj, Wonsook S. Ha, Lance R. Gruhn, Emilia L. Bristow, Amy M. Gahala, Joshua F. Valder, Carole D. Johnson, Eric A. White, and Shelby P. Sterner

Abstract

Between July 2011 and February 2013, the City of Cedar Rapids observed water level declines in their horizontal collector wells approaching 11 meters. As a result, pumping from these production wells had to be halted, and questions were raised about the reliability of the alluvial aquifer under future drought conditions. The U.S. Geological Survey, in cooperation with the City of Cedar Rapids, completed a study to better understand the effects of drought stress on the Cedar River alluvial aquifer using a numerical groundwater flow model. Previously published groundwater flow models were combined with newly collected airborne, waterborne, down-hole, and land-based geophysical survey data and provided a detailed three-dimensional lithologic model of the Cedar River alluvial aquifer and surrounding area. An improved conceptual model for the groundwater flow system and a lithologic model were used to build and inform a numerical groundwater flow model capable of simulating water levels observed in the City of Cedar Rapids horizontal collector wells during the 2012 drought. Model performance was assessed primarily on the ability of the model to simulate water table elevation at six monitoring wells. Statistical tests were used to assess the numerical model during the calibration period, and results varied from satisfactory to unsatisfactory, likely because of stage changes in the Cedar River and production well withdrawal rates near monitoring wells. Simulated water levels during the 2012 drought indicated a depression near the horizontal collector wells, although simulated elevations at these locations and at monitoring wells were generally overestimated compared to measured values. The numerical groundwater flow model was modified to account for a decrease in seepage rate caused by low flow in the Cedar River and increased production. With seepage rate modification, model results improved; the simulated water table elevations were like those observed in horizontal collector and monitoring wells. Results demonstrated the ability of the model to simulate water levels observed in the horizontal collector wells during the 2012 drought when accounting for a decrease in infiltration from the Cedar River.

Introduction

The Cedar River alluvial aquifer is the principal source of municipal water for the City of Cedar Rapids, Iowa, and is generally composed of alluvial sand and gravel deposits (Iowa Department of Natural Resources, 1998c; Schulmeyer and Schnoebelen, 1998). Historically, the aquifer supported the production needs of the City of Cedar Rapids and surrounding area (fig. 1) with an estimated population of about 264,000 in 2010 (U.S. Census Bureau, 2018). Between July 2011 and February 2013, Iowa experienced severe drought conditions (generally referred to as the "2012 drought") that affected water availability for communities that relied on alluvial aquifers for their production needs (Hillaker, 2012). During that time, the City of Cedar Rapids observed water level declines in their horizontal collector wells (HCWs) approaching 11 meters (m; 36 feet), nearing the top of the lateral opening (fig. 2). Pumping from affected production wells had to be halted to prevent damage to the pumps and wells and caused concern about the reliability of the alluvial aquifer under future drought conditions (fig. 2; B. Jacobs, City of Cedar Rapids, written commun., 2018).

In 2013, the U.S. Geological Survey (USGS), in cooperation with the City of Cedar Rapids, began a study to better understand the effects of drought stress on the Cedar River alluvial aquifer using a numerical groundwater flow model. Previously published groundwater flow models were constructed before the 2012 drought and did not simulate water level declines like those observed during the 2012 drought (Schulmeyer and Schnoebelen, 1998; Turco and Buchmiller, 2004). The USGS groundwater flow model developed during the 2013 study combined published hydrogeologic data with airborne, waterborne, down-hole, and land-based geophysical

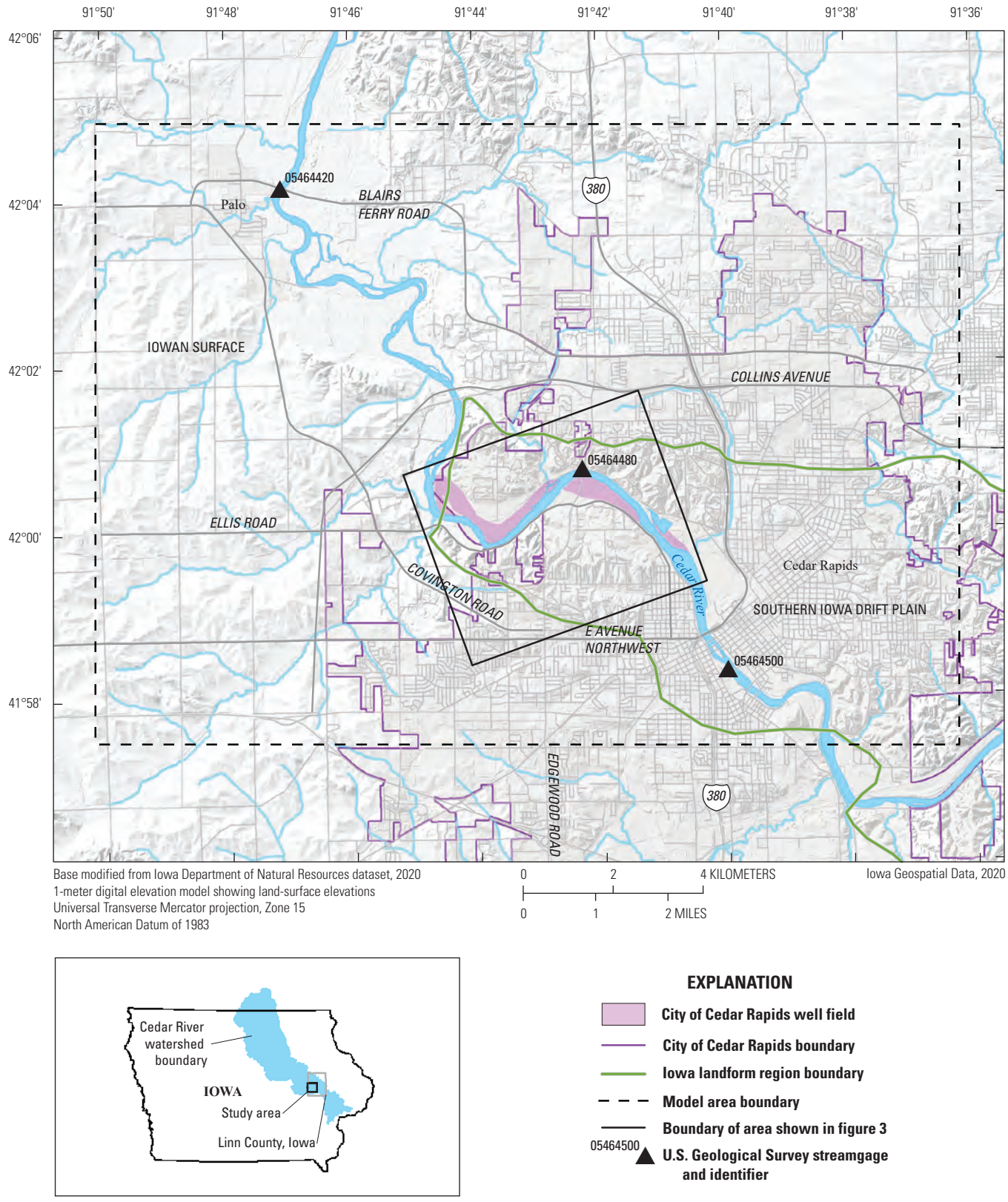

Figure 1. Groundwater flow model area, the Cedar River channel, and U.S. Geological Survey streamgages.

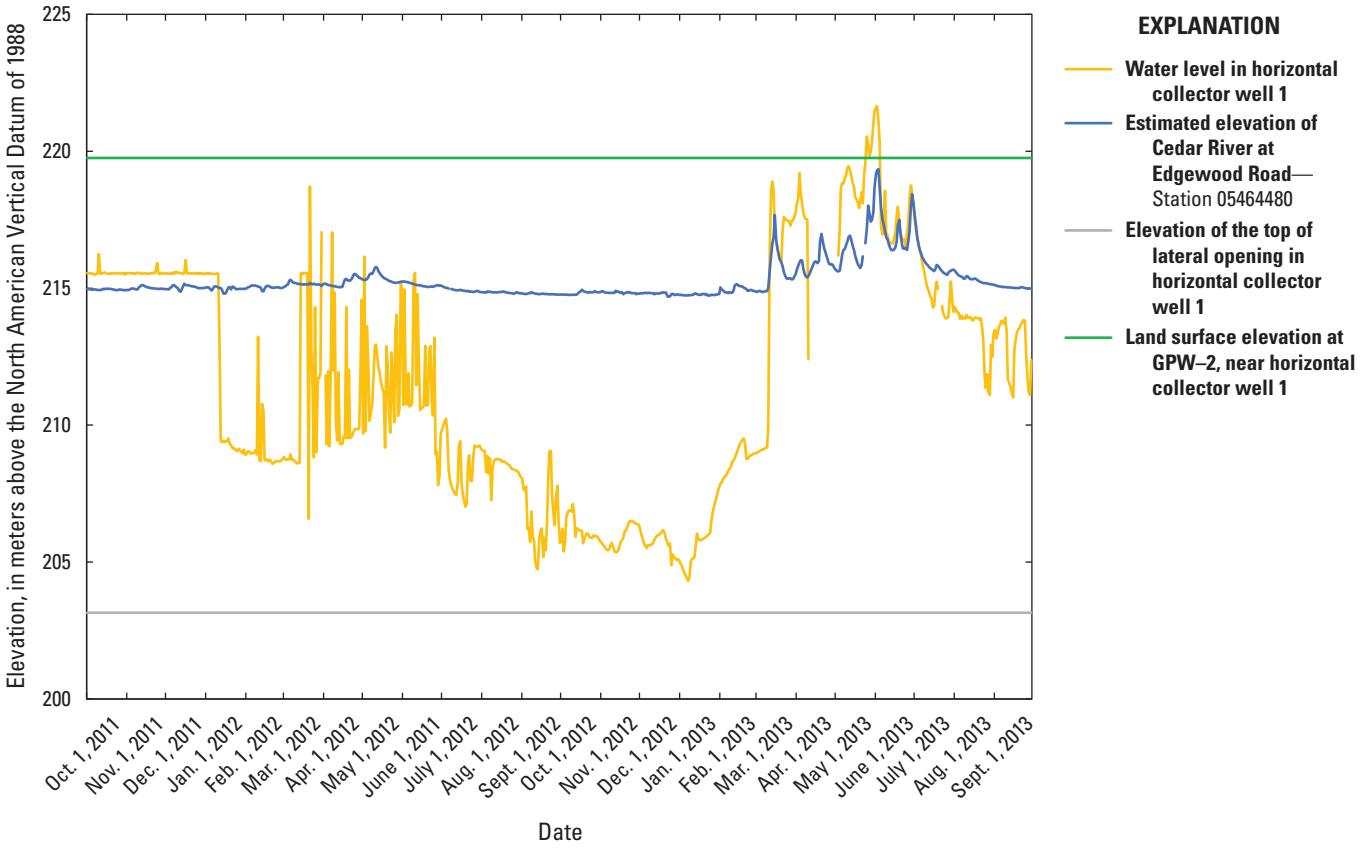

Figure 2. Water level decline in horizontal collector well 1 (HCW1) from October 2011 through September 2013. Stream elevation estimated at U.S. Geological Survey (USGS) streamgage at Edgewood (05464480) using stream elevation measurements from USGS streamgage at Cedar Rapids (05464500). Land surface elevation taken from USGS monitoring well GPW–2 (415954091440401) about 88 meters (289 feet) west of HCW1.

survey data collected from 2015 to 2017 that (1) provided a detailed three-dimensional lithologic model of the Cedar River alluvial aquifer and surrounding area, (2) improved the conceptual model for the groundwater flow system, and (3) evaluated hydrogeologic characteristics of aquifer materials. These new conceptual and lithologic models and data were used to build and inform new numerical groundwater flow models using MODFLOW-NWT (version 1.0.9; Niswonger and others, 2011) capable of simulating water levels observed in the City of Cedar Rapids HCWs during the 2012 drought.

This report describes the conceptualization, construction, and calibration of numerical groundwater flow models and interpretation of numerical model results for the 2012 drought period with and without streambank seepage rate reduction. The geophysical data are available as part of USGS data releases (Deszcz-Pan and others, 2018; Johnson and others, 2020) and a USGS Scientific Investigations Map (Valder and others, 2019) and are not included in this report. The groundwater flow models and supporting data are available as part of an accompanying USGS data release (Ha and Haj, 2021).

Purpose and Scope

The purpose of this report is to describe the conceptual and numerical groundwater flow models and numerical model scenario results for the Cedar River alluvial aquifer during the 2012 drought. This report includes hydrologic data collected from October 1, 2011, to April 30, 2013; October 1, 2015, to November 30, 2015; and October 1, 2016, to August 31, 2018, for parts of the Cedar River alluvial aquifer near the Cedar River between the cities of Palo and Cedar Rapids, Iowa (fig. 1). Also described are the hydrologic and geophysical data collection methods and how these data were used to construct and inform the conceptual and numerical models. The conceptual model includes a hydrogeologic framework, hydrogeologic units, and water budget components. The numerical model documentation includes explanations of (1) boundary conditions, (2) model input parameters, (3) calibration approach, (4) water budget calculations, and (5) sensitivity analysis. Previously collected geophysical data were documented by Deszcz-Pan and others (2018) and Johnson and others (2020). Documentation and run instructions for the Cedar River alluvial aquifer groundwater flow model are provided in an accompanying data release (Ha and Haj, 2021).

Other data sources included lithologic data from Valder and others (2019), geologic and hydrogeologic data published by the Iowa Department of Natural Resources and the Iowa Geological Survey (Iowa Department of Natural Resources, 1998a, b, c; Bettis and others, 2005; Iowa Geological and Water Survey, 2010; Gannon and others, 2011; Iowa Geological Survey, 2017a, b, 2018; Iowa Geospatial Data 2017), and water level data from the USGS National Water Information System database (U.S. Geological Survey, 2018). Results from this study could assist the City of Cedar Rapids with evaluating aquifer response to drought and with developing a drought management plan.

Previous Groundwater Flow Models and Investigations

A previous groundwater flow model developed by Schulmeyer and Schnoebelen (1998) provided a hydrogeological study of the Cedar River in Benton (not shown) and Linn Counties, Iowa, and a steady-state numerical groundwater flow model that identified sources of recharge to the Cedar River alluvial aquifer and quantified recharge rates to the aquifer near Cedar Rapids under hypothetical municipal pumping regimes. The study used geophysical data to characterize the hydrogeologic characteristics of aquifer materials and reported surface and groundwater conditions from 1992 to 1996. The results of the model indicated that as streamflow in the Cedar River declined, riverbed leakage into the underlying alluvial aquifer decreased. Riverbed leakage accounts for an estimated 74 percent of recharge to the alluvial aquifer (Schulmeyer and Schnoebelen, 1998). As riverbed leakage decreased, water table elevation in the alluvial aquifer declined. As a result, the underlying carbonate bedrock, hereafter referred to as "bedrock," may have become the primary source of recharge to the alluvial aquifer.

Turco and Buchmiller (2004) refined the Schulmeyer and Schnoebelen (1998) groundwater flow model to better understand interactions among the Cedar River, the alluvial aquifer, and the City of Cedar Rapids well fields (fig. 1; Turco and Buchmiller, 2004). The 2004 model also was designed to demonstrate the response of recharge (from streambed leakage) to the aquifer from various municipal pumping scenarios. The resulting steady-state numerical groundwater flow model indicated that infiltration from the Cedar River accounted for more than 99 percent of the water withdrawn by production wells and infiltration rates changed proportionately with pumping rates in transient model simulations (Turco and Buchmiller, 2004).

The 2012 drought conditions combined with an increased production demand caused water levels in HCW1 and HCW2 of the City of Cedar Rapids well fields to steadily decrease in July 2012 and remain low until February 2013 (fig. 2; B. Jacobs, City of Cedar Rapids, written commun., 2013). Attempts were made by Cedar Rapids and by USGS scientists to simulate observed water levels with the Turco and Buchmiller (2004) groundwater flow model (and modified versions), but none of the attempts were successful (G. Littin, U.S. Geological Survey, oral commun., 2013). The groundwater flow models built by Schulmeyer and Schnoebelen (1998) and Turco and Buchmiller (2004) were used to construct and inform the conceptual groundwater flow model and the numerical groundwater flow models presented in this report.

Description of Model Area

The model area is a rectangular area encompassing about 265 square kilometers (km^2) of the Cedar River valley, west of Cedar Rapids, Iowa, and a 37-kilometer (km) reach of the Cedar River (fig. 1). The model area generally is characterized as a flat alluvial valley (lowlands) underlain by fluvial and glaciofluvial sands and gravels (the Cedar River alluvial aquifer) and adjacent uplands underlain by eolian (wind deposited sand and silt) sediment and glacial till (Iowa Department of Natural Resources, 1998c). The model area is within the Dissected Tills section of the Central Lowlands physiographic province (not shown), a region characterized by flatlands with geomorphic remnants of glaciation (Vigil and others, 2000). The land surface elevation within the model area ranges from 214 to 283 m above the North American Vertical Datum of 1988 (NAVD 88; Iowa Geospatial Data, 2017).

Three USGS streamgages were within the model area: Cedar River at Blairs Ferry Road at Palo, Iowa (05464420); Cedar River at Cedar Rapids, Iowa (05464500); and Cedar River at Edgewood Road at Cedar Rapids, Iowa (05464480; fig. 1; U.S. Geological Survey, 2018). Water level data were collected from 14 USGS monitoring wells within the model area (table 1, fig. 3; U.S. Geological Survey, 2018).

During the period for this study, the City of Cedar Rapids operated 3 production well fields along the Cedar River with 50 active wells: the Seminole well field had 20 vertical production wells, the west well field had eight vertical collection wells, and the east well field had 17 vertical collection wells (table 2, fig. 3). Production from the vertical wells was supplemented by five horizontal collection wells, HCW1, 2, 3, 4, and 6. Most groundwater withdrawals from the Cedar River alluvial aquifer near Cedar Rapids occurred from the City of Cedar Rapids production well fields.

Iowa has a typical continental, subhumid climate characterized by seasonal variations (Schulmeyer and Schnoebelen, 1998). The mean annual temperature from 1981 to 2010 at the Cedar Rapids Municipal Airport weather station (USW00014990, not shown) 8 km (5 miles) south of the model area was 9 degrees Celsius (°C; 48.2 degrees Fahrenheit [°F]) (National Centers for Environmental Information, 2019). Summer months (June, July, and August) tended to be hot with heavy precipitation and a mean temperature of 21.78 °C (71.2 °F), whereas winter months (December, January, and February) were dry and mild with a mean temperature of −5.33 °C (22.4 °F) and a maximum temperature of −0.56 °C (31 °F) (National Centers for Environmental Information,

Table 1. U.S. Geological Survey monitoring wells used in this study.

[Site_ID, site identification; mm/dd/yyyy, month/day/year; ft, foot; NAVD 88, North American Vertical Datum of 1988; --, no data; TR_sim, transient model simulations; SS, steady-state model; TR_cal, transient model calibration]

Site number	Site name	Site_ID	Field measurement period of record for study (mm/dd/yyyy)	Sensored period of record for study (mm/dd/yyyy)	Site elevation (ft, NAVD 88)	Model use	Model row	Model column
415953091435003	083N08W13CBDA 2009USGS CRM–3A	CRM–3a	06/06/2011–03/11/2015	--	727.06	TR_sim	78	73
415953091435302	083N08W13CBDA 2009USGS CRM–4A	CRM–4a	07/20/2010–10/30/2018	10/09/2014–10/29/2018	727.93	SS/TR_cal/TR_sim	78	73
415954091435302	083N0W13ADBC 2010USGS CRM–6A	CRM–6a	06/06/2011–10/30/2018	10/09/2014–06/09/2017	727.88	SS/TR_sim	78	73
420030091424601	083N07W07CCCB 1994USGS CRM–10	CRM–10	03/02/1994–12/04/2012	--	720.65	TR_sim	68	85
420033091420302	083N07W07DDBD 1993USGS CRM–11	CRM–11	12/01/1994–05/22/2019	01/02/2001–05/21/2019	719.24	SS/TR_cal	67	93
415949091405402	083N07W17DAC 1993USGS CRM–12	CRM–12	12/01/1994–05/22/2019	04/20/2016–05/21/2019	721.99	SS/TR_cal	78	107
420014091442701	083N08W14A 1996USGS CRM–18	CRM–18	01/22/1997–11/18/2019	03/26/2015–11/17/2019	723	SS/TR_cal/TR_sim	73	66
415954091440301	083N08W13CBBC 1997USGS CRM–20	CRM–20	12/05/2012–06/14/2019	02/07/2017–05/21/2019	720	SS/TR_cal/TR_sim	77	70
420018091430801	083N08W13AACA 1998USGS CRM–26	CRM–26	08/12/1998–12/04/2012	--	722	TR_sim	71	81
420031091443301	2015USGS GPW1	GPW–1	09/14/2015–11/18/2019	04/20/2016–11/17/2019	721.58	SS/TR_cal	68	65
415954091440401	2015USGS GPW2	GPW–2	09/15/2015–11/18/2019	03/12/2016–11/17/2019	720.98	SS/TR_cal	77	70
420026091423001	2015USGS GPW3	GPW–3	09/15/2015–05/22/2019	04/20/2016–05/21/2019	721	SS/TR_cal	69	88
420031091422601	2015USGS GPW4	GPW–4	09/16/2015–11/18/2019	04/20/2016–11/17/2019	720.11	SS/TR_cal	68	89
415939091400201	2015USGS GPW5	GPW–5	09/16/2015–05/22/2019	04/20/2016–05/21/2012	729	SS/TR_cal	81	117

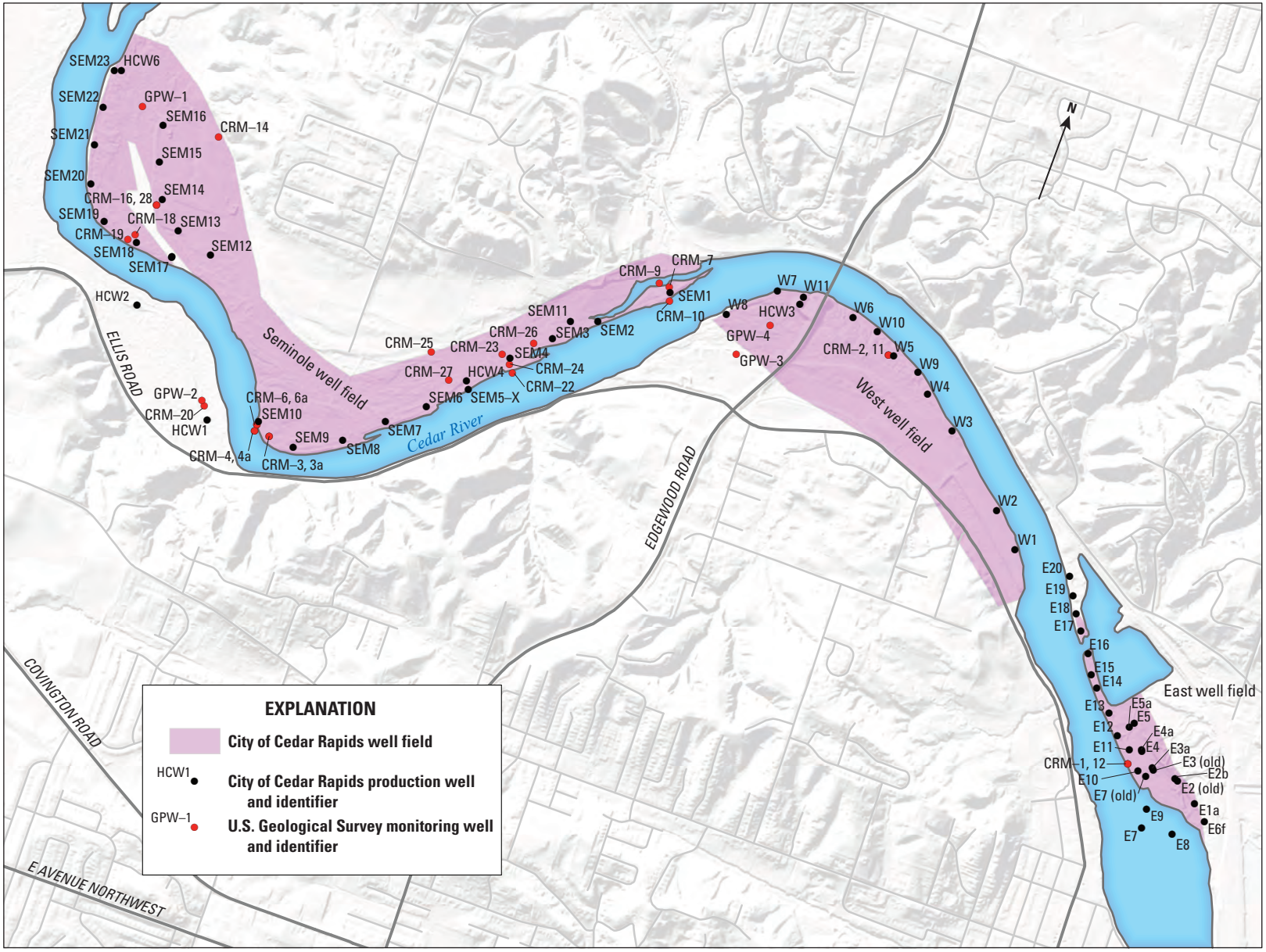

Figure 3. The approximate location of U.S. Geological Survey monitoring wells, City of Cedar Rapids production wells, and production well fields.

Table 2. Production wells modeled as withdrawal wells in this study.

[Production wells described as "plugged" were removed before this study; production wells described as "not used" were not active during this study but remain part of the production well network. Site_ID, site identification; ft, foot; --, no data]

Station number	Station name	Site_ID	Operational status	Site elevation (ft)	Model row	Model column
415946091403901	083N07W17DADD 1961 Cedar Rapids East 1	E1	Active	720.34	79	110
415949091405201	083N07W17 DACC 1980 Cedar Rapids East 10	E10	Active	722.44	78	107
415950091405501	083N07W17DBDA 1984	E11	Active	725.9	78	107
415952091405701	083N07W17DBDA 1984 Cedar Rapids East 12	E12	Active	727.22	78	106
415955091410101	083N07W17DBAC 1984 Cedar Rapids East 13	E13	Active	736.16	77	106
415959091410501	083N07W17DBAB 1984 Cedar Rapids East 14	E14	Active	725.12	76	105
420000091410701	083N07W17ABBD 1984 Cedar Rapids East 15	E15	Active	724.09	76	105
420002091410701	083N07W17ACCD 1984 Cedar Rapids East 16	E16	Active	723.71	75	104
420005091411101	083N07W17ACCB 1984 Cedar Rapids East 17	E17	Active	720.99	74	104
420007091411201	083N07W17ACBC 1984 Cedar Rapids East 18	E18	Active	720.67	74	103
420010091411501	083N07W17BDAA 1984 Cedar Rapids East 19	E19	Active	719.02	73	103
415949091404301	083N07W17DADC 1961 Cedar Rapids East 2	E2	Active	730.26	78	109
420013091411601	0803N07W17BADD 1984 Cedar Rapids East 20	E20	Active	721.29	73	103
415949091404901	083N07W17DACD 1961 Cedar Rapids East 3	E3	Active	728.55	78	108
415954091405101	083N07W17DABC 1961 Cedar Rapids East 4	E4	Active	727.15	78	107
415952091404401	083N07W17DBAD 1961 Cedar Rapids East 5	E5	Active	720	77	107
415940091402801	083N07W16CCBC 1961 Cedar Rapids East 6	E6	Not used	717	--	--
415941091404001	083N07W17DDBD 1961 Cedar Rapids East 7	E7	Not used	720	--	--
415941091404101	083N07W17DDAD 1963 Cedar Rapids East 8	E8	Not used	722.39	--	--
415944091404801	083N07W17DDBA 1977 Cedar Rapids East 9	E9	Active	725.13	80	108
415952091440400	083N08W13CBCB 1994 Cedar Rapids Ranney 1	HCW1	Active	721.62	77	70
420004091442300	083N08W14ADCC 1995 Cedar Rapids Ranney 2	HCW2	Active	724.9	75	67
420035091422301	083N07W07DCBC 2002 Cedar Rapids West Ranney 3	HCW3	Active	734.61	67	90
420010091431801	083N08W13ACAD 2002 Cedar Rapids Seminole Ranney 4	HCW4	Active	720.63	73	79
420036091444001	083N08W11DCBC 2013 Cedar Rapids Ranney 6	HCW6	Active	726.8	67	63
420030091424901	083N07W07CCD 1971 Cedar Rapids Seminole 1	S1	Active	719	68	65
415953091435201	083N08W13CBDA 37817 1971 Cedar Rapids 10	S10	Active	725.4	77	73
420024091430401	083N08W13AAAB 1980 Cedar Rapids Seminole 11	S11	Active	717.61	70	82
420015091441301	083N08W14AADC 1990 Cedar Rapids Seminole 12	S12	Plugged	722.08	--	--
420017091442101	083N08W14AACA 1990 Cedar Rapids Seminole 13	S13	Active	722.62	72	67
420020091442501	083N08W14ACDA 1990 Cedar Rapids Seminole 14	S14	Active	725.12	71	67

Table 2. Production wells modeled as withdrawal wells in this study.—Continued

[Production wells described as "plugged" were removed before this study; production wells described as "not used" were not active during this study but remain part of the production well network. Site_ID, site identification; ft, foot; --, no data]

Station number	Station name	Site_ID	Operational status	Site elevation (ft)	Model row	Model column
420024091442701	083N08W14ABDB 1990 Cedar Rapids Seminole 15	S15	Active	726.37	70	66
420029091443001	083N08W11DCDB 1990 Cedar Rapids Seminole 16	S16	Not used	725.9	--	--
420013091442000	083N08W14ADBB 1991 Cedar Rapids Seminole 17	S17	Active	723.52	73	68
420013091442501	083N08W14ACAA 1991 Cedar Rapids Seminole 18	S18	Active	723.95	73	66
420014091443201	083N08W14ABDC 1991 Cedar Rapids Seminole 19	S19	Active	721.22	72	65
420025091425801	083N08W13AAAA 1971 Cedar Rapids Seminole 2	S2	Active	719.98	70	83
420017091443701	083N08W14ABCC 1991 Cedar Rapids Seminole 20	S20	Active	721.57	71	64
420022091444001	083N08W14ABBC 1991 Cedar Rapids Seminole 21	S21	Active	721.38	70	63
420029091444101	083N08W11DCCC 1991 Cedar Rapids Seminole 22	S22	Active	719.24	69	63
420034091444101	083N08W11DCBC 1991 Cedar Rapids Seminole 23	S23	Active	723.27	67	63
420020091430601	083N08W13AACA 1971 Cedar Rapids Seminole 3	S3	Active	720.89	71	82
420015091430601	083N08W13AACC 1971 Cedar Rapids Seminole 4	S4	Active	720.53	72	81
420009091431901	083N08W13ACAD 1971 Cedar Rapids Seminole 5	S5	Plugged	718.03	--	--
420006091432201	083N08W13ACDB1971 Cedar Rapids Seminole 6	S6	Active	722.19	75	78
415959091433001	083N08W13DBBB 1971 Cedar Rapids Seminole 7	S7	Active	724.72	76	77
415955091433601	083N08W13CAAC 1970	S8	Active	721.4	77	76
415952091434301	083N08W13CACA 1971 Cedar Rapids Seminole 9	S9	Active	724.85	78	74
420007091411801	083N07W17BDCC 1964 Cedar Rapids West 1	W1	Not used	716	--	--
420036091420901	083N07W07DCAA 1980 Cedar Rapids West 10	W10	Active	723.78	67	93
420039091422101	083N07W07DCBB 1980 Cedar Rapids West 11	W11	Active	723.97	66	90
420017091413401	083N07W17BBDA 1964 Cedar Rapids West 2	W2	Not used	724.21	--	--
420024091414601	083N07W17BBBB 1964 Cedar Rapids West 3	W3	Active	722.18	69	97
420029091415501	083N07W07DDDA 1964 Cedar Rapids West 4	W4	Active	723.13	68	95
420034091410501	083N07W07DDBC 1964 Cedar Rapids West 5	W5	Active	722	67	94
420037091421401	083N07W07DCAB 1964 Cedar Rapids West 6	W6	Active	722.24	66	92
420036091422701	083N07W07CDAA 1964 Cedar Rapids West 7	W7	Active	724.05	66	89
420032091423301	083N07W07CDCA 1964 Cedar Rapids West 8	W8	Plugged	724.59	--	--
420031091415701	083N07W07DDDB 1980 Cedar Rapids West 9	W9	Active	722.5	67	95

2019). The mean annual precipitation from 1981 to 2010 was about 879.1 millimeters (mm; 34.61 inches) per year; most precipitation occurred during summer months (National Weather Service, 2019). Monthly precipitation recorded at the Cedar Rapids Municipal Airport weather station from October 1, 2016, to September 30, 2018, ranged from 10.92 to 236.73 mm (0.43 to 9.32 inches) with a total of 1,662.68 mm (65.46 inches). During the 2012 drought, from October 1, 2011, to September 30, 2013, monthly precipitation ranged from 2.79 to 217.17 mm (0.11 to 8.55 inches) with a total of 1,629.92 mm (64.17 inches).

The model area is within the Middle Cedar River drainage basin of the broader Cedar River drainage basin, an area of about 16,860 km^2 (6,510 square miles) upstream from the USGS streamgage Cedar River at Cedar Rapids (05464500; fig. 1). The river flows from its headwaters in southern Minnesota to its confluence with the Iowa River in Louisa County in southeastern Iowa and flows southeast through the alluvial valley in the central part of the model area (fig. 1). Former river-channel meanders, sloughs, and oxbow lakes are adjacent to the Cedar River and are more abundant in the northwestern part of the model area.

Land use in the northwestern regions of the model area is primarily agricultural and becomes increasingly urban towards Cedar Rapids in the southeastern part of the model area. Forest cover is common in riparian areas throughout the model area, and areas of steep topography are found in the southeastern part of the model area (Turco and Buchmiller, 2004).

The study area has parts within the Southern Iowa Drift Plain and Iowan Surface landform regions that include sediment deposits and weathering zones formed during several glacial and interglacial intervals over the past 2.2 million years (fig. 1; Hallberg, 1986; Prior, 1991; Bettis and others, 2005). The Southern Iowa Drift Plain was glaciated several times from 2.2 million to 500,000 years before present, referenced to calendar year 1950 (Hallberg, 1986). These glaciations deposited predominantly basal till on an irregular bedrock surface, generally composed of 22 lithologic formations ranging from Silurian to Devonian in age (Tucci and McKay, 2006; Iowa Geological Survey, 2017a, b). The tills were assigned to the Pleistocene Alburnett and younger Wolf Creek Formations by Hallberg (1980); both formations consist of multiple till units and paleosols (weathering surfaces with soil formation) deposited during several glacial and interglacial episodes. These till units are primarily silty clay and sandy clay loams with interbedded, discontinuous sand and gravel bodies that vary in thickness from 1 to 3 m.

Before the Illinoian glaciation, a drainage network formed, like the one observed on the modern landscape. On the uplands, deep weathering profiles and erosional surfaces developed, removing till entirely in places; in the lowlands, stream channels incised, in some areas to bedrock, and over the millennia (500,000 years before present), many cut-and-fill episodes left behind sand and gravel deposits (Hallberg, 1980). During the Wisconsinan glaciation, about 23,000 and 11,000 years before present, the last advance of continental ice occurred in North America. Although glacial ice did not reach the study area, two episodes of eolian sediment (loess) deposition occurred (Prior, 1991) on high alluvial terraces and upland surfaces near the Cedar River valley.

The Cedar River alluvial aquifer is generally composed of 13–22 m of sand and gravel deposits that are Pleistocene to Holocene in age and eolian sand deposits in areas of the valley where wind has reworked older alluvial deposits (Iowa Department of Natural Resources, 1998c; Schulmeyer and Schnoebelen, 1998). The Cedar River alluvial aquifer system has two principle components: the unconsolidated Quaternary-age surficial deposits and the underlying Silurian to Devonian-age bedrock (Iowa Department of Natural Resources, 1998a; Iowa Geological and Water Survey, 2010). These two components are hydraulically connected and vary in thickness, extent, and hydrologic characteristics (Turco and Buchmiller, 2004). The Quaternary-age surficial deposits include the alluvial and eolian sediments that make up the Cedar River alluvial aquifer and the glacial till that overlies the bedrock in much of the study area. Bedrock underlying the surficial deposits was interpreted by Schulmeyer and Schnoebelen (1998) as two aquifers: a Devonian aquifer and a Silurian aquifer separated by a semiconfining unit, the Otis and Bertram Formations (Iowa Department of Natural Resources, 1998a; Iowa Geological and Water Survey, 2010).

Geophysical Methods and Supplemental Data

This study integrated several geophysical methods and supplemental data to characterize the lithologic and hydrologic properties of the aquifers within the model area. Geophysical methods described in this report were land based, waterborne, and borehole. Additionally, an airborne electromagnetic (AEM) geophysical survey was completed and independently published (Valder and others, 2019). Data collected from the surveys are available in two USGS data releases (Deszcz-Pan and others, 2018; Johnson and others, 2020). The data were used to create a hydrogeologic framework, to provide estimates of hydrogeologic properties to refine the conceptual groundwater flow model, and to characterize and delineate lithologic materials. Results from one geophysical method were used to help constrain or interpret data from other methods, and corroboration between different methods improved the robustness of the interpretations.

During the geophysical surveys, complimentary data were collected for use during data analysis, interpretation, and mapping. These data included global positioning system (GPS) coordinates, groundwater conductivity, temperature, and water level from available boreholes. After the land-based surveys, soil borings were collected at geophysical survey locations and later described and documented for comparison to the geophysical data (Johnson and others, 2020). Soil boring descriptions provided lithologic information and served as control data. Other complimentary data are included in an accompanying USGS data release (Johnson and others, 2020).

Land-Based Geophysical Surveys

Land-based geophysical surveys were completed to characterize unconsolidated materials, estimate depth to bedrock, and delineate bedrock topography beneath the adjacent floodplain terraces of the Cedar River (fig. 4, appendix). For this investigation, electrical resistivity tomography (ERT) and horizontal-to-vertical spectral ratio (HVSR) passive seismic methods were used, and often used concurrently. ERT is a geophysical technique that measures electrical properties of subsurface geologic materials and can be used to better understand the makeup and extent of underlying earth materials and estimate depth to bedrock. HVSR measurements were made at each end, the middle, and other locations along the ERT survey lines as time allowed. Additional HVSR measurements were made at independent locations where depth to bedrock was known (for calculating an average shear-wave velocity) and in areas where depth to bedrock was unknown. A handheld GPS unit was used to record coordinates for the HVSR measurements and the orientation and location of the ERT survey lines.

ERT surveys were completed using a cable with 56 takeouts spaced every 5 m. The takeouts on the cable were connected to stainless-steel metal stakes inserted into the ground to inject electrical current. Electric potential was measured between selected pairs of electrodes along the cable. For this investigation, a total of five ERT surveys were completed and survey lines were 275 m long. Data collection and processing were completed applying methods described by Loke (2018). At each ERT survey location, several types of measurement arrays were used, including dipole-dipole, Schlumberger, and inverse Schlumberger arrays (Ward, 1990). These arrays were chosen for their respective geometries and sensitivity to changes in resistivity (Loke, 2018). The depths of investigation for these geometries are generally 20–25 percent of the length of the ERT survey line (Ward, 1990).

EarthImager software (Advanced Geosciences, Inc., 2009) was used to process the ERT survey data. Threshold settings in the software were applied to automatically remove data points that exceeded threshold values. Additional problematic data points were manually processed out of the dataset and were typically associated with electrode stakes being poorly coupled to the ground. After minimal processing of the raw data, these data were inverted to generate two-dimensional resistivity cross sections of the subsurface electrical properties (fig. 4). Inversion settings that were used included the selection of a smooth inversion model with a starting model equal to the mean apparent resistivity for the line. Smoothness and damping factors were set to 10, and layer thickness was allowed to increase with depth by 10 percent. Vertical to horizontal roughness ratio values were set to 1 to accommodate flat lying features, and a fine mesh was used between electrodes to obtain more accurate resistivity values from inversion results. A resolution factor of 0.2 was selected to improve model sensitivity at depth. Inversion models converged after two or three iterations. Resistivity values ranged from 25 to 325 ohm-meters. Resistivity cross sections indicated a geologic contact between the lower resistivity near-surface geologic materials and underlying higher resistivity geologic material (fig. 4). The top of the higher resistivity materials was interpreted as the bedrock surface.

HVSR passive seismic surveys can be used to estimate depth to bedrock where there is a significant acoustic impedance contrast (greater than 2:1) between overlying unconsolidated sediments and underlying bedrock (Nakamura, 2000; Lane and others, 2008). A total of 34 HVSR measurements were made with 23 measurements associated with ERT lines and nine independent measurements (fig. 4; Johnson and others, 2020). Field methods described in Johnson and Lane (2016) were used to determine an average shear-wave velocity for five HVSR measurements made at locations with known depth to bedrock (Johnson and others, 2020). At each site, three-component, passive seismic data were collected for 20 minutes. Details on equipment, data collection, and data processing are provided by Johnson and others (2020).

Data from the HVSR surveys were assessed to determine the resonance frequency from analysis of the spectral ratio (horizontal to vertical) of the horizontal and vertical components of the seismic data using Grilla (Micromed S.p.A., 2015), version 6.1, and methods described by Koller and others (2004). Grilla software allows the user to set the window size for the collected data, and a value of 20 seconds was used. Passive seismic data were filtered to remove low-frequency information less than 1 hertz. High-amplitude transients in the windowed data were avoided through use of the anti-triggering algorithm. For each 20-second window, the mean spectrum was computed for the two horizontal components and the vertical component, and the ratio of the horizontal and vertical amplitude spectra was calculated. The plotted spectrums were examined to determine the resonance frequency (f_0), which was expressed as a peak in the frequency spectrum.

At five locations where the depth to bedrock was known, an average shear-wave velocity (Vs) was computed using the formula $Vs=Z\times4f_0$ (Ibs-von Seht and Wohlenberg, 1999), where Z is the thickness of the unconsolidated deposits and f_0 is the measured resonance frequency . An average shear-wave velocity of 300 meters per second (m/s) was calculated from field measurements in the survey area and was consistent with published values (Building Seismic Safety Council, 1994; Johnson and others, 2020). The sediment thickness was computed using methods described by Johnson and Lane (2016) using a shear-wave velocity (Vs) of 300 m/s and the measured resonance frequency (f_0) at each location. The Z value was calculated as $0.25Vs$ divided by the resonance frequency ($Z=0.25\times Vs/f_0$).

The quality of the HVSR curves was assessed using the SESAME guidelines (Koller and others, 2004). Where HVSR surveys were determined to have poor coupling, the poor-quality data were not included in the data release (Johnson and others, 2020). Where sufficient coupling to the ground was determined, the HVSR method was effective for determining the thickness of the unconsolidated deposits overlying

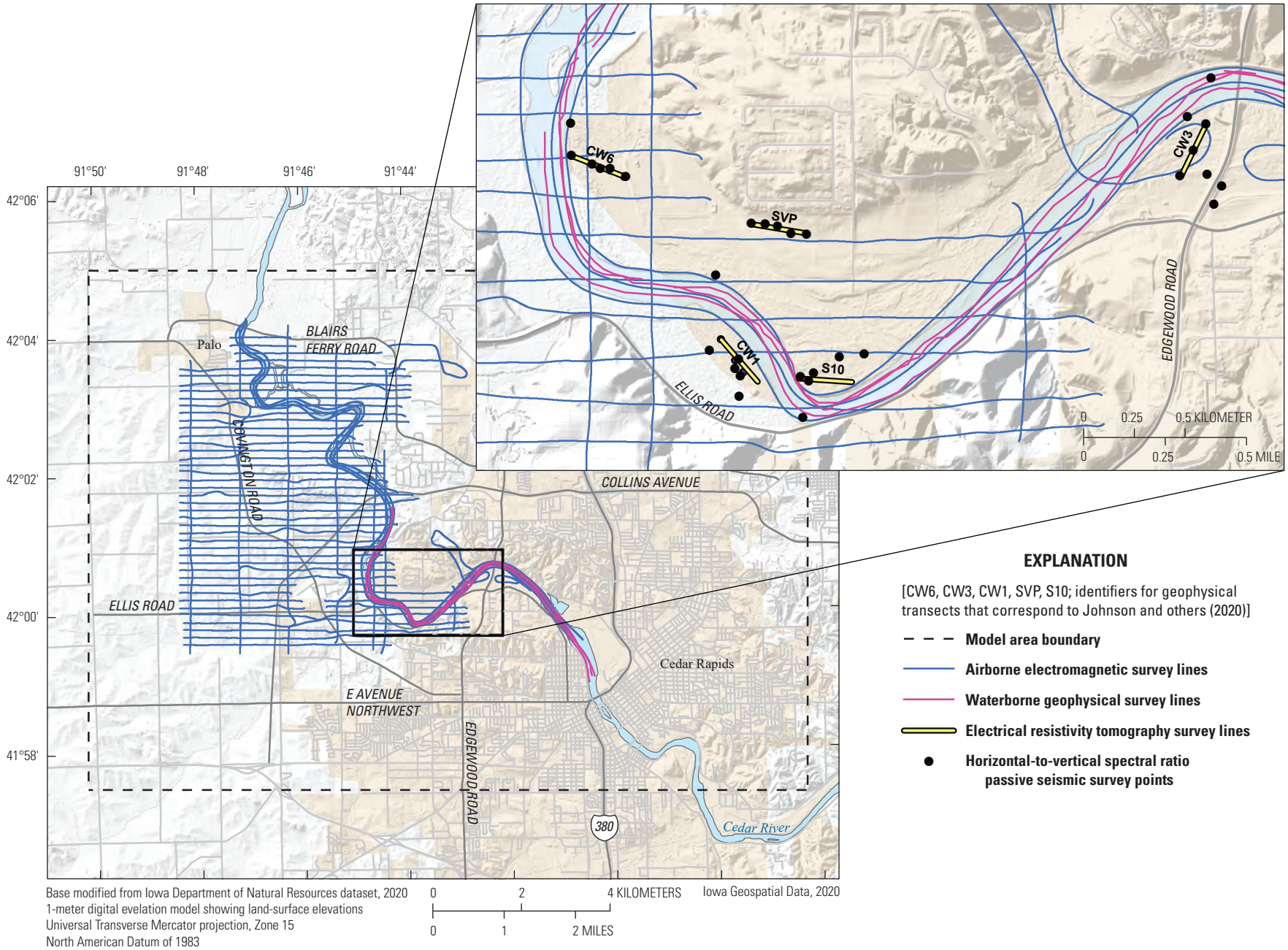

Figure 4. Location of airborne, waterborne, and land-based geophysical survey lines and sites within the model area, Cedar Rapids, Iowa.

bedrock. HVSR results indicated overburden depths ranging from 4 to 28 m. The HVSR determined that the overburden/bedrock contact generally was consistent with the depth of a resistive layer observed in the ERT resistivity profiles (appendix).

Waterborne Geophysical Surveys

Waterborne surveys using continuous resistivity profiling (CRP) and continuous seismic profiling (CSP) methods were completed to characterize the subsurface below the Cedar River. Surveys were concurrent, with the CSP instrument deployed alongside a boat and the CRP streamer deployed behind a boat. A Trimble GPS was used to georeference the location of the boat during data collection, and offset corrections were made to determine the CRP streamer location. Survey lines generally were along the right bank, the left bank, and the center of the river channel (fig. 4). Slightly more CSP data (about 35.4 km) than CRP data (about 30.6 km) were collected because of the difficulty in deploying and maintaining the CRP streamer in a straight line behind the boat; a straight line is not required for the CSP instrument.

The CRP streamer was used to measure the electrical properties of the surface water and geologic materials below the riverbed for characterization and distribution of conductive sediments such as clays, sands, and bedrock (Johnson and White, 2007). CRP data were collected and processed following field methods described in Day-Lewis and others (2006), and these data are presented in Johnson and others (2020). The streamer used for CRP surveys had 11 electrodes with 10-m spacing. A dipole-dipole array geometry was set for the first two electrodes used to inject electrical current into the water, and the remaining nine electrodes were used to measure electrical potential (Day-Lewis and others, 2006). The depth of investigation was about 16 m below the water surface.

The CRP data were processed with EarthImager 2D (version 2.4.4; Advanced Geosciences, Inc., 2009) to remove noise and outliers in the data using methods detailed in Loke (2018). The remaining data were inverted using model inversion. The L2 norm and root mean square error were used to assess the model fit and convergence (Loke, 2018). In general, the resistivity profiles indicated electrically resistive zones underlying shallow unconsolidated deposits below the water bottom (appendix). The resistive zones were interpreted as hard or cemented materials. Electrically resistive zones that occurred at the water bottom were interpreted as coarse-grained materials.

CSP can provide depth to the water bottom, and where signal penetration is achieved with sufficient contrast in acoustic properties, CSP can potentially image sediment layers under the river bed and delineate depth to bedrock (Johnson and White, 2007). Waterborne CSP data were collected using a swept-frequency seismic system that transmits a range of frequencies ranging from 4 to 10 kilohertz (kHz). An acoustic signal was transmitted through the water and reflected off the river bottom and other geologic material layers below the river bottom. A seismic velocity of 1,500 m/s through the water column was applied, and the measured two-way travel time of the acoustic signal was converted to distance. CSP provided the depth to water bottom, and where sufficient signal penetration was achieved, CSP also provided data on the depth to geologic material beneath the river bottom. Data were collected and processed using field methods described in Johnson and White (2007). The survey data are provided in an accompanying data release (Johnson and others, 2020).

The CSP data were interpreted using SonarWiz (version 6.01.0023) software (Chesapeake Technology, 2015). The water bottom and underlying geologic material were interpreted, and output data files were generated that provided location reported as latitude and longitude (in decimal degrees) and depth to the reflector material (in meters). In general, some of the reflectors that could be traced within materials below the streambed in the CSP profiles were consistent with layers observed in the CRP profiles; however, the CSP did not image as deep as the CRP methods (appendix).

Borehole Geophysical Surveys

Borehole geophysical methods can be helpful for mapping vertical variations in lithology, as well as estimating the electrical and hydraulic conductivity of the aquifer. For this investigation, borehole logs also were used to benchmark other geophysical surveys. From June 19 to 22, 2017, borehole surveys were completed in nine USGS groundwater monitoring wells. Four of the wells, CRM–4a, CRM–6a, CRM–11, and CRM–12, were previously established, and the other five wells, GPW1, GPW2, GPW3, GPW4, and GPW5 (not shown), were installed specifically to monitor water levels and complete borehole geophysical surveys for this study (fig. 3). Natural gamma, electromagnetic induction (EMI), and nuclear magnetic resonance (NMR) were three borehole methods used in this study. Of the 9 wells, 8 were logged using all 3 borehole methods. The remaining well was logged with gamma only because the well casing was bent near the top, which prevented insertion of the EMI and NMR probes. Fluid conductivity, temperature, and specific conductance were measured in the water in the casing using a YSI model 30 conductivity meter before each geophysical survey (Johnson and others, 2020).

Natural-gamma logs were collected using a Mount Sopris Instruments gamma probe, model 2PGA–1000. The gamma probe passively measured ambient gamma-ray radiation in counts per second. The tool had a radius of investigation of about 0.3 m and a vertical resolution of about 0.3–0.6 m (Keys, 1990). The data were used to infer intervals of fine-grained sediments and clay, which typically have a higher gamma emission than other earth materials (Keys, 1990). These layers may indicate materials with low hydraulic conductivity. Logs were collected while continuously trolling up the well at about 4–5 meters per minute.

The EMI logs were collected using a Mount Sopris Instruments EMI probe, model 2PIA–1000. The EMI probe measured bulk electrical conductivity of the formation and the water in the formation surrounding the borehole in millisiemens per meter (mS/m). The zone of effect was about a 1.5-m radius from the measuring point with the zone of maximum response about 0.5 m from the measurement point. Increases in electrical conductivity were used to infer silt and clay content, increased water content, and increased total dissolved solids of fluids in the formation. The EMI tool was calibrated in the field using a Mount Sopris Instruments calibration ring and a free-air (0 mS/m) measurement.

A pulsed NMR tool was used to characterize hydraulic properties of the aquifer including water content, pore-size distribution, and hydraulic conductivity. The benefits of NMR measurements are that they can be collected in open holes or through casing. Also, the tool does not require contact with the water, pumping or injection of water, or use of active nuclear sources. During NMR measurement, water molecules surrounding the tool align with strong static magnets in the tool. Then, a pulsed radio-frequency field is used to excite the water molecules and tip the molecules into the transverse plane and emit a magnetic field that is measured by the tool. The signal strength of the magnetic field decreases exponentially with time in what is called the transverse decay (T_2 decay). The initial magnetic field strength in the T_2 decay is directly proportional to the amount of water in the measurement zone. In general, the timing or rate of the T_2 decay indicates the pore-size distribution, with short T_2 decay times indicating small pore sizes and long decay times indicating large pore sizes. The theory and application of NMR measurements is reviewed in detail by Behroozmand and others (2015).

The NMR logs were collected with either the Vista Clara Javelin Probe JP175 or JP238, depending on the casing diameter of the borehole (Walsh and others, 2013). The JP175 and JP238 are 45 and 64 mm (1.75 and 2.38 inches) in diameter, respectively. NMR data were collected in step-mode logging with measurements made in 0.5- or 0.25-m depth increments. Dual-frequency measurements were made with the JP238 at center frequencies of about 290 and 245 kHz, which relate to measurements focused at 14.0 and 15.2 centimeters (5.5 and 6.0 inches) radially from the center of the tool. The vertical resolution of the JP238 tool is 0.5 m. Dual-frequency measurements were made with the JP175 at center frequencies of about 290 and 245 kHz, which relate to measurements focused at 9.5 and 10.2 centimeters (3.6 and 4 inches) radially from the center of the tool. The vertical resolution of the JP175 is 1.0 m. In addition, two recovery times (T_rs) were used for each frequency including a full T_r of 3 to 4 seconds, and a burst-mode (short) T_r of 1.2 seconds. At each depth, several measurements were stacked to improve the signal to noise ratio. The full T_r was stacked 30 times, and the burst-mode T_r was stacked 120 times. For both tools, a total of four binary files were generated for each depth interval, and the results were combined in postprocessing. Additional details of the NMR measurements made with these tools are discussed in Hull and others (2019).

The NMR data were processed using the manufacturer's postprocessing software (Vista Clara, Inc., Javelin Processor, version 3.4.3). During postprocessing, data from each frequency measurement were processed separately. The full T_r and burst-mode T_r measurements were combined for each depth increment. An impulse noise filter was used to remove high-amplitude noise in the T_2-decay data. The data also were adjusted by removing the ambient noise collected with an external reference coil measured concurrently with the subsurface measurement. The outputs for each frequency from the postprocessing program were combined and further processed in a second proprietary software (Vista Clara, Inc., [VC] Javelin Interpretation, version 1.5). Multiexponential decay curves were fit to the T_2-decay data combined from both frequencies with both T_r times for each depth using specified regularization and vertical averaging. The multiexponential decay curves from the combined datasets were inverted to estimate the pore-size distribution. For each depth interval, the total-, mobile-, and immobile-water fractions were determined using empirically derived cutoff values of T_2-relaxation times. The total-water content included the mobile and immobile fractions of water. The mobile fraction, the fraction that decays after the 33-millisecond cutoff, is under saturated conditions and represents the effective porosity (Morriss and others, 1997). The immobile fraction, which includes the clay and capillary fractions that decay earlier than the 33-millisecond cutoff, represents bound water.

Estimates of hydraulic conductivity were made using NMR data and two unit-dependent equations: the Schlumberger-Doll research equation (Kenyon and others, 1988) and the sum of echoes equation (Allen and others, 2000). The parameters used for these equations were the default settings for unconsolidated deposits in the Vista Clara Javelin Interpretation software. The estimates of hydraulic conductivity were considered relative and within 1 to 1.5 orders of magnitude. Data processing and parameter settings are provided in an accompanying data release (Johnson and others, 2020) and by Hull and others (2019).

All borehole geophysical survey results, including gamma, EMI conductivity, and NMR, were combined into a single composite plot for comparison. Additionally, lithologic descriptions were included in the composite plots. The plots are provided in an accompanying data release (Johnson and others, 2020). The suite of logs was effective for identifying the major lithologic contacts. In general, the gamma and EMI were effective for identifying the zones of fine-grained and coarse-grained sediments. The NMR logs were effective for quantifying the water content and pore-size distribution and estimating the relative hydraulic conductivity of the materials. Where the boreholes penetrated the underlying bedrock, such as in CRM–12, the water content and hydraulic conductivity were greatly reduced, and the borehole EMI log indicated a

sharp reduction in the conductivity in the bedrock. This observation was consistent with the sharp increase in resistivity observed in the ERT and CRP profiles at depth.

Borehole logging surveys indicated layers of fine-grained sediments characterized by high gamma counts and high electrical conductivity. Conversely, zones of coarse-grained sediments generally have low gamma, lower electrical conductivity (relative to the fine layers), and higher hydraulic conductivity (as compared to that of the fine-grained sediment layers). NMR survey results characterized zones that are likely good aquifer materials and demonstrate larger amounts of long T_2-decay times, associated with higher mobile-water content (higher hydraulic conductivity). These zones seem to coincide with the midrange electrical resistivity values that are less than the highly resistive bedrock and more than the thin electrically conductive layer observed in the near surface.

Representation of the Conceptual Model in the Groundwater Flow Model

A simple conceptual model was developed for the model area and illustrates the hydrogeologic framework and sources and sinks of groundwater. In the model area, bedrock and surficial sediments were conceptualized as seven hydrogeologic units: alluvial sediment (including the Cedar River alluvial aquifer), eolian sediment (including windblown sands and silts), residual soils, weathered glacial till, unweathered glacial till, weathered bedrock, and unweathered bedrock (fig. 5, table 3). Sources of groundwater recharge include seepage from the stream channel and precipitation. Sources of groundwater loss include evapotranspiration, stream base flow, and withdrawals from vertical and horizontal collector wells. Groundwater flows between the hydrogeologic units and surface waters, primarily rivers and streams in the model area.

Turco and Buchmiller (2004)—and supporting data from Schulmeyer (1995) and Schulmeyer and Schnoebelen (1998)—described a conceptual model that included a hydrogeologic framework, groundwater flow, hydrologic properties, and water budget of a groundwater flow model constructed by Turco and Buchmiller (2004). In general, the Cedar River alluvial aquifer system was composed of multiple aquifers: (1) the Cedar River alluvial aquifer; (2) aquifers associated with tributary stream alluvium, eolian sand, and silt (loess) that overlie glacial till; (3) a buried-channel aquifer that is in direct hydraulic connection with underlying bedrock units and that underlies the Cedar River alluvial aquifer; (4) glacial till in the upland areas primarily composed of clay with an oxidized and fractured upper part; (5) the Devonian and Silurian bedrock

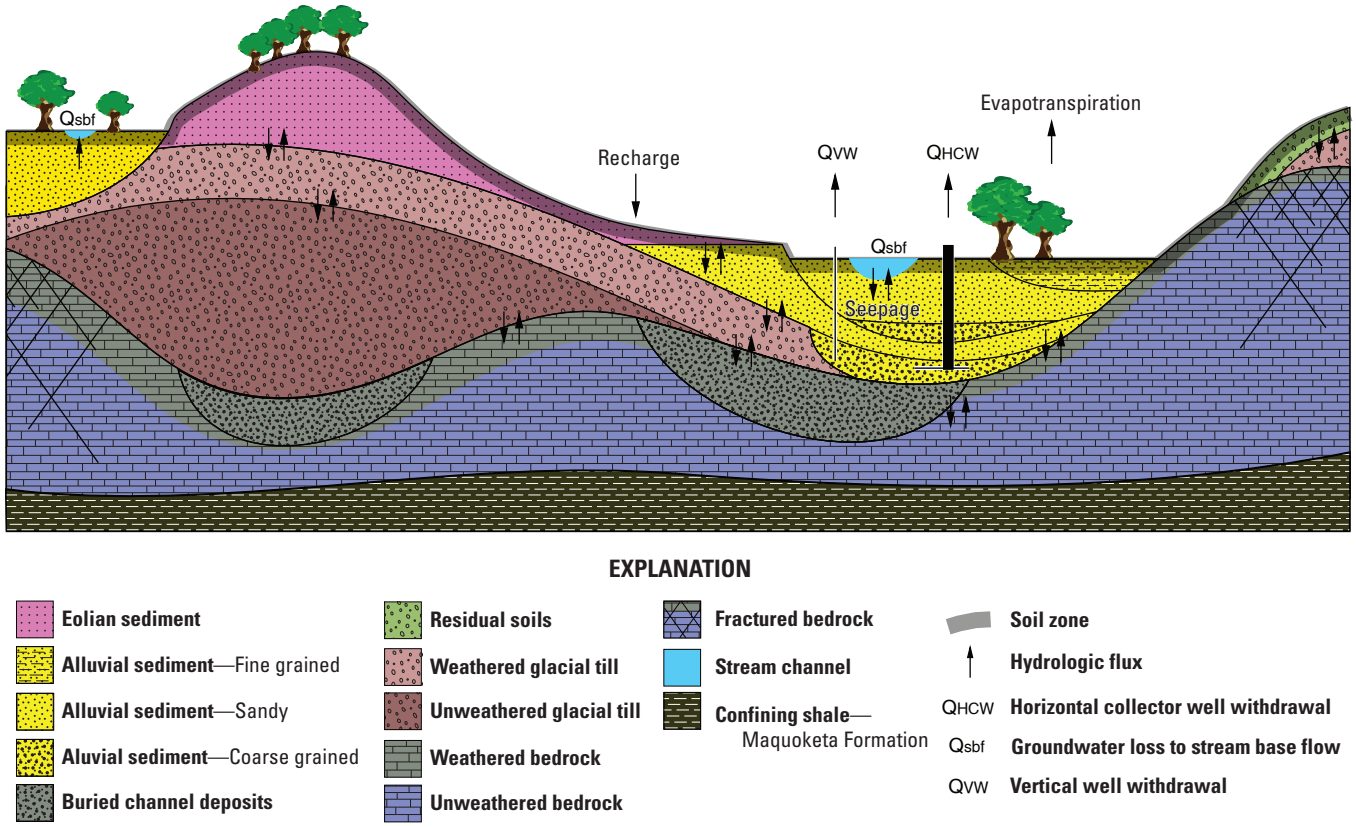

Figure 5. Representation of the conceptual model for seven hydrogeologic units in the model area near Cedar Rapids, Iowa. Groundwater stresses for the system include evapotranspiration, well withdrawals, losses and gains to rivers and streams, and flow into and out of the model boundaries.

Table 3. Conceptual model hydrogeologic units and zones and geologic units mapped by the Iowa Department of Natural Resources (1998c).

[IDNR, Iowa Department of Natural Resources; N/A, not available]

Geologic unit from IDNR, 1998c	Model zone	Hydrogeologic zone description	Hydrogeologic unit	Model layers
Qal, Qpt	1	Fine to medium alluvial sand	Alluvial sediments	1, 2, 3
Qnw	2	Fine to coarse alluvial sand and gravel		
Qal	3	Medium to coarse alluvial sand and gravel		
Qps1	4	Eolian silt loam with sand	Eolian sediments	1
Qps4, Qps1, Qpt	5	Eolian silt loam and sand		2
Qnw, Qps2	6	Fine to medium eolian sand		1, 2
Qwa1, Qps4	7	Loamy sand and gravel erosional surface sediment	Residual soils	1, 2
Qwa2	8	Sandy loam erosional surface sediment		
N/A	9	Weathered till	Weathered till	2, 4
N/A	10	Unweathered till	Unweathered till	2, 4, 5
N/A	11	High hydraulic conductivity	Weathered bedrock	2, 4, 5, 6
N/A	12	Moderate hydraulic conductivity		
N/A	13	Low hydraulic conductivity		
N/A	14	Unweathered bedrock	Unweathered bedrock	4, 5, 6, 7

aquifers consisting of bedrock of Devonian and Silurian age that are separated by a local confining unit, the Otis and Bertram Formations; and (6) the Maquoketa Shale, a regional confining unit that is the lowermost unit in the conceptual model of the flow system. These aquifers were then represented in the hydrogeologic framework as 5 hydrogeologic units and 5 model layers in the groundwater flow model.

The 7 hydrogeologic units in the conceptual model for this study were like those described in previous studies and were further subdivided into 14 subunits with specific hydraulic characteristics, further described in the following "Hydrogeologic Framework" section (table 3). The AEM survey results (Deszcz-Pan and others, 2018); waterborne, land-based, and downhole geophysical survey data collected in 2014 and 2015 (Johnson and others, 2020); and a newly published groundwater flow model for the Silurian and Devonian aquifers (Gannon and others, 2011) were used to improve the Turco and Buchmiller (2004) conceptual model and delineate hydrogeologic units and subunits in the hydrogeologic framework. For example, the Cedar River alluvial aquifer and aquifers associated with tributary stream alluvium, eolian sand, and silt from Turco and Buchmiller (2004) were represented in the hydrogeologic framework as two hydrogeologic units—alluvial sediment and eolian sediment—and further subdivided into subunits with specific hydrogeologic characteristics. Additionally, the Silurian and Devonian aquifers and the confining unit associated with the Otis and Bertram Formations described by Turco and Buchmiller (2004) were represented in the conceptual model as two hydrogeologic units: a thin, weathered upper part of bedrock having a high hydraulic conductivity and a thick, unweathered lower part of bedrock with low hydraulic conductivity. The specifics of these modifications are described in the following "Hydrogeologic Framework" section and are intended to better capture hydrogeologic processes within the scope of this study.

The primary groundwater flow direction for the bedrock aquifer is toward the Cedar River and to the southeast (Gannon and others, 2011), and groundwater flow in the bedrock aquifer is considered primarily regional and not substantially affected by local hydraulic conditions (Turco and Buchmiller, 2004). The primary discharge area for the bedrock aquifer is the Cedar River alluvial aquifer and to the southeast of the study area. Groundwater flow in the Cedar River alluvial aquifer is primarily toward the Cedar River and down the Cedar River valley; however, groundwater flow direction can change during periods of rapid stage increase of the Cedar River or near production wells (Turco and Buchmiller, 2004). The main sources of recharge to the Cedar River alluvial aquifer are infiltration from precipitation, infiltration of runoff from adjacent upland areas, leakage from adjacent aquifers, and leakage from the Cedar River that includes bank storage and induced infiltration caused by pumping from production wells (Schulmeyer and Schnoebelen, 1998). A low-head dam, Five in One Dam, located downstream from the east well field beneath the Interstate 380 bridge, is designed to maintain a minimum river stage by forming a pool that acts as a source of recharge to the Cedar River alluvial aquifer in the east and west well fields (fig. 1; Schulmeyer and Schnoebelen, 1998).

Hydrogeologic Framework

A hydrogeologic framework (framework) for this study was a three-dimensional model of the hydrogeologic units (units) and subunits (zones) for the groundwater flow system. The framework was developed using previously conceptualized hydrogeologic units (Schulmeyer and Schnoebelen, 1998; Turco and Buchmiller, 2004), the lithostratigraphic model from Valder and others (2019), AEM survey data (Deszcz-Pan and others, 2018), detailed surficial geology and depth to bedrock maps (Iowa Department of Natural Resources, 1998b, c), and hydraulic relations and characteristics published in previous USGS reports (Schulmeyer, 1995; Schulmeyer and Schnoebelen, 1998; Turco and Buchmiller, 2004). The framework was used to determine the number of model layers, layer thicknesses, and hydrogeologic units and zones ascribed to each cell of each model layer; this is further discussed in the "Numerical Model Design" section.

Hydrogeologic Units

The primary hydrogeologic units in the model were determined from three-dimensional maps from AEM survey data (Deszcz-Pan and others, 2018), a lithostratigraphic model (Valder and others, 2019), and existing bedrock elevation maps and surficial geology maps (Iowa Department of Natural Resources, 1998a, c). The hydrogeologic units included (1) weathered bedrock, (2) unweathered bedrock, (3) weathered glacial till, (4) unweathered glacial till, (5) alluvial sediment, (6) eolian sediment, and (7) residual soils. A description of each unit and a brief explanation for determination of unit thickness and extent are described in the next sections in order of construction.

Weathered Bedrock and Unweathered Bedrock Hydrogeologic Units

The weathered bedrock and unweathered bedrock units composed the bedrock aquifer and were conceptualized as separate units to simulate interaction of the alluvial aquifer with weathered rock and buried valley sediments that overlie unweathered bedrock. The weathered bedrock unit represents the highly permeable weathered bedrock and sediments in the upper part of the bedrock. The weathered bedrock unit could interact more with the alluvial aquifer than the unweathered bedrock where in hydraulic connection. Both hydrogeologic units were delineated from the thicknesses of Silurian and Devonian-age geologic formations that compose the bedrock aquifer (fig. 6). A 120-m grid raster file was created in a geographic information system (GIS) for the thickness of the bedrock aquifer using the difference of the elevation of the top of bedrock and the elevation of the top of the Maquoketa Formation, a regional confining unit that underlies the bedrock aquifer (Iowa Department of Natural Resources, 1998a, b; fig. 6). The elevation of the top of the bedrock was determined as a 120-m raster in a GIS using data published by Valder and others (2019) for the part of the model area covered by the AEM survey. For the part outside the AEM survey, a depth to bedrock map published by the Iowa Department of Natural Resources (1998b) and the digital elevation map (Iowa Geospatial Data, 2017) were used in a GIS to create a 120-m raster grid that defined the elevation of the top of the bedrock for the model area. These two raster grids were merged in a GIS; some manual adjustments were made to the raster elevation values to correct for abrupt changes in the mapped elevations, usually at survey boundaries.

The thickness of the weathered bedrock unit was determined using four bedrock topographic categories based upon published bedrock elevation values converted in a GIS to a 120-m raster grid for the model area (Iowa Department of Natural Resources, 1998b). Two categories are associated with areas of low elevation on the bedrock surface and are associated with pre-Quaternary valley (erosional) systems (Turco and Buchmiller, 2004). In the first of these two areas, where bedrock elevation was lower than 700 m, the weathered bedrock unit was assigned a thickness of 9 m; this area included buried alluvial sediments described as buried valley aquifers by Turco and Buchmiller (2004). In the second areas where the bedrock elevation was greater than 700 m but less than 780 m, the weathered bedrock unit was assigned a thickness of 8 m (fig. 6). Two categories were assigned to areas of high elevation on the bedrock surface, generally expressed as bedrock plateaus, created when glacial ice advances removed bedrock, exposing a broad, flat, unweathered bedrock surface. In the first of these two areas, where bedrock surface elevation was 780–835 m, the weathered bedrock unit was assigned a thickness of 6 m; in the second area, where elevations were greater than 835 m, the weathered bedrock unit was assigned a thickness of 5 m (fig. 6). Weathered bedrock unit thickness values for the four categories were determined using maximum and minimum thickness values from available lithologic logs (Iowa Geological Survey, 2018).

Weathered Glacial Till and Unweathered Glacial Till Hydrogeologic Units

The thickness, extent, and character of glacial till were generalized from subsurface geophysical profiles (Deszcz-Pan and others, 2018; Valder and others, 2019) for upland (higher elevation) and lowland (lower elevation) parts of the model area. Generally, glacial till overlies the bedrock surface (Iowa Department of Natural Resources, 1998c); however, in lowland parts of the study area, or lowland (fig. 7), and the Cedar River valley, glacial till was eroded and alluvial sediments overlie the bedrock surface, except where deep valleys are present in the bedrock surface (fig. 7). In the bedrock valleys, glacial till underlies the Cedar River alluvium, filling the bedrock valley, and in turn, is underlain by glacial outwash gravels or older alluvial sediments and referred to as "buried-channel deposits" (fig. 5). In the lowland, the thickness of glacial till was determined to be zero, except where deep bedrock valleys were present. In those areas, a glacial till thickness was

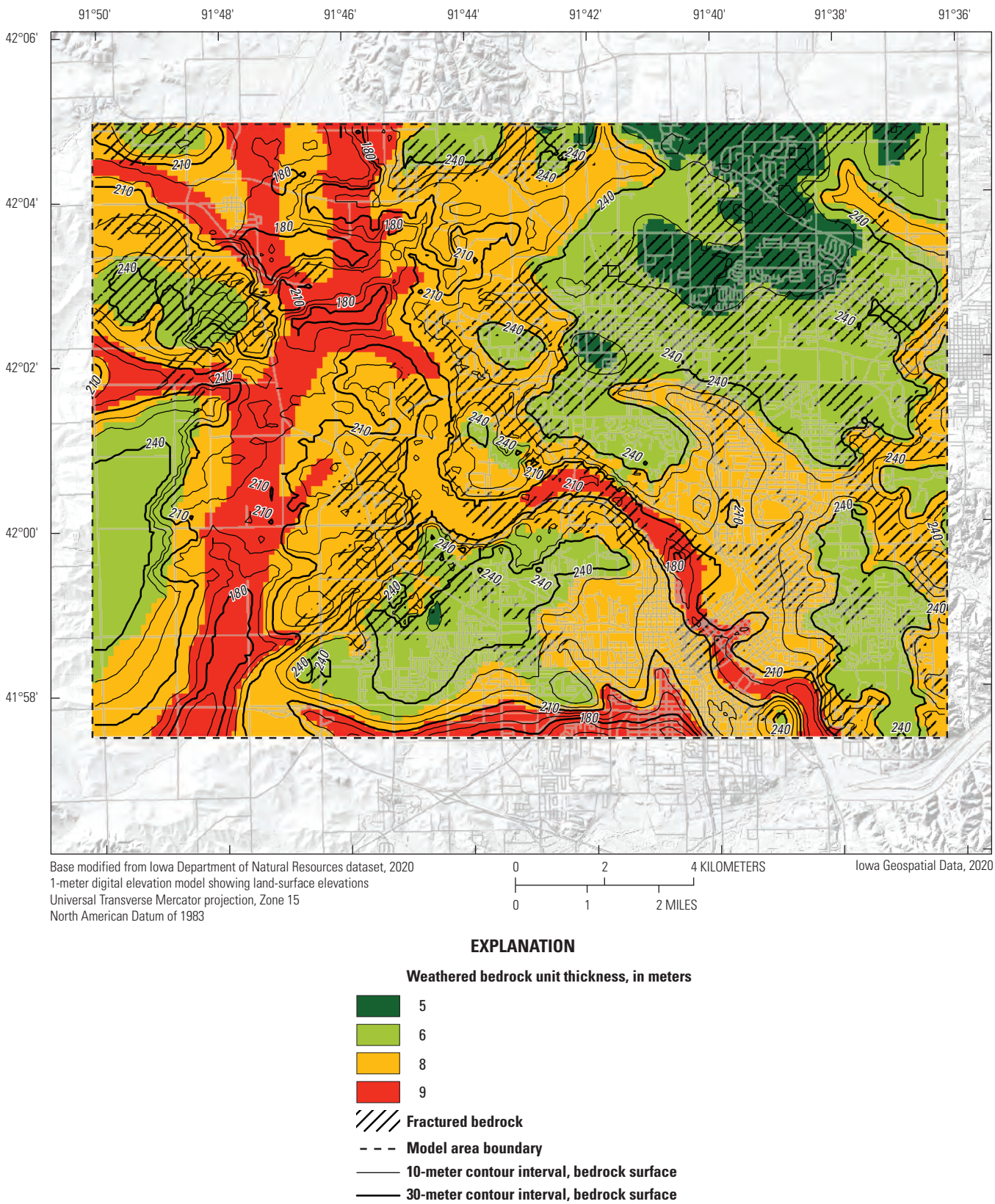

Figure 6. The elevation contours of the bedrock surface and the thickness of the weathered bedrock hydrogeologic unit.

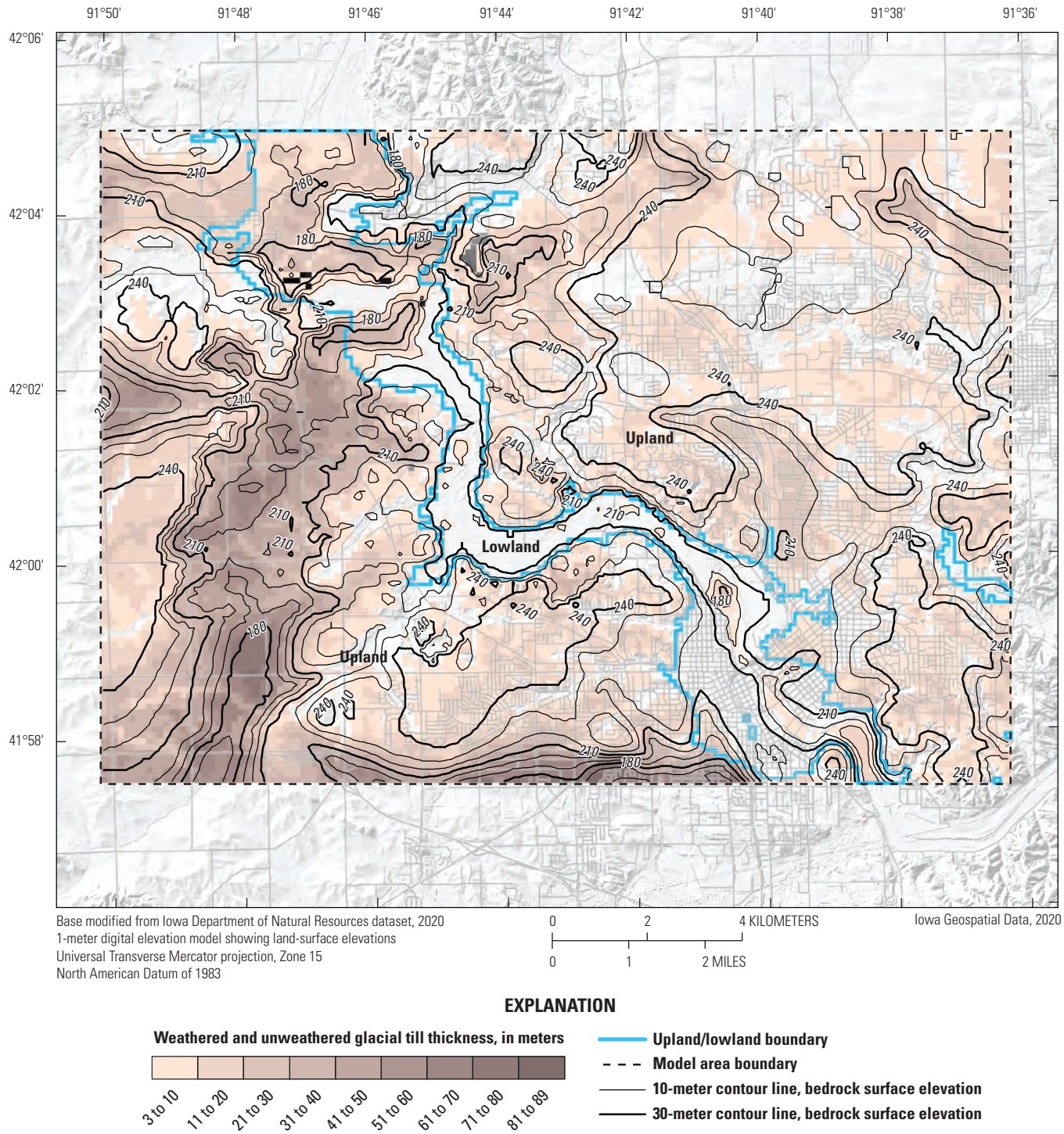

Figure 7. Elevation contours of the bedrock surface and the thickness and extent of weathered and unweathered glacial till.

the difference of till surface elevation and bedrock elevation. In upland parts of the model area, or upland, the glacial till surface generally coincided with land surface, except where overlain by eolian or alluvial sediments, and has a uniform, deep weathering profile. This weathered thickness can be identified in the upper part of AEM profiles in the glacial till as a distinct zone of lower electrical resistivity (Deszcz-Pan and others, 2018; Valder and others, 2019). The thickness of glacial till in the upland was the difference of the till surface elevation and the bedrock surface elevation. Two units were designated for the glacial till: weathered glacial till and unweathered glacial till. The weathered glacial till unit represented the uppermost part of the glacial till that was fractured, oxidized, and leached with a higher hydraulic conductivity than the underlying unweathered glacial till unit.

A 120-m raster grid for the elevation of the till surface was determined in a GIS using data collected during the AEM survey (fig. 4 in Valder and others, 2019). Till surface elevation, thickness, and extent were estimated using mapped surficial geology (Iowa Department of Natural Resources, 1998c), depth to bedrock maps published by Iowa Department of Natural Resources (1998b), Iowa Geological and Water Survey (2010), and the digital elevation map (Iowa Geospatial Data, 2017) in areas outside the AEM survey. Some manual adjustments were made to till surface elevation raster values to account for abrupt changes in the elevation values, the transition at the AEM survey boundary, and mapped (Iowa Department of Natural Resources, 1998c) or observed (in AEM profiles) thicknesses of overlying alluvial and eolian sediments. The glacial till thickness map and contours of the bedrock surface are shown in figure 7; a contour map of the till surface is illustrated in figure 8.

The extent and thickness of the weathered glacial till and unweathered glacial till units were determined with data from AEM profiles (Deszcz-Pan and others, 2018), mapped characteristics of surficial geology (Iowa Department of Natural Resources, 1998c), bedrock elevation raster, and the elevation raster of the glacial till surface. A smoothed 120-m raster map was created in a GIS from land surface elevations and lowered in elevation value by 8 m to represent the approximate depth of the weathering profile and to determine an initial elevation of the top of the unweathered glacial till unit. In the part of the model area where the bedrock elevation was below the elevation of the top of the unweathered glacial till unit, a thickness for the unweathered glacial till unit was calculated by subtracting the elevations. In areas where the bedrock surface elevation was greater than the elevation of the top of the unweathered glacial till unit, the thickness of the unweathered glacial till unit was set to zero. The thickness for the weathered glacial till unit was determined for upland and lowland areas by using the difference of till surface elevation and the elevation of the top of the unweathered glacial till.

In lowland areas (fig. 8), weathered and unweathered glacial till unit thicknesses were adjusted by considering stream erosion. An elevation of 190 m, representing the potential bottom of alluvial sediment, was determined from analysis of alluvial sediment thicknesses described in boring, lithologic, and geophysical logs for each cell in a 120-m raster grid in a GIS (Iowa Geological Survey, 2018; Johnson and others, 2020). The part of the thickness of the weathered and (or) unweathered glacial till units above the elevation of the potential bottom of the alluvial sediment was removed; any remaining thickness of the weathered glacial till unit below the alluvial sediment was assigned to the unweathered glacial till unit. The remaining unweathered till thickness in the Cedar River lowland occurred in deep bedrock valleys under the Cedar River alluvial aquifer. Results were comparable to the occurrence of weathered and unweathered glacial till units from the AEM profiles (Deszcz-Pan and others, 2018; Valder and others, 2019) and with mapped locations of deep bedrock valleys and buried valley aquifers (Iowa Department of Natural Resources,1998a, b; Iowa Geological and Water Survey, 2010).

The thickness and extent of the weathered and unweathered glacial till units in upland and lowland areas were adjusted (in most cases decreased) to accommodate a minimum thickness for the overlying eolian sediments, alluvial sediments, and residual soils without changing surface elevation, and this adjustment is further explained in the "Alluvial Sediment, Eolian Sediment, and Residual Soils Hydrogeologic Units" section. The thickness and extent of the weathered and unweathered glacial till units are shown in figure 7; the thickness and extent of the weathered glacial till unit is shown in figure 8.

Alluvial Sediment, Eolian Sediment, and Residual Soils Hydrogeologic Units

The thickness and extent of the alluvial sediment, eolian sediment, and residual soils units were determined primarily from mapped extents of geologic units, lithologic descriptions, and stratigraphic information (Iowa Department of Natural Resources, 1998c). The thicknesses of these units are small, compared to the other unit thicknesses in the study area, and were not distinguished in AEM profiles. Geologic units mapped by the Iowa Department of Natural Resources (1998c) were grouped into alluvial sediments, eolian sediments, and residual soils hydrogeologic units (table 3). The approximate combined thickness and extent of the alluvial sediment, eolian sediment, and residual soils ranged from 3.0 to 51 m (fig. 9), and the extent and stratigraphic relation of each unit are shown in figure 10. The determination of thickness and extent for each unit is explained in this section.

Eolian sediments in the study area (table 3) are primarily composed of sands and silts (loess) deposited on the upland surface and alluvial terraces near the valley margin of the study area (Iowa Department of Natural Resources, 1998c). The description, thicknesses, and distribution of three geologic units from the Iowa Department of Natural Resources (1998c) were used to determine the thickness and extent of the eolian sediment unit in the model area (table 3), especially where eolian sediments are thin. AEM profiles also were used to identify eolian sediments in the study area, especially where eolian sediments were thick, typically greater than 3 m (Valder and others, 2019). Geologic unit thicknesses (or in some cases, ranges of thicknesses) were projected below land surface elevation and compared to available thickness, which was the difference in land surface elevation and elevation of the top of weathered glacial till, at each grid cell in the 120-m raster grid framework. The thickness for the eolian sediment unit was determined with some manual adjustments made to the grid cell raster thickness of the weathered glacial till, typically a reduction in the weathered glacial till thickness to adequately represent the thickness of the eolian sediment unit. The thickness and extent of the eolian sediment unit is illustrated in figures 9 and 10.

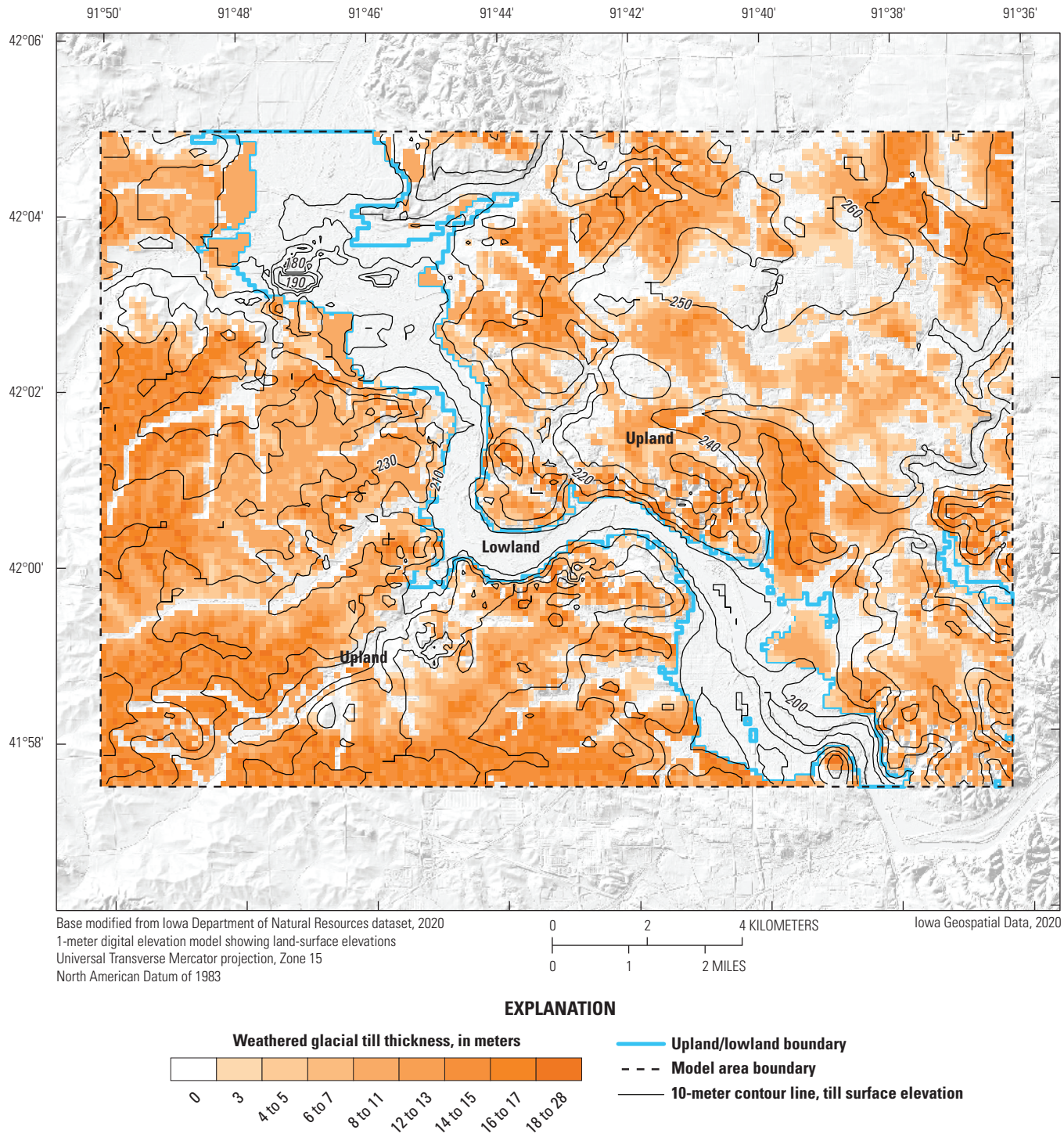

Figure 8. Elevation contours of the till surface and the thickness and extent of the weathered glacial till unit.

The alluvial sediment unit in the model area (table 3) is primarily composed of sands and gravels deposited by the Cedar River and its tributaries; although, some of the alluvial sediments include older sands and gravels underlying alluvial terraces and within and beneath glacial tills (Schulmeyer and Schnoebelen, 1998). The extent and estimated thicknesses of alluvial geologic units mapped by the Iowa Department of Natural Resources (1998c) were used for upland areas to determine a thickness value for a 120-m raster grid in a GIS; in the lowland areas, AEM profiles (table 3; Deszcz-Pan and others, 2018; Valder and others, 2019), existing well logs (Iowa Geological Survey, 2018; Johnson and others, 2020), and waterborne and land-based geophysical surveys (Johnson and others, 2020) were used to verify and modify the thickness

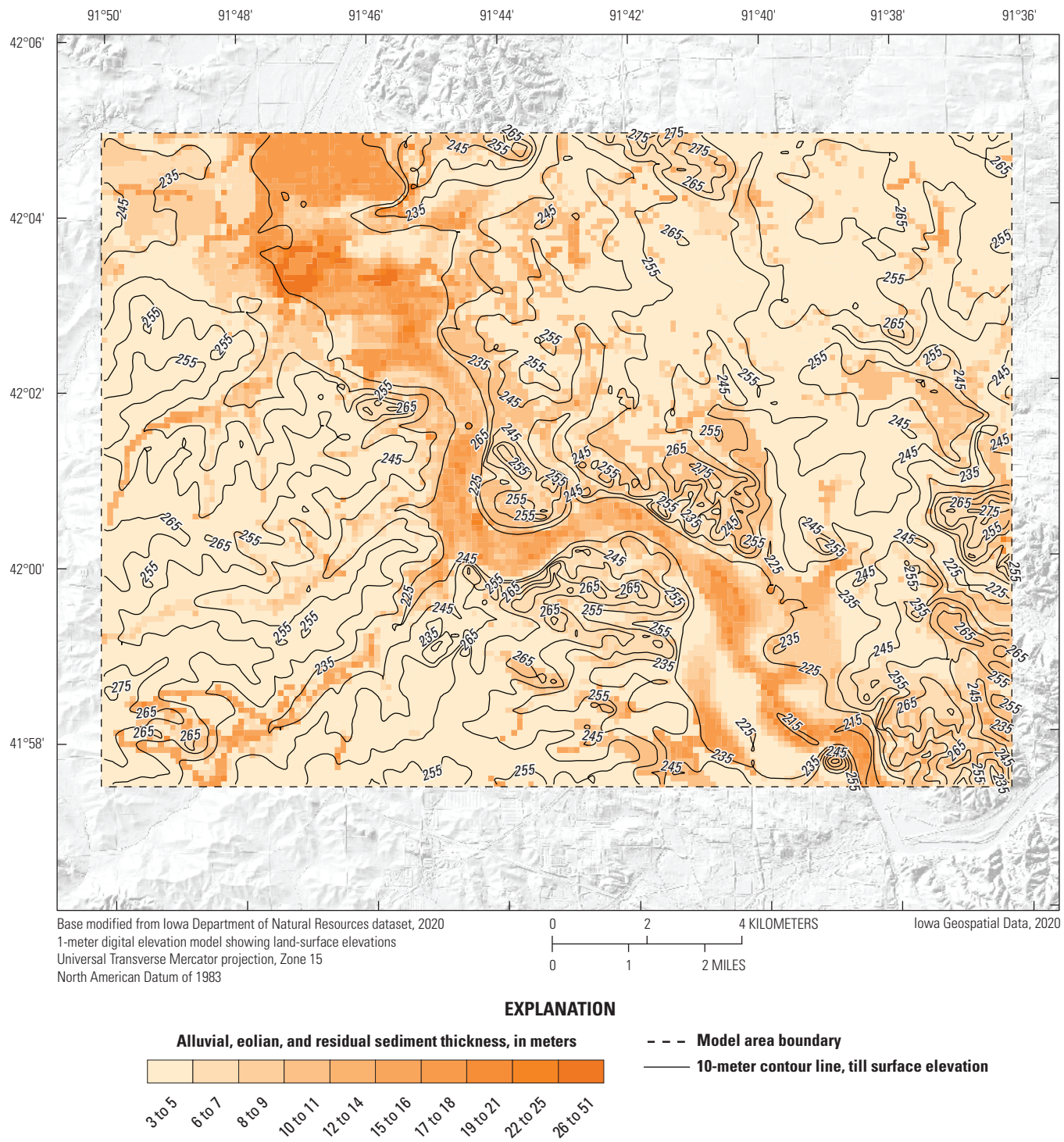

Figure 9. Elevation contours for land surface and the thickness of alluvial sediment, eolian sediment, and residual soils units.

of the alluvial sediment unit, which was the difference in land surface elevation and tentative elevation of the top of weathered glacial till or bedrock surface, at each raster grid cell of the framework. Decreases were made to the thicknesses of underlying hydrogeologic units to adequately represent the thickness of the alluvial sediment unit. Lastly, in the Cedar River valley, thicknesses for three alluvial sediment zones were determined using generalized lithologic changes interpreted in AEM survey profiles, waterborne and land-based geophysical surveys, and existing well logs. The thickness and extent of the alluvial sediment unit are illustrated in figures 9 and 10.

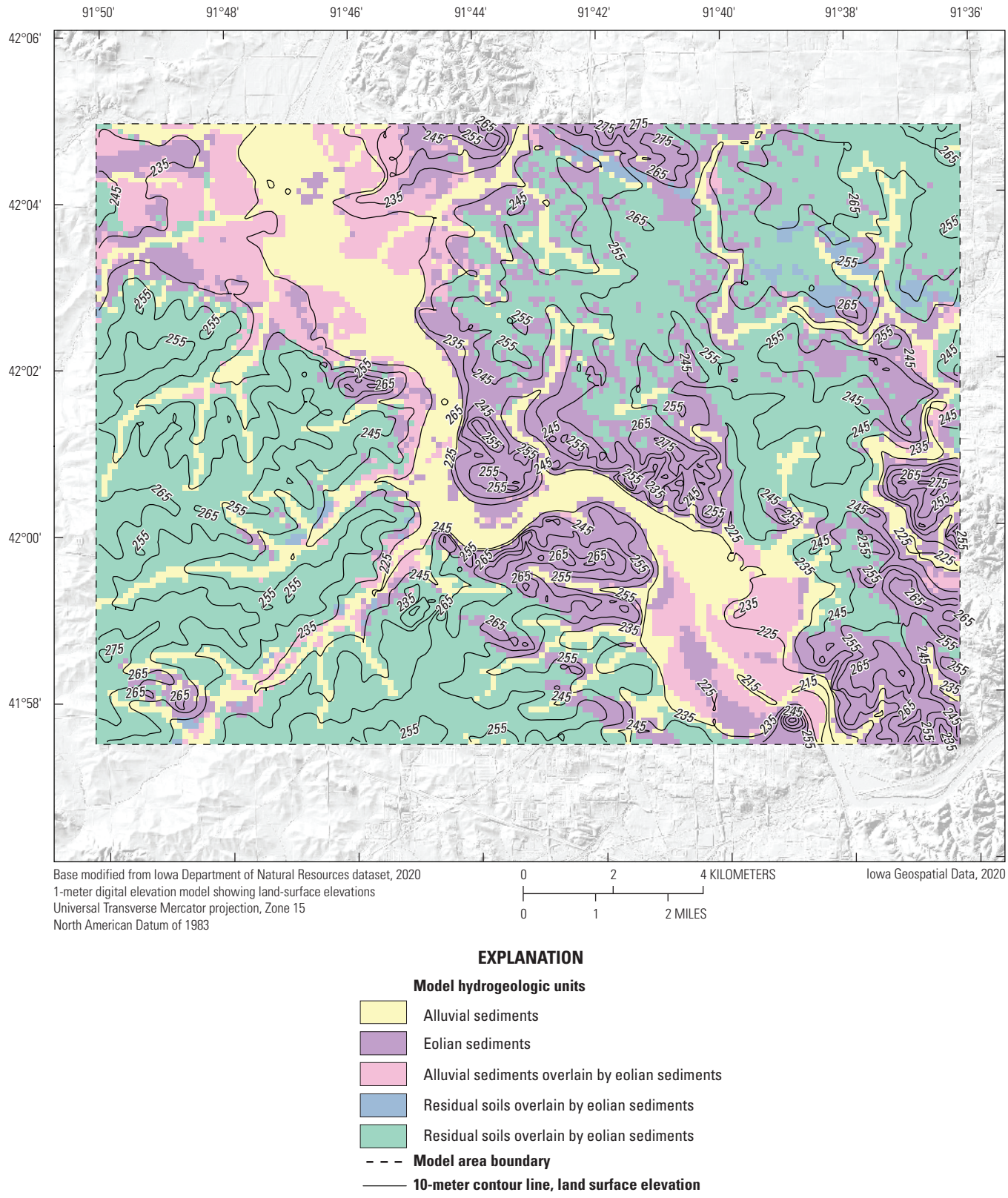

Figure 10. Elevation contours for land surface and distribution of alluvial sediment, eolian sediment, and residual soils units.

The residual soils unit (table 3) in the model is composed of sandy erosional sediments that accumulated on the surface of weathered glacial till. Two zones were determined for the residual soils unit, loamy sand and gravel erosional surface sediment and sandy loam erosional surface sediment, based upon lithologic information from the Iowa Department of Natural Resources (1998c) and AEM profiles where glacial till was observed at or near land surface (table 3; Deszcz-Pan and others, 2018; Valder and others, 2019). The minimum thickness of the residual soil unit was set to a value of 3 m. Decreases were made manually to the 120-m raster grid thickness values of underlying hydrogeologic units to compensate for the 3-m minimum thickness of the residual soils unit. The thickness and extent of the residual soils unit are illustrated in figures 9 and 10.

Water Budget Components

Water budget components consist of the inflows and outflows of the water cycle and include precipitation, streamflow (base flow and runoff), groundwater recharge, evapotranspiration, and groundwater withdrawal. For this study, selected water budget components were estimated to develop, calibrate, and simulate groundwater flow in the numerical model. Specifically, monthly recharge was estimated for the calibration period (October 1, 2016, through August 31, 2018) and simulation period (October 1, 2011, through April 30, 2013) using the Groundwater Toolbox, an open-source software that incorporates streamflow to calculate stream base-flow, runoff, and groundwater recharge using data from the U.S. Geological Survey (2018) and methods published by Barlow and others (2015). Remaining water budget components were calculated from evaporation field measurements and well withdrawal rates provided by the City of Cedar Rapids (Ha and Haj, 2021). Constant head values were assigned for the bedrock aquifer based on previously published information (Gannon and others, 2011) and are discussed in more detail in the "Boundary Conditions" section. Constant head boundaries at groundwater divides determined inflows and outflows from model boundaries.

Recharge

Monthly mean recharge was calculated from streamflow data from the USGS streamgage Cedar River at Cedar Rapids (05464500) using the Groundwater Toolbox by applying the RORA recession-curve displacement and RECESS computer program techniques to streamflow data (Rutledge, 1998) from October 1, 2011, through September 30, 2018. The RECESS program estimates the recession index needed by the RORA program to calculate recharge from streamflow data. A recession index of 41.86 was determined by analyzing a total of 21 recession curves for a 10-day period during the months of October through March for years 1999–2018 (Rutledge, 1998; Barlow and others, 2015). These months were selected for analysis because it was assumed that riparian evapotranspiration was minimal during these months. The recession index and the RORA program were used to obtain the estimates of monthly recharge for model calibration and simulation periods: November 2015 (steady state), from October 2011 to April 2013, and from October 2016 to August 2018 (table 4).

Evapotranspiration and Extinction Depth

Mean monthly potential evapotranspiration (PET) values were obtained from the Iowa Environmental Mesonet (IEM) station CIR14 near Cedar Rapids, Iowa, about 3.5 km south of the Cedar River (not shown) using the available period of record from April 3, 2014, to August 14, 2019 (https://mesonet.agron.iastate.edu/agclimate/et.phtml). Mean monthly estimates of PET obtained from the IEM were calculated using the American Society of Civil Engineers standardized reference evaporation equation (Walter and others, 2001). First, daily PET values from the IEM were estimated by using the Penman-Monteith method (Walter and others, 2001) with calculated net radiation (in megajoules per square meters per day), soil heat flux (in megajoules per square meters per day), mean hourly air temperature (in degrees Celsius) at 2 m, mean daily wind speed (in meter per second, vapor pressure deficit (in kilopascals), slope of the saturation vapor pressure-temperature curve (in kilopascals per degrees Celsius), and psychrometric constant (in kilopascals per degrees Celsius). The IEM calculated monthly PET from daily PET estimates (https://mesonet.agron.iastate.edu/agclimate/#tmpf). Mean monthly PET values were used in the numerical groundwater flow simulations from the IEM period of record and applied uniformly to the model area (table 5). Extinction depth in the model was considered shallow, about 2 m.

Groundwater Water Withdrawal

The City of Cedar Rapids withdraws water from the Cedar River alluvial aquifer at three well fields: the Seminole, east, and west (fig. 3). The well fields have 52 vertical wells (45 active wells) and five HCWs completed in the alluvial aquifer adjacent to the Cedar River (table 2, fig. 3). The City of Cedar Rapids Water Department maintains well withdrawal data that include single-day pumping rates and daily volume totals from the Seminole, east, and west well fields (City of Cedar Rapids, written commun., 2019). The peak mean withdrawal rate exceeded 50 million gallons per day in July of 2012. The HCW withdrawal data included single-day pumping rates and total raw water delivered to water treatment facilities. Single-day pumping rates for vertical wells were not recorded, but daily operation (on/off) data were recorded. The on/off data were correlated with HCW daily pumping rates and inflow rates to raw water treatment facilities to estimate daily pumping rates for vertical wells. Estimated daily well withdrawal data are available in an accompanying data release (Ha and Haj, 2021).

Table 4. Estimated monthly recharge from streamflow used for the Cedar River alluvial aquifer model simulations, from October 1, 2011, to September 30, 2013, and from October 1, 2016, to August 31, 2018.

[mm, millimeter; --, no data]

Simulation period		Calibration period	
Month and year	Recharge (mm)	Month and year	Recharge (mm)
Oct. 2011	0.00	Oct. 2016	0.00
Nov. 2011	7.11	Nov. 2016	32.51
Dec. 2011	8.64	Dec. 2016	41.40
Jan. 2012	0.00	Jan. 2017	0.00
Feb. 2012	3.81	Feb. 2017	75.18
Mar. 2012	23.62	Mar. 2017	0.00
Apr. 2012	16.76	Apr. 2017	105.41
May 2012	13.72	May 2017	31.75
June 2012	11.18	June 2017	0.00
July 2012	3.05	July 2017	30.73
Aug. 2012	3.05	Aug. 2017	0.00
Sept. 2012	2.29	Sept. 2017	4.83
Oct. 2012	0.00	Oct. 2017	26.92
Nov. 2012	0.00	Nov. 2017	16.26
Dec. 2012	0.00	Dec. 2017	0.00
Jan. 2013	0.00	Jan. 2018	10.16
Feb. 2013	7.87	Feb. 2018	0.00
Mar. 2013	30.99	Mar. 2018	32.00
Apr. 2013	44.70	Apr. 2018	65.79
May 2013	32.00	May 2018	49.53
June 2013	136.91	June 2018	93.73
July 2013	12.95	July 2018	3.81
Aug. 2013	5.84	Aug. 2018	8.64
Sept. 2013	7.11	--	--

Table 5. Mean monthly potential evapotranspiration values for groundwater flow simulations.

[mm, millimeter]

Month	Mean monthly potential evapotranspiration (mm)
January	0.6
February	1.1
March	2.3
April	3.8
May	3.7
June	4.6
July	4.2
August	3.9
September	3.6
October	2.3
November	1.3
December	0.6

Numerical Model of Groundwater Flow

Numerical models of groundwater flow (numerical models) were constructed and used to simulate the elevation of the water table from October 1, 2016, to August 31, 2018, and for drought conditions from October 1, 2011, to April 30, 2013. The numerical models were developed as a tool for use by water managers to better understand the potential effects of drought and increased demand on production wells. All numerical model input and output files are available in an accompanying USGS data release (Ha and Haj, 2021).

Numerical Model Design

MODFLOW-NWT (version 1.1.4; Niswonger and others, 2011) was used to simulate groundwater flow for seven hydrogeologic units in the model area. MODFLOW-NWT, a Newtonian-Rapson formulation for MODFLOW-2005, solves the groundwater flow equations for a set of discrete blocks,

called "cells," and balances all inflows and outflows for each cell in the model area. Various components of the water budget were simulated using MODFLOW model packages that are included in MODFLOW-NWT. A MODFLOW model package is a part of the model that deals with a single aspect of the simulation. Packages used in the numerical models include the Discretization, Initial Conditions, and Upstream Weighting Packages (Harbaugh and others, 2000). The Discretization Package was used to define the extent and geometry of layers included in the numerical models; the Initial Conditions Package was used to provide initial starting hydraulic heads for each model layer; and the Upstream Weighting Package was used to specify properties controlling flow between cells such as hydraulic conductivity, anisotropy, specific storage, and specific yield. Aquifer stress was simulated using the Drain (DRN; Harbaugh, 2005), Well (WEL; Harbaugh and others, 2000), Recharge (RCH; Harbaugh and others, 2000), Basic (Harbaugh and others, 2000), Time-Variant Specified Head (Harbaugh and others, 2000), and Evapotranspiration (EVT; McDonald and Harbaugh, 1988) Packages. The DRN Package was used to simulate head-dependent flux boundaries (Winston, 2018). The WEL Package was used to simulate groundwater withdrawals from wells in the model area. The RCH Package was used to represent infiltration from precipitation in the model area. The Basic and Time-Variant Specified Head Packages were used to distribute initial heads to model cells, and the EVT Package was used to represent evapotranspiration from groundwater in the model area. Packages resulting from MODFLOW-NWT output were used to generate output files associated with the groundwater flow model simulation. Output files included cell by cell, hydraulic head, and drawdown.

Spatial, Vertical, and Temporal Discretization

The model area included about 265 km^2 of the Cedar River alluvial aquifer and adjacent uplands (fig. 1). The study area was discretized spatially into cells that were 120 square meters with 115 rows (oriented east to west) and 160 columns (oriented north to south). The model was vertically discretized into 7 layers used to represent the 7 hydrogeologic units with the numerical model layer thickness determined by unit thickness from the framework.

Layer 1 represented the soil zone in the conceptual model; was 3, 4, 5, or 6 m in thickness; and consisted of eolian sediment, alluvial sediment, or residual soils units represented in the framework (fig. 11). Layer 2 ranged in thickness from 1 to 49 m and represented additional thicknesses of eolian sediment, alluvial sediment, or residual soils units below the soil zone (fig. 12). Where no thickness of these units remained below the soil zone (layer 1), the layer 2 cell was assigned the underlying unit value from the framework and a layer thickness value of 1 m. Layer 3 was designed to accommodate vertical heterogeneity for the alluvial sediment in future model development and was assigned the underlying unit value from the framework and a layer thickness value of 1 m (not shown). Layer 4 ranged in thickness from 1 to 28 m and represented the thickness and extent of the weathered glacial till unit (fig. 13). Layer 5 ranged in thickness from 1 to 73 m and represented the thickness and extent of the unweathered glacial till unit (fig. 14). Layer 6 was 1, 2, 4, or 5 m in thickness and represented the thickness and extent of the weathered rock unit (fig. 15). Layer 7 represented the thickness and extent of the unweathered rock unit and ranged in thickness from 219 to 560 m (layer thickness not shown). In all model layers, if the units were not present, then the cell in the layer was assigned the underlying unit value from the framework and a thickness of 1 m. The resulting model consisted of 7 layers with 128,800 active cells, unit top elevations and boundaries like those in the framework, and layer flexibility to incorporate additional vertical and horizontal discretization of units in future model development.

The elevation of the top of layer 1 was set to the mean land surface elevation in each model cell in the framework, determined from digital elevation models (fig. 10; Iowa Geospatial Data, 2017). The elevation of the bottom of layer 7 was set to the mean elevation of the top of the Maquoketa Shale in each model cell in the framework (fig. 16; Gannon and others, 2011). Elevations of the top and bottom of each cell for each layer, thicknesses, and unit values used in the numerical model are available in an accompanying USGS data release (Ha and Haj, 2021).

Two models were constructed for this study. The first model was used to represent steady-state (mean) conditions for general drought/low-flow conditions (referred to in this report as the "steady-state" model) and was simulated in steady-state mode. Aquifer storage is considered negligible during steady state and, therefore, is not used in the formulations of the groundwater flow equation (Niswonger and others, 2011). The steady-state model was used to simulate mean hydrologic conditions from November 1 to November 30, 2015, and to provide starting conditions for the second model used for time-varying (transient) simulations (referred to in this report as the "transient model").

The second model, or transient model, was used to simulate conditions from October 1, 2016, to August 31, 2018 (calibration period), and from October 1, 2011, to April 30, 2013 (simulation period). This model was discretized into discrete blocks of time, called "stress periods," during which all stresses were held constant. The calibration period was divided into 165 stress periods that vary from 3 to 7 days in length, and the simulation period was divided into 70 stress periods that vary from 3 to 14 days in length. The transient stress periods represent subweekly to submonthly conditions and were simulated in transient mode. Aquifer storage is considered during the transient stress periods and is used in the formulations of the groundwater flow equation. Stress period discretization details (ending date and number of days) used for numerical model calibration and simulations are available in an accompanying data release (Ha and Haj, 2021).

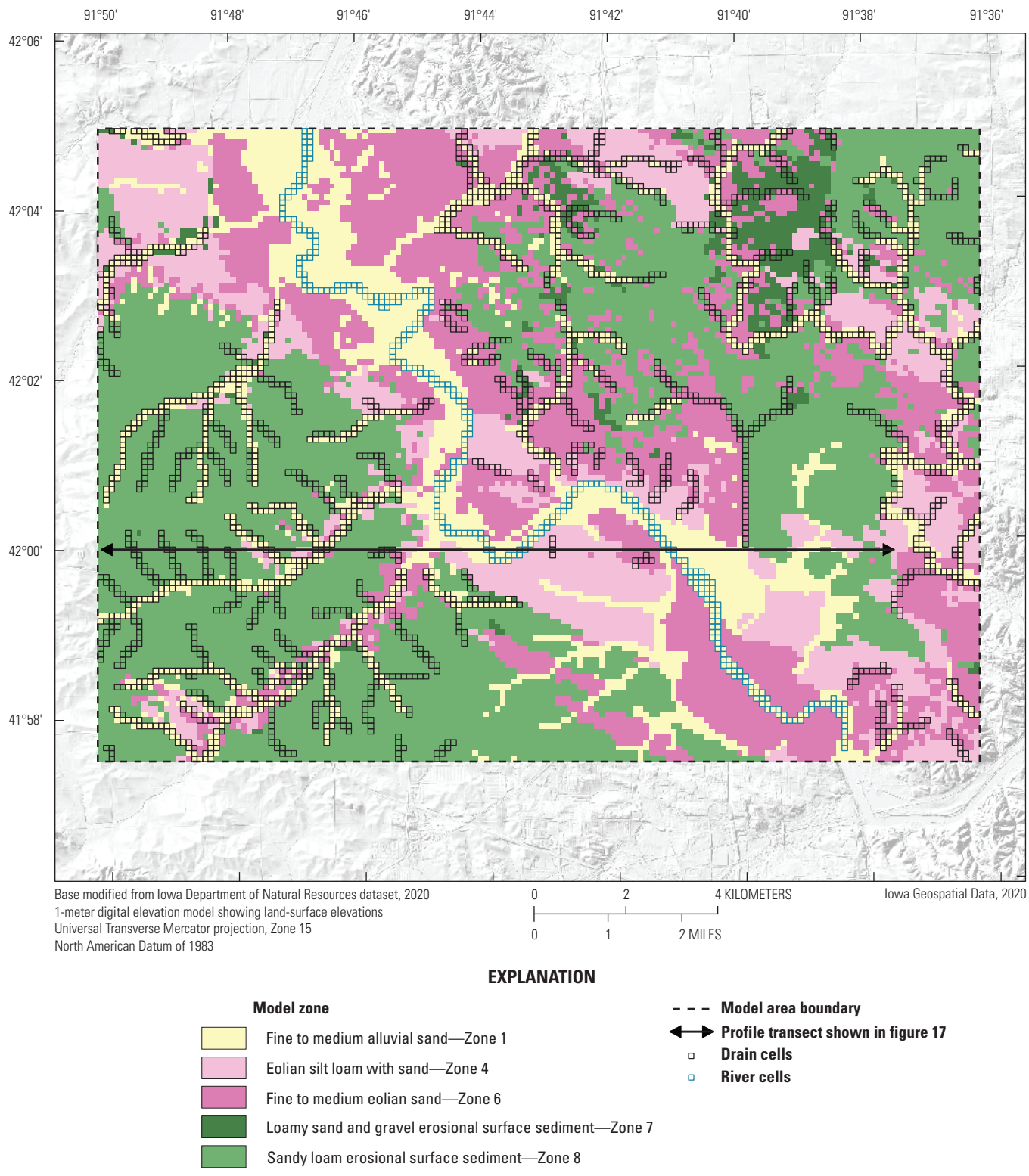

Figure 11. Model layer 1 hydrogeologic units and boundary conditions.

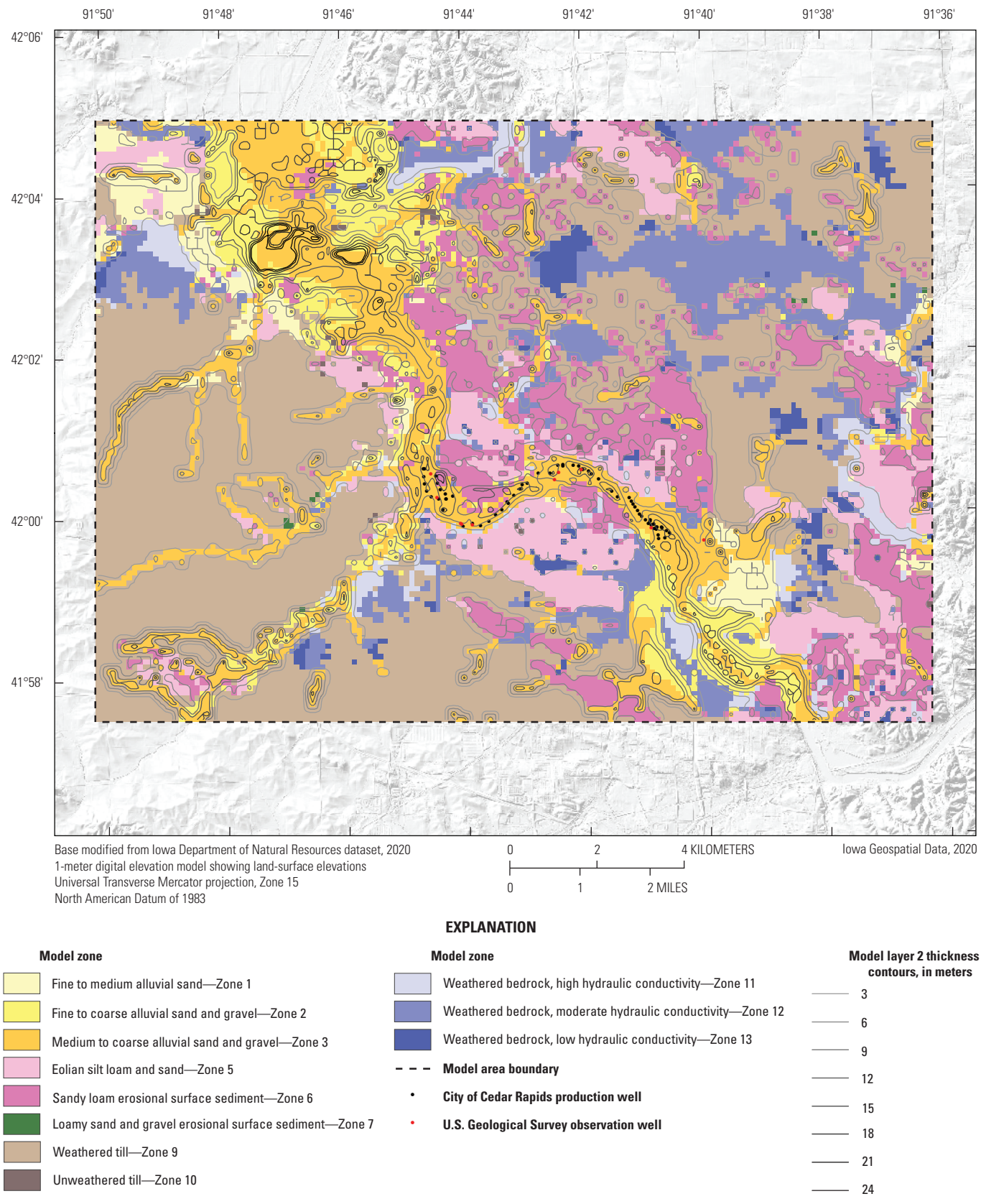

Figure 12. Model layer 2 thickness contours, hydrogeologic units, and zones.

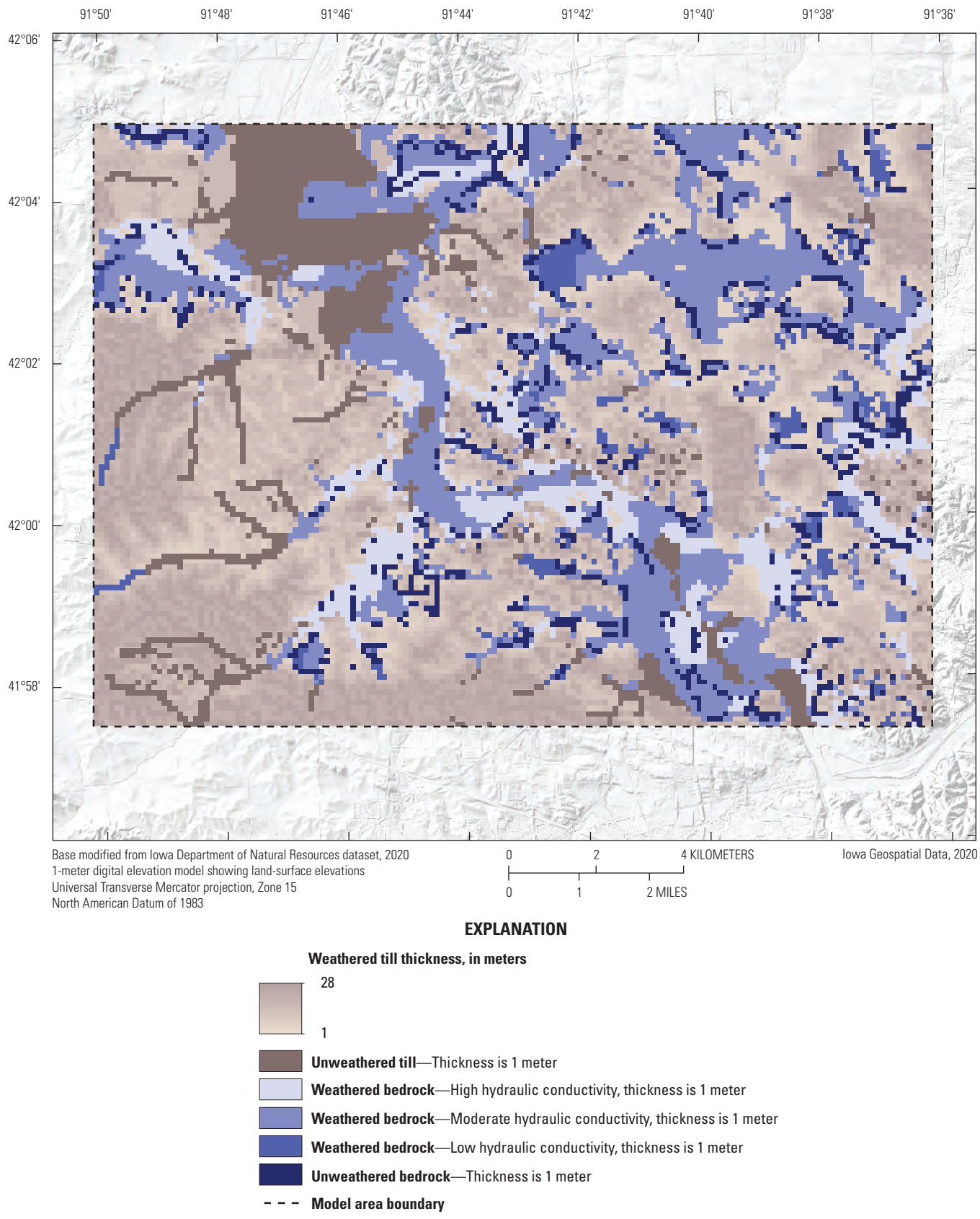

Figure 13. Model layer 4 hydrogeologic units, zones, and weathered till unit thickness.

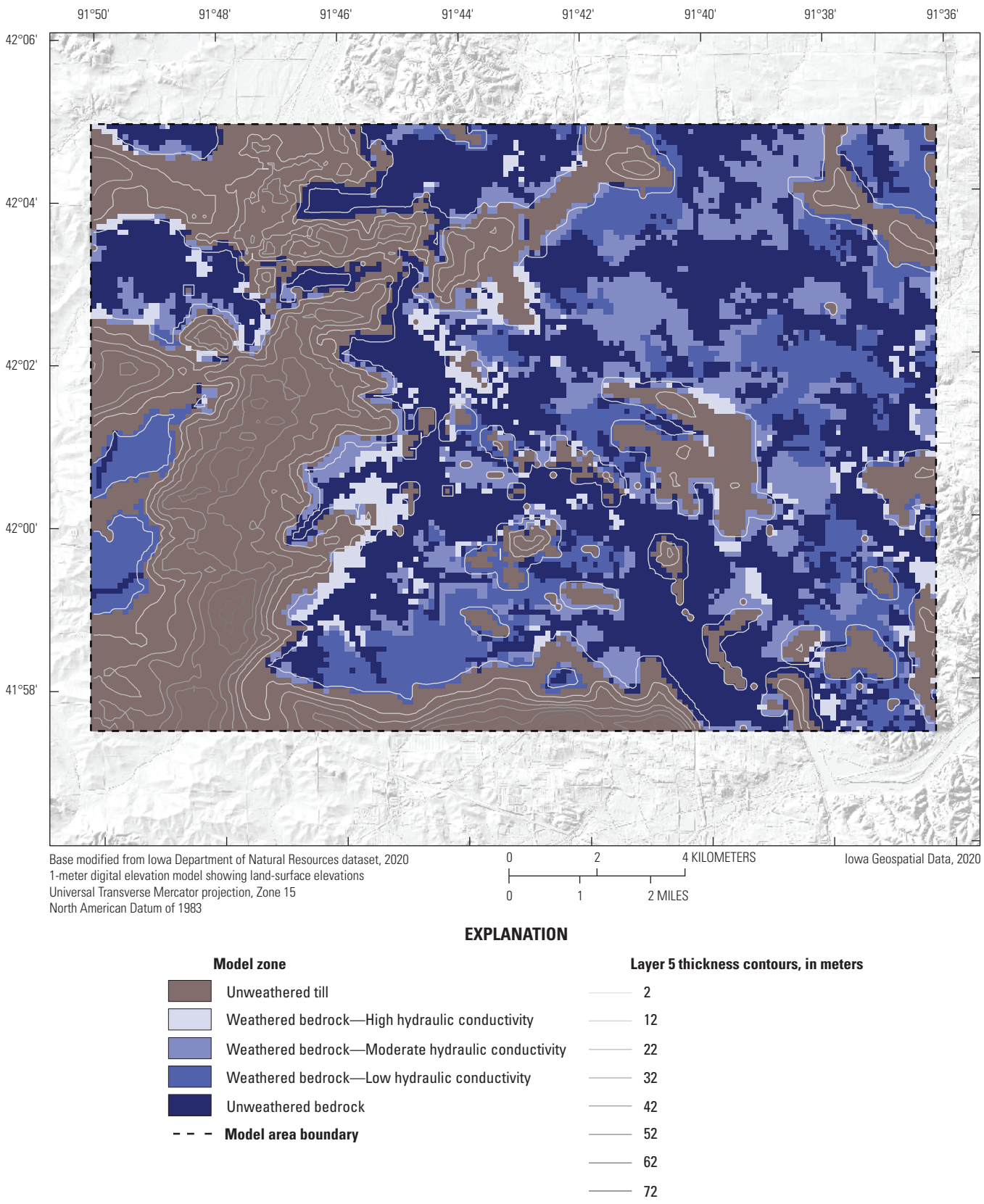

Figure 14. Model layer 5 thickness contours, hydrogeologic units, and zones.

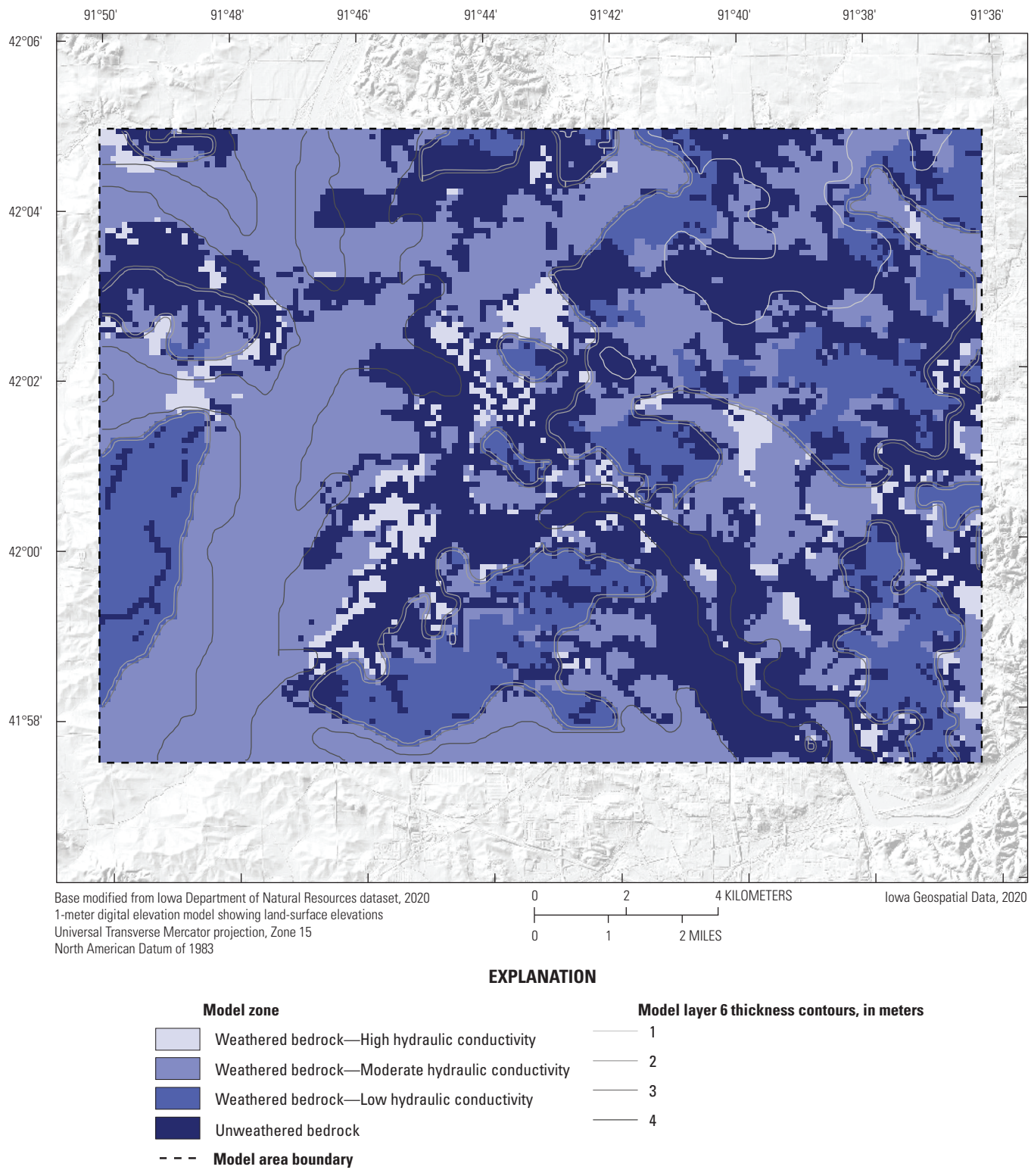

Figure 15. Model layer 6 thickness contours, hydrogeologic units, and zones.

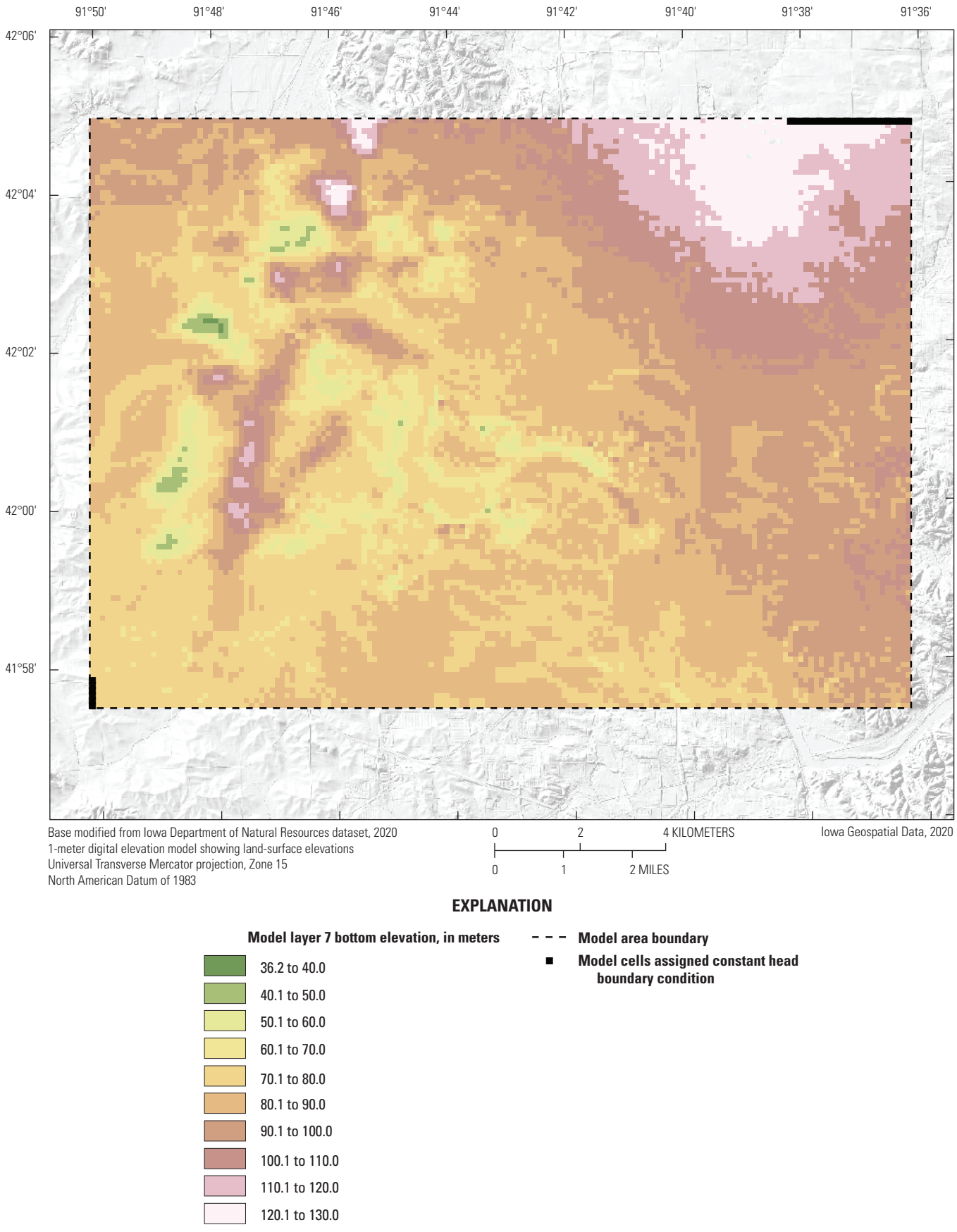

Figure 16. Model layer 7 bottom elevation and boundary conditions.

Hydrogeologic Properties

A total of 14 hydrogeologic zones, subunits of the 7 hydrogeologic units, were constructed for the numerical model (table 3). Vertical and horizontal hydraulic conductivity, specific yield, and specific storage were specified for each zone. Aquifer storage properties (specific yield and specific storage) were assigned to zones in the transient model and allowed to vary during calibration. Zone discretization and characteristics were determined from interpretation of mapped geologic data, geophysical subsurface information, lithologic logs, and previously published ranges and estimates for hydrogeologic properties (Schulmeyer, 1995; Iowa Department of Natural Resources, 1998a, b, c; Schulmeyer and Schnoebelen, 1998; Turco and Buchmiller, 2004; Gannon and others, 2011; Deszcz-Pan and others, 2018; Valder and others, 2019; Johnson and others, 2020). Weathered glacial till, unweathered glacial till, and unweathered bedrock units were each assigned a unique zone. Multiple zones were developed for alluvial sediment, eolian sediment, residual soils, and weathered bedrock units to better represent variability of lithologic characteristics and hydrogeologic properties. Hydrogeologic property values for zones are summarized in table 6, and spatial distributions of zones are illustrated for layers 1, 2, 4, 5, 6, and 7 (figs. 11, 12, 13, 14, 15, 16, and 17). Initial values were assigned based on published values and adjusted further during model calibration.

Three alluvial sediment zones were determined for the alluvial sediment unit, fine to medium alluvial sand, fine to coarse alluvial sand and gravel, and medium to coarse alluvial sand and gravel, using lithological descriptions of the texture of alluvial sediments (table 3; Iowa Department of Natural Resources, 1998c). Lithologic information from boring logs and AEM profiles were used to assign zone values to all alluvial sediment unit cells in model layers 1 and 2 (Deszcz-Pan and others, 2018; Iowa Geological Survey, 2018; Johnson and others, 2020). Each zone was assigned horizontal and vertical hydraulic conductivity, specific yield, and specific storage values based upon textural differences and previously published values (table 6). Fine to medium alluvial sand was assigned a specific yield of 0.35, a specific storage value of 0.00016 per meter, a horizontal hydraulic conductivity value of 18.11 meters per day (m/d), and a vertical hydraulic conductivity value of 1.81 m/d; fine to coarse alluvial sand and gravel was assigned a specific yield of 0.45, a specific storage value of 0.00016 per meter, a horizontal hydraulic conductivity value of 82.30 m/d, and a vertical hydraulic conductivity value of 8.23 m/d; medium to coarse alluvial sand and gravel was assigned a specific yield of 0.45, a specific storage value of 0.00016 per meter, a horizontal hydraulic conductivity value of 117.35 m/d, and a vertical hydraulic conductivity value of 11.73 m/d. Vertical and horizontal discretization of the alluvial sediment zones are shown in figures 11 and 12.

Three eolian sediment zones were determined for the eolian sediment unit, eolian silt loam with sand, eolian silt loam and sand, and fine to medium eolian sand using lithologic descriptions of eolian surficial sediments (table 3; Iowa Department of Natural Resources, 1998c). All cells in model layers 1 and 2 having a unit value of eolian sediment were assigned to one of the three eolian sediment zones. Each zone was assigned horizontal and vertical hydraulic conductivity, specific yield, and specific storage values based upon textural differences and previously published values (table 6). Eolian silt loam with sand was assigned a specific yield of 0.41, a specific storage value of 0.00066 per meter, a horizontal hydraulic conductivity value of 3.05 m/d, and a vertical hydraulic conductivity value of 9.14 m/d; eolian silt loam and sand was assigned a specific yield of 0.41, a specific storage value of 0.00066 per meter, a horizontal hydraulic conductivity value of 3.05 m/d, and a vertical hydraulic conductivity value of 9.14 m/d; fine to medium eolian sand was assigned a specific yield of 0.35, a specific storage value of 0.00016 per meter, a horizontal hydraulic conductivity value of 3.05 m/d, and a vertical hydraulic conductivity value of 9.14 m/d. Preferential vertical flow was assigned to eolian silt loam with sand and eolian silt loam and sand zones (Wang and others, 2018). Vertical and horizontal discretization of the eolian sediment zones are shown in figures 11 and 12.

Two residual soils zones were determined for the residual soils unit, loamy sand and gravel erosional surface sediment and sandy loam erosional surface sediment, using lithologic descriptions of erosional surface sediments (table 3; Iowa Department of Natural Resources, 1998c). All residual soils unit cells in model layers 1 and 2 were assigned one of the two residual soils zone values. Each zone was assigned horizontal and vertical hydraulic conductivity, specific yield, and specific storage values based upon textural differences and previously published values (table 6). Loamy sand and gravel erosional surface sediment and sandy loam erosional surface sediment were assigned a specific yield of 0.10, a specific storage value of 0.0016 per meter, a horizontal hydraulic conductivity value of 2.44 m/d, and a vertical hydraulic conductivity value of 0.24 m/d. Vertical and horizontal discretization of the residual soils zones are shown in figures 11 and 12, respectively.

Weathered glacial till and unweathered glacial till units were each assigned one zone. Weathered glacial till zone had a horizontal hydraulic conductivity of 12.19 m/d, a vertical hydraulic conductivity of 1.22 m/d, a specific yield of 0.10 per meter, and specific storage of 0.00066 m/d based on previously published values (table 6; Schilling and Tassier-Surine, 2006). The unweathered glacial till zone was assigned a horizontal hydraulic conductivity of 1.22 m/d, a vertical hydraulic conductivity of 0.12 m/d, a specific yield of 0.05 per meter, and specific storage of 0.0066 m/d (table 6; Schilling and Tassier-Surine, 2006).

Three weathered bedrock zones were determined for the weathered bedrock unit: high, moderate, or low hydraulic conductivity (table 3). The zones were delineated based on the mapped distributions of fractures in bedrock (fig. 6; Iowa Department of Natural Resources, 1998c) and the thickness categories for the weathered bedrock unit. Parts of the model areas were modified using lithologic descriptions from boring

Table 6. Hydrogeologic characteristics for hydrogeologic zones.

[K_h, horizontal hydraulic conductivity; m/d, meter per day; K_v, vertical hydraulic conductivity; Sy, specific yield; SS, specific storage; K_x, K_y, horizontal hydraulic conductivity for x and y axes, respectively; m/d, meter per day; K_z, vertical hydraulic conductivity; E, denotes exponentiation; K, hydraulic conductivity]

Zone number	Zone description	Published zone hydrogeologic characteristics				Precalibration values				Steady-state calibrated values		Transient calibrated values	
		K_h (m/d)	K_v (m/d)	Sy	SS, per meter	Sy	SS, per meter	K_x, K_y (m/d)	K_z (m/d)	K_x, K_y (m/d)	K_z (m/d)	K_x, K_y (m/d)	K_z (m/d)
1	Fine to medium alluvial sand	1.22–30.48[a]	0.12–3.05	0.30–0.40	1.6E−04	0.35	1.6E−04	18.11	1.81	18.11	1.81	18.11	1.81
2	Fine to coarse alluvial sand and gravel	12.19–152.40	5.18–15.24	0.45	1.6E−04	0.45	1.6E−04	82.30	8.23	82.30	8.23	82.30	8.23
3	Medium to coarse alluvial sand and gravel	51.82–182.88	5.18–18.28	0.45	1.6E−04	0.45	1.6E−04	117.35	11.73	176.02	17.60	211.23	17.60
4	Eolian silt loam with sand	3.048	9.14[b]	0.4–0.42	6.6E−04	0.41	6.6E−04	3.05	9.14	3.05	9.14	3.05	9.14
5	Eolian silt loam and sand	3.048	9.14[b]	0.4–0.42	6.6E−04	0.41	6.6E−04	3.05	9.14	3.05	9.14	3.05	9.14
6	Fine to medium eolian sand	3.048	9.14[b]	0.30–0.40	1.6E−04	0.35	1.6E−04	3.05	9.14	3.05	9.14	3.05	9.14
7	Loamy sand and gravel erosional surface sediment	2.43[c]	0.25	0.1[d]	1.6E−03	0.10	1.6E−03	2.44	0.24	2.44	0.24	2.44	0.24
8	Sandy loam erosional surface sediment	2.43[c]	0.25	0.05[d]	1.6E−03	0.10	1.6E−03	2.44	0.24	2.44	0.24	2.44	0.24
9	Weathered till	12.19[e]	1.22	0.1	6.6E−04	0.10	6.6E−04	12.19	1.22	12.19	1.22	12.19	1.22
10	Unweathered till	1.21[e]	0.3	0.05	6.6E−03	0.05	6.6E−03	1.22	0.12	1.22	0.12	1.22	0.12
11	Weathered bedrock, high K	2.44–54.88[c]	0.24–5.5	0.1–0.15	3.3E−05	0.18	3.3E−05	50.00	5.00	50.00	5.00	50.00	5.00
12	Weathered bedrock, moderate K	2.44–54.88[c]	0.24–5.5	0.1–0.15	3.3E−05	0.18	3.3E−05	25.00	2.50	25.00	2.50	25.00	2.50
13	Weathered bedrock, low K	2.44–54.88[c]	0.24–5.5	0.1–0.15	3.3E−05	0.18	3.3E−05	10.00	1.00	10.00	1.00	10.00	1.00
14	Unweathered bedrock	2.44–54.88[c]	0.24–5.5	0.1–0.15	3.3E−05	0.18	3.3E−05	5.00	0.50	10.00	1.00	12.00	1.31

[a]Modified for fine-grained sediments.

[b]Modified for preferential vertical flow (Wang and others, 2018).

[c]Schulmeyer and Schnoebelen (1998).

[d]Johnson (1967).

[e]Schilling and Tassier-Surine (2006).

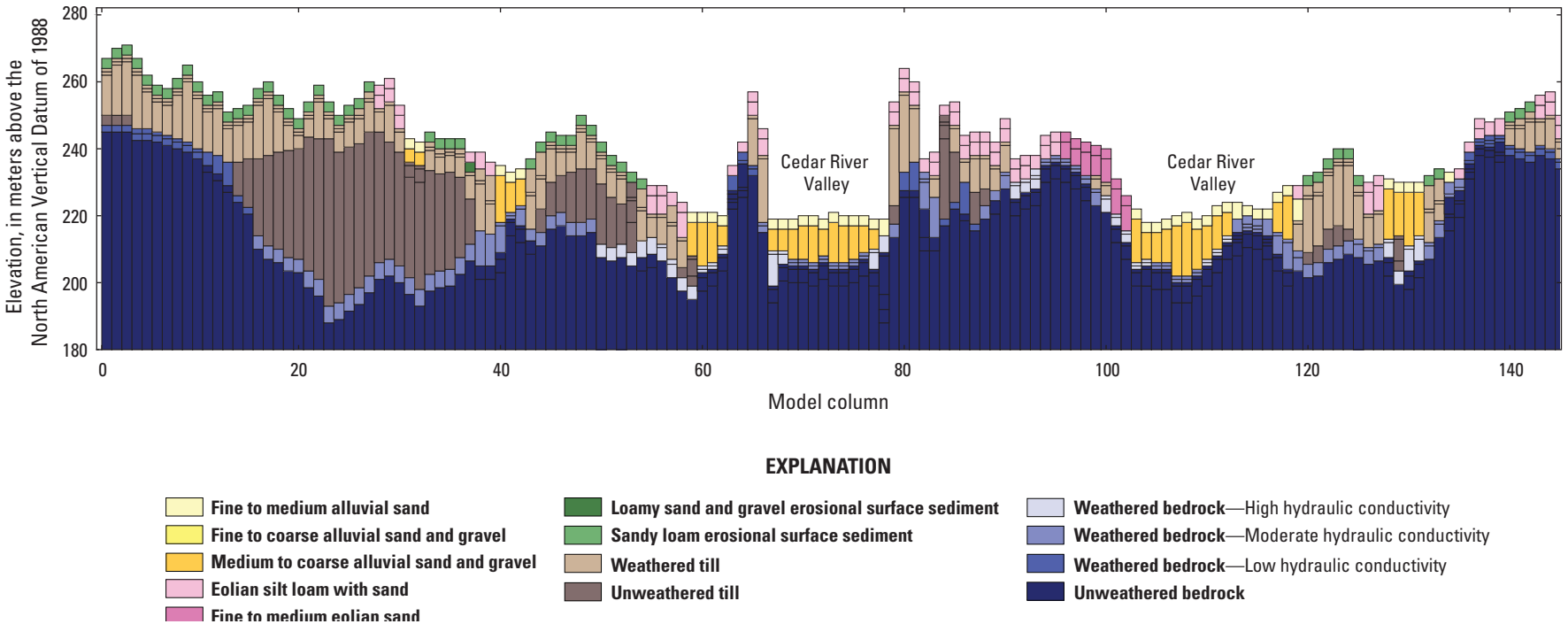

Figure 17. Cross-sectional profile A–A′ (row 77, columns 1 through 150) depicting the vertical relation of hydrogeologic units and zones for model layers. The total thickness of layer 7 is not shown.

logs and AEM profiles (Deszcz-Pan and others, 2018; Iowa Geological Survey, 2018; Johnson and others, 2020). Each zone was assigned horizontal and vertical hydraulic conductivity, specific yield (0.18), and specific storage (0.000033 m/d) values based upon textural differences and previously published values (table 6; Schulmeyer, 1995; Schulmeyer and Schnoebelen, 1998; Turco and Buchmiller, 2004; Gannon and others, 2011). The high zone was assigned a horizontal hydraulic conductivity value of 50.00 m/d and a vertical hydraulic conductivity value of 5.00 m/d, the moderate zone was assigned a horizontal hydraulic conductivity value of 25.00 m/d and a vertical hydraulic conductivity value of 2.50 m/d, and the low zone was assigned a horizontal hydraulic conductivity value of 10.00 m/d and a vertical hydraulic conductivity value of 1.00 m/d. Vertical and horizontal discretizations of the weathered bedrock hydrogeologic unit are shown in figures 13–15. One zone was created for the unweathered bedrock unit that had a horizontal hydraulic conductivity of 5.00 m/d, a vertical hydraulic conductivity of 0.50 m/d, a specific yield of 0.18 per meter, and specific storage of 0.000033 m/d based on previously published values (table 6; Schulmeyer and Schnoebelen, 1998).

Boundary Conditions

Boundary conditions in the numerical model were simulated using various MODFLOW-NWT packages. Constant head boundaries were simulated using the CHD Package, recharge from infiltration of precipitation in the model area was simulated using the RCH Package, direct evapotranspiration from groundwater was simulated using the EVT Package, groundwater withdrawal was simulated using the WEL Package, and the interaction of groundwater and surface water in the model area was simulated using the RIV and DRN Packages.

Constant head boundaries were assigned to several cells in layer 7 in the northeastern corner ranging from 251 to 256 m and the southwestern corner with a value of 230 m at the model boundary and were constant for all model stress periods (fig. 16). Values for these cells were determined using contour maps of the elevation of the water table for the Silurian and Devonian aquifer system from Horick (1984) and minimum values recorded during drought periods (Iowa Geological Survey, 2018; U.S. Geological Survey, 2018) and are provided in an accompanying data release (Ha and Haj, 2021). The interpolated elevation of the water table for the Silurian and Devonian aquifer system (weathered and unweathered bedrock units in this study) and constant head cell values are available in an accompanying data release (Ha and Haj, 2021). Boundary conditions were set on mapped groundwater divides in the Silurian and Devonian aquifer system (weathered and unweathered bedrock units) near the margin of the model area to better simulate potential groundwater flow contribution from the bedrock aquifer to the Cedar River alluvial aquifer during drought periods.

Recharge from infiltration of precipitation on the land surface was simulated using the RCH Package. The RCH Package is designed to simulate aerially distributed recharge to the groundwater system (Langevin and others, 2017). The rate of recharge was specified for each stress period, in units of meters per day, and the rate is multiplied by the cell horizontal area to obtain the recharge flow rate for each model cell (Langevin and others, 2017). Recharge rates were estimated using the RORA/RECESS model (table 4) and used as initial estimates of recharge for the model. The initial recharge value for November 2015 steady state was about zero, a value of 0.0012 cubic meter per day (m^3/d); initial monthly values used for transient model simulations are listed in table 4. The calculated recharge rates were adjusted during model calibration using a single recharge multiplier; this is further discussed in the "Groundwater Model Calibration Approach" section of this report.

Evapotranspiration occurs from direct evaporation of groundwater and from plant transpiration and was simulated using the EVT Package. The EVT Package simulates the effects of plant transpiration and direct evaporation by removing water from the saturated groundwater regime (Langevin and others, 2017). The initial rate of evapotranspiration assigned to the steady-state model for drought conditions was 0.0027 m/d, estimated as about 10 times less than the lowest observed values recorded in mean monthly PET values from April 3, 2014, to August 14, 2019 (https://mesonet.agron.iastate.edu/agclimate/et.phtml; table 5). An evapotranspiration value was assigned to each stress period in units of meters per day. Mean monthly PET values (table 5) were divided by the number of days in each month, and then daily values were aggregated for each stress period. PET estimates used in the model are available in an accompanying data release (Ha and Haj, 2021).

Groundwater withdrawal from wells in the model area was simulated using the WEL Package. The WEL Package is designed to simulate features such as wells that withdraw water from or add water to the aquifer at a specified rate during a stress period, where the rate is independent of the cell area and the head in the cell (Langevin and others, 2017). Groundwater withdrawal rates were specified for each stress period in units of cubic meters per day. Groundwater withdrawal rates for the steady-state stress period and each stress period for transient model simulations were determined from data provided by the City of Cedar Rapids (Ha and Haj, 2021). Only groundwater withdrawal for City of Cedar Rapids production was considered in the numerical model. Groundwater withdrawal for other uses existed in the model area but was considered small in comparison to all other water budget components and not included in the model. Production well locations in the Seminole, east, and west well fields; withdrawal rates for HCWs; and inflows to raw water treatment facilities were provided by the City of Cedar Rapids (Ha and Haj, 2021). Production well locations were converted to the

equivalent model row, column, and layer coordinates (table 2). All modeled production well information is available in an accompanying USGS data release (Ha and Haj, 2021).

Streams and rivers were the only surface-water features represented in the model and were simulated using the RIV and DRN Packages (Langevin and others, 2017). The RIV Package was assigned to cells in layer 1 that intersected segments of the Cedar River in the model area. Attributes required to define each model cell simulated by the RIV Package (RIV cell) include the top elevation of the river bed, in meters above NAVD 88; the river stage, in meters above NAVD 88; and conductance of the riverbed material, in meters squared per day. River bed top elevations for each RIV cell were estimated from the digital elevation model elevations of the streambank and water surface, from the estimated depths of the river channel, and by calculating a change in elevation for each RIV cell to ensure that the elevation of the river bed top was not above the land surface elevation of adjacent cells. River stage for each RIV cell was interpolated using a GIS and low-flow stage measurements from Cedar River at Blairs Ferry Road at Palo, Iowa (05464420); Cedar River at Edgewood Road at Cedar Rapids, Iowa (05464480); and Cedar River at Cedar Rapids, Iowa (05464500; U.S. Geological Survey, 2018).Riverbed thickness was set to 1 m for all RIV cells. Conductance of the riverbed material was calculated by the RIV package to be 3,600 meters squared per day (m^2/d) with a stream width and length of 60 m and riverbed hydraulic conductivity set to 1 m/d for each RIV cell.

The DRN Package was assigned to cells in layer 1 that intersected tributaries of the Cedar River in the model area. Attributes required to define each model cell simulated by the DRN Package (DRN cell) include drain altitude, in meters above NAVD 88, and conductance of the drain bed (streambed) material, in meters squared per day. Drain altitudes for each DRN cell were estimated at 3 m below elevation of the top of model layer 1. Conductance of the drain bed material was calculated by the DRN Package to be 3,600 m^2/d with a drain width and length of 60 m and drain bed hydraulic conductivity set to 1 m/d for each DRN cell.

Groundwater Model Calibration Approach

Model calibration is the process of estimating model parameters to minimize the differences, or residuals, between model outputs and hydraulic observations (calibration targets). Model calibration uses a process called history matching, which is an iterative process of matching calibration targets to model-simulated values at a defined period (stress period). The difference between a calibration target and model-simulated value, or the "residual," is calculated for the calibration targets. History matching is completed by attempting to reduce the sum of squared residuals for all calibration targets.

Model calibration was completed, using the Parameter ESTimation (PEST) software package, by completing a single model simulation using a user-defined set of model input parameters and comparing model outputs to the calibration dataset (Doherty, 2004, 2015). Subsequent model runs were completed with small changes in model input parameters, and the model outputs again were compared to the calibration dataset. PEST mathematically determined which input parameters to adjust to provide a better match between the model outputs and the calibration dataset. PEST continued the process until the optimal set of model input parameters was obtained, which provided the statistically best comparison of model outputs and the calibration dataset. In this study, the singular value decomposition method was used within PEST, which allowed the model to find the improved fit to observations among many parameters by suppressing variability of insensitive parameters during the regression process (Doherty and Hunt, 2010).

Calibration Targets

Calibration targets used for steady-state and transient model calibration were derived from daily water table elevation measurements (water levels) obtained from USGS National Water Information System water level data and equally weighted (U.S. Geological Survey, 2018). Calibration targets for the steady-state groundwater flow model were created for mean conditions for the month of November 2015 using published field measurements and daily values of water level at 11 USGS monitoring wells from November 1 to November 30, 2015 (table 1, fig. 3). The transient model was calibrated using daily observations of water level at 10 USGS monitoring wells during the transient calibration period, from October 1, 2016, to August 31, 2018 (table 1, fig. 3). Daily values were determined from continuous measurements made by pressure sensors. Water levels were determined by subtracting the depth of the water table from the USGS National Water Information System well elevation (U.S. Geological Survey, 2018). Targets may differ from recently published values in the USGS National Water Information System because of an update of station elevations that occurred after calibration of the steady-state model and from adjustments made to accommodate land surface elevation values for the model grid. Each calibration target for water level was assigned to model layer 2 based on the well depth and to a model cell-based well location (table 1). Calibration targets are listed in an accompanying data release (Ha and Haj, 2021).

Calibration Parameters

Parameters adjusted during model calibration were horizontal hydraulic conductivity, vertical hydraulic conductivity, a recharge multiplier, and an evapotranspiration multiplier. Horizontal and vertical hydraulic conductivity were estimated for zones in the model area. Recharge and evapotranspiration multipliers were applied to the recharge and evaporation matrices of the model.

Horizontal and Vertical Hydraulic Conductivity

Horizontal and vertical hydraulic conductivity were calibrated for zones of the steady-state and transient models. Each zone was assigned an initial value of horizontal and vertical hydraulic conductivity, specific storage, and specific yield values determined from previously published studies (table 6; Schulmeyer, 1995; Schulmeyer and Schnoebelen, 1998; Turco and Buchmiller, 2004; Gannon and others, 2011). The upper parameter bound applied during calibration was the maximum value reported in the literature plus 20 percent; the lower parameter bound applied during model calibration was the minimum value reported minus 20 percent. (table 6; Schulmeyer, 1995; Schulmeyer and Schnoebelen, 1998; Turco and Buchmiller, 2004; Gannon and others, 2011).

Recharge and Evapotranspiration

The estimates of recharge and evapotranspiration were adjusted individually during the calibration process for the steady-state model using recharge and evapotranspiration multipliers; these parameters were not calibrated during transient model calibration. Estimates of recharge from the water budget were used to define the upper and lower limits of recharge applied to the model during calibration (table 4).

Numerical Model Calibration Results

Calibration results, including optimal parameter estimates, a comparison of calibration targets to model-simulated values, and a parameter sensitivity analysis, are described in this section. Optimal parameter estimates for zone horizontal and vertical hydraulic conductivity, recharge, and evapotranspiration multipliers compared well with literature values (table 6). Optimal parameter estimates were evaluated by comparing model-simulated values to calibration targets. Model-simulated potentiometric surfaces, groundwater flow directions, and groundwater budgets also were also described. Secondary assessments of model performance also included a qualitative assessment of model-simulated groundwater and surface-water interactions and the ability of the model to adequately simulate groundwater withdrawal. A model parameter sensitivity analysis was completed and used to indicate which parameters had the greatest effect on model outputs. The parameter sensitivity analysis was completed using PEST.

Optimal Parameter Estimates

In general, the steady-state and transient model calibration resulted in few changes in parameter values. Calibrated values that resulted from the steady-state calibration for recharge and evapotranspiration were similar to initial estimates. A small adjustment was made to recharge estimates with an optimal value of 0.00008 m^3/d, nearly zero; no further adjustments were made to recharge inputs (table 4) during transient model calibration. Only small changes were made to evapotranspiration values, from 0.0027 to 0.0023 m/d during steady-state calibration. The optimization change was considered small and a validation of the initial evapotranspiration input estimates from the PET data, and no further adjustments were made to evapotranspiration inputs (table 5) for transient model calibration.

Calibrated parameter values for zone hydraulic conductivity were similar to initial values, with steady-state calibrated hydraulic conductivity values for zones 3 (medium to coarse alluvial sand and gravel) and 14 (unweathered bedrock) changed from initial values of 117.35 and 5.0 m/d to calibrated values of 176.02 and 10 m/d, respectively (table 6). Calibrated values were reasonable and compared well to previously published value ranges.

Comparison of Simulated and Observed Water Table Elevations

Model performance was assessed primarily on the ability of the model to match the calibration targets (water table elevation) for all calibration stress periods at six monitoring wells: CRM–4a, CRM–18, GPW–1, GPW–2, GPW–3, and GPW–4. Daily simulated water table elevations were compared to calibration targets using statistical tests, time series plots for select target locations, and water table maps for select stress periods.

Statistical Tests of Simulated Water Table Elevations

Statistical tests were used to assess the numerical model-simulated water table elevation during the model calibration period, for October 1, 2016, through August 31, 2018, and for October 17, 2017, through February 28, 2018. The percentage bias (*PBIAS*), root mean square error to observation standard deviation ratio (*RSR*), Nash-Sutcliffe efficiency (*NSE*), and coefficient of determination (R^2) statistics (Nash and Sutcliffe, 1970; Singh and others, 2004; Moriasi and others, 2007) were used to evaluate model performance.

The *PBIAS* measures the tendency of the simulated data to be larger or smaller than their observed counterparts (Gupta and others, 1999). A *PBIAS* value of 0.00 indicates ideal performance, whereas positive values indicate underestimation bias and negative values indicate overestimation bias (Moriasi and others, 2007). For hydrologic models, a simulation is considered “very good” if the *PBIAS* is between

0 and plus or minus (±) 10 percent, "good" if the *PBIAS* is between ±10 and ±15 percent, "satisfactory" if the *PBIAS* is between ±15 and ±25 percent, and "unsatisfactory" if the *PBIAS* is ±25 percent or greater (Moriasi and others, 2007). Model simulations of water table elevations were less than the observed value, except at GPW–2, where water table elevation is overpredicted (table 7). This may be due to the proximity of the well to RCW–1's depression of the water table during the simulation. The *PBIAS* values indicate the model predicted water table elevation is rated as good or satisfactory, except at GPW–4 (−30 percent) and CRM–4a (−70 percent). The higher *PBIAS* values for GPW–4 and CRM–4a may be explained by more variability in water table elevation because of their proximity to HCW4 and HCW1, both highly productive wells that cause more pronounced local depression of the water table.

The *RSR* was developed to use the standard deviation of the difference in simulated and observed water to define a low root mean square error for model performance (Singh and others, 2004). The *RSR* incorporates the benefits of error index statistics and includes a normalization/scaling factor. The *RSR* ranges from 0, which is an optimal value, to a large positive value, which means a poor fit (Singh and others, 2004). Model performance is considered "very good" if the *RSR* is between 0 and 0.5, "good" if the *RSR* is between 0.5 and 0.6, "satisfactory" if the *RSR* is between 0.6 and 0.7, and "unsatisfactory" if the *RSR* is greater than 0.7 (Moriasi and others, 2007). The *RSR* values for the model ranged from 0.58 to 3.06 at monitoring wells, with all but one (GPW–4 from October 17, 2017, to February 28, 2018) rated as unsatisfactory with the best performance at GPW–3 and GPW–4 (from October 17, 2017, to February 28, 2018). This was not an unexpected result because of the small-time step of the model simulation, unmodeled stage changes in the Cedar River, and assumptions in the vertical well production rates.

The *NSE* is a normalized statistic that provides a measure of how well simulated values match measured datasets. The *NSE* values range from −∞ to 1. A value of less than 0 indicates that the mean measured value is a better predictor than the simulated value, a value of 0.00 indicates the simulated value is as good as using the mean value of all the measured data, and a value of 1 indicates a perfect fit between measured and simulated values (Moriasi and others, 2007). The *NSE* values for all but one monitoring well (CRM–18) were less than 0, which indicated that the mean measured values at each well were better predictors than simulated values (table 7). The *NSE* values for the model ranged from −8.42 to 0.65 and indicated that the mean measured value of the water table elevation was generally a better predictor of observed water table values than simulated values. The best model performance was at GPW–3 and GPW–4 from October 17, 2017, to February 28, 2018, with values of 0.39 and 0.65, respectively.

The R^2 evaluates the accuracy that the simulated model results reflect the variability in the measured data that is explained by the simulated output. The R^2 can reveal the strength of the linear relation between the predicted and the measured values and ranges from 0 to 1. Values approaching 1 indicate a linear correlation between simulated and measured values (Kalin and Hantush, 2006). For hydrologic modeling, values greater than 0.5 are considered satisfactory (Gassman and others, 2007). The R^2 values at the monitoring wells ranged from 0.65 to 0.72 with the model rated as satisfactory at GPW–3 and GPW–4 from October 17, 2017, to February 28, 2018. The increased performance of the model in the areas of GPW–3 and GPW–4 was likely due to the model being less affected by stage changes in the Cedar River and vertical well production rates in these areas.

Graphical Comparison of Simulated and Observed Water Table Elevations

Simulated water table elevations were compared to values at 6 of the 10 calibration target locations for the Cedar River alluvial aquifer. All observed and modeled values for

Table 7. Statistical comparison of simulated and observed water table elevations for October 1, 2016, through August 31, 2018.

[m, meter; obs, observations; *PBIAS*, percentage bias; *RSR*, ratio of the root mean square error to the standard deviation of the observations; *NSE*, Nash-Sutcliffe efficiency; R^2, coefficient of determination; *, values calculated from October 17, 2017, to February 28, 2018]

Statistic	CRM–4a	CRM–18	GPW–1	GPW–2	GPW–3	GPW–4
Residual mean, m	1.07	−0.78	These areas	−0.82	1.02	0.32
Range in obs, m	1.34	1.71	1.92	3.21	1.05	1.86
PBIAS	−0.70	0.00	−0.10	0.20	−0.10	−0.30
RSR	3.06	0.85	1.05	1.05	1.12	1.56
NSE	−8.42	0.27	−0.10	−0.10	−0.25	−1.45
R^2	0.02	0.28	0.00	0.02	0.11	0.12
*PBIAS**	−0.60	0.30	0.40	0.50	0.10	0.00
*RSR**	2.96	1.85	1.91	1.59	0.77	0.58
*NSE**	−8.06	−2.53	−2.76	−1.61	0.39	0.65
R^2*	0.16	0.08	0.01	0.15	0.65	0.72

water level were plotted and compared to a 1:1 perfect-fit line (fig. 18) to evaluate the overall simulation-to-observation performance. Plots indicate little to no correlation; however, this relation may be a result of the large residual value as compared to the range in values for calibration targets; for example, the residual mean at CRM–4a is 1.07 m, and the range in observations is 1.34 m (table 7). Time series plots were created for further evaluation of modeled and observed water level comparison (fig. 19). Generally, modeled values do not capture the fluctuations in elevation observed for the calibration period and may further explain the little to no correlation of modeled and observed values illustrated in figure 18. Changes in the simulated water level at all targets do reflect the general seasonal trends in water level change in the observed data. This is likely due to seasonal changes in pumping demand or variability in stage of the Cedar River (not simulated by the model).

In October 2017, a USGS streamgage was installed at Edgewood Road (fig. 1) that measured stream stage (elevation) and allowed for the direct comparison of simulated and observed water level values with stream stage near the calibration targets. Increases in stream stage correlated with increases in water level in the calibration target data. These changes are not reflected in model-simulated water level because of the boundary conditions of the model—modeled stream stage was held constant at a minimum value; therefore, evaluating simulated groundwater elevation changes during these periods of stage variability is not appropriate. Alternatively, the stage of the Cedar River from October 19, 2017, to February 28, 2018, was relatively constant and low (fig. 19). During that part of the calibration period, the model seems to better predict changes in water level and, at some targets, elevation values (fig. 19, GPW–1 and GPW–4). Statistical comparison of most (all but CRM–18) of the modeled and observed water level data from October 19, 2017, to February 28, 2018, indicated improved correlation (table 7; fig. 18).

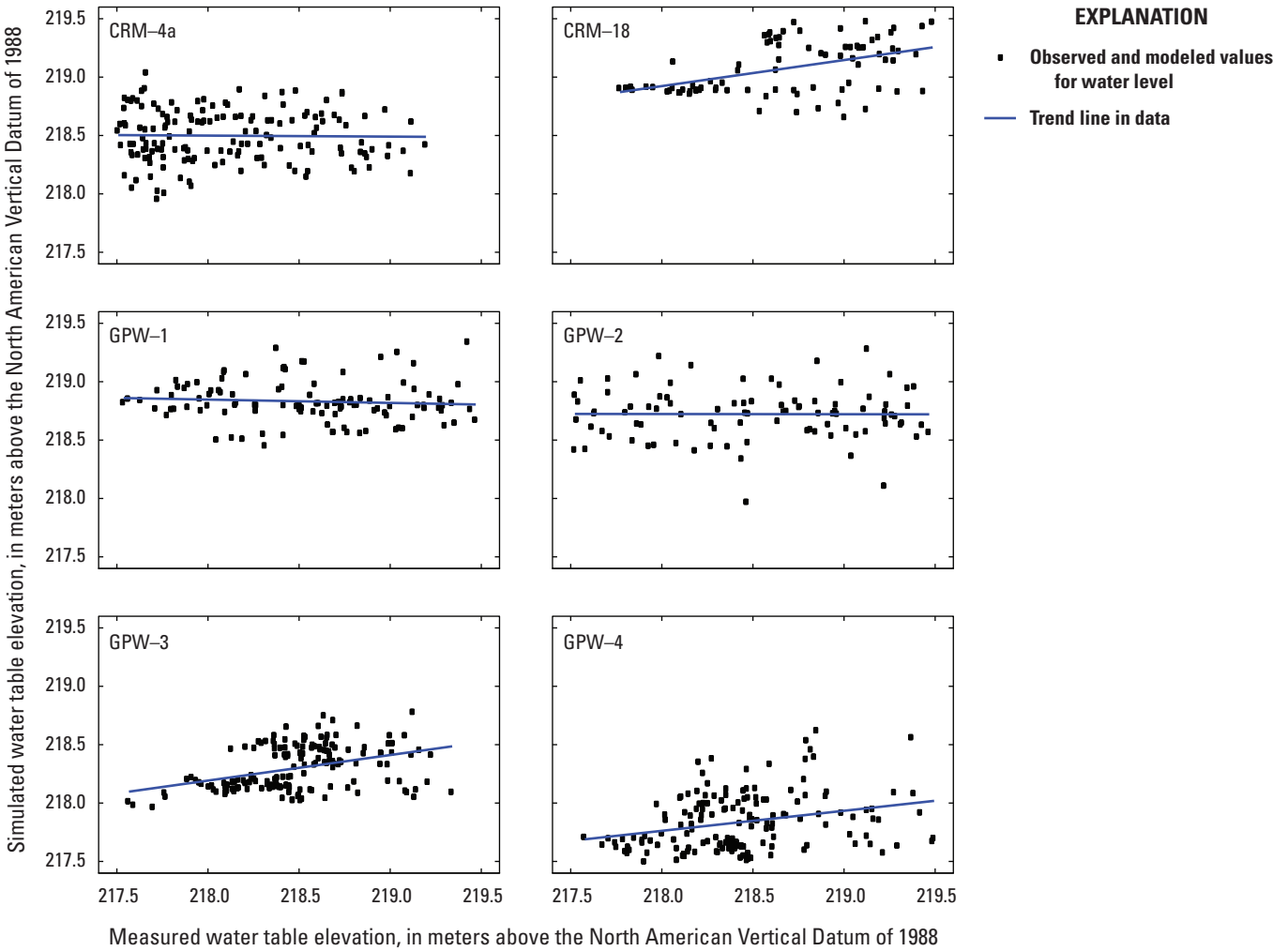

Figure 18. Model-simulated versus observed water level values at calibration targets from October 19, 2017, to February 28, 2018.

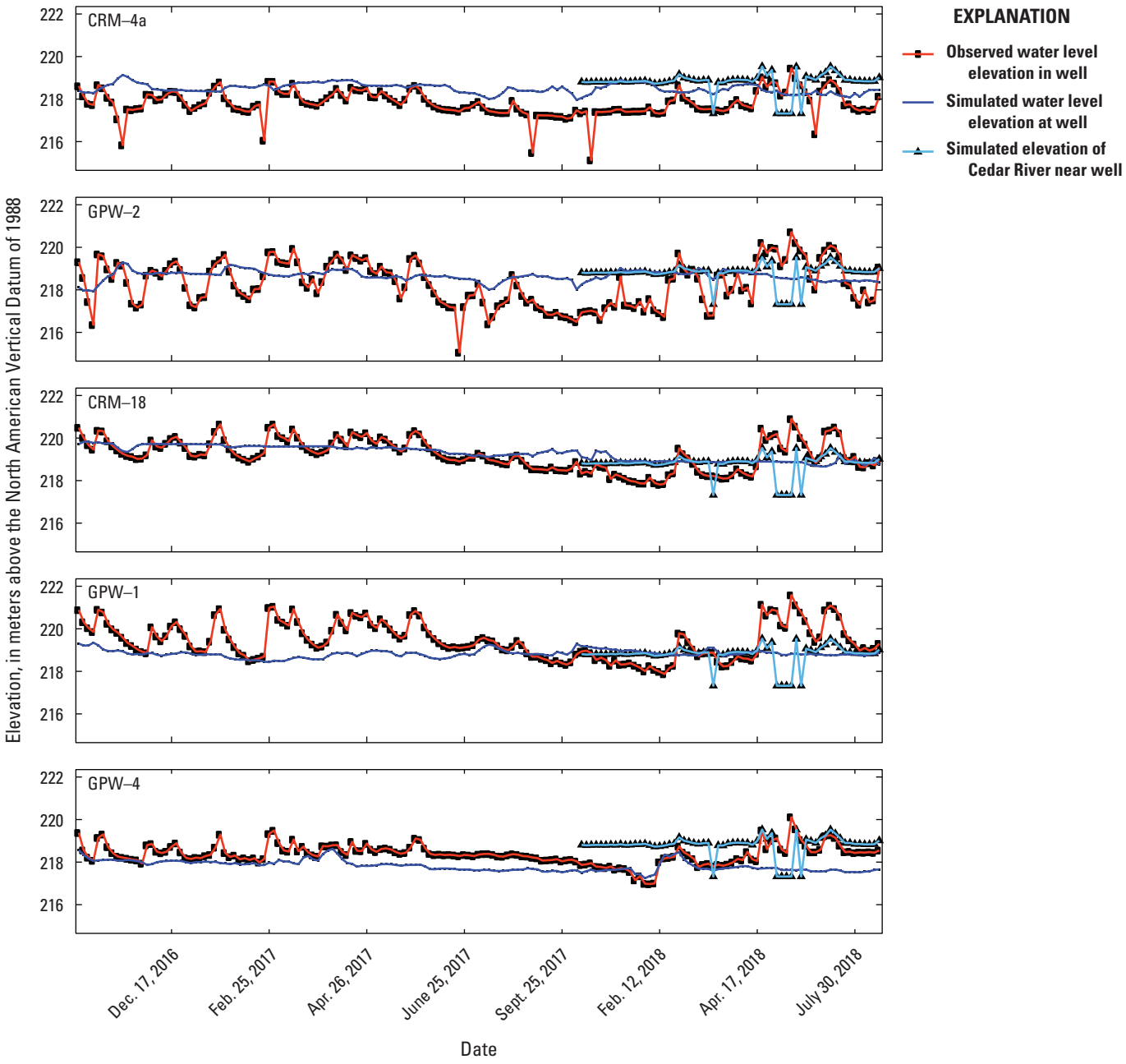

Figure 19. Model-simulated versus observed water level values at calibration targets compared to elevation of the Cedar River for the calibration period, from October 1, 2016, to August 31, 2018.

Spatial Comparison of Simulated Water Table Elevations for Selected Stress Periods

The positive and negative mean residuals, the mean difference of observed and simulated values for water level during the calibration period, were mapped in the model area for examination of spatial bias. Residuals for the calibration period are evenly distributed spatially in the model area with a potential bias for lower than observed water levels at a distance from HCWs (fig. 20). Residuals for October 19, 2017, to February 28, 2018, demonstrate an even distribution of positive and negative mean residuals and indicate that the model results are not spatially biased (fig. 21).

Simulated Groundwater Budget

Simulated groundwater budgets were calculated using Zone Budget, version 3.01—a software that characterizes inflows and outflows from MODFLOW output files (Harbaugh, 1990). Budgets were calculated for the 14 model zones in the 7 model layers and included groundwater fluxes

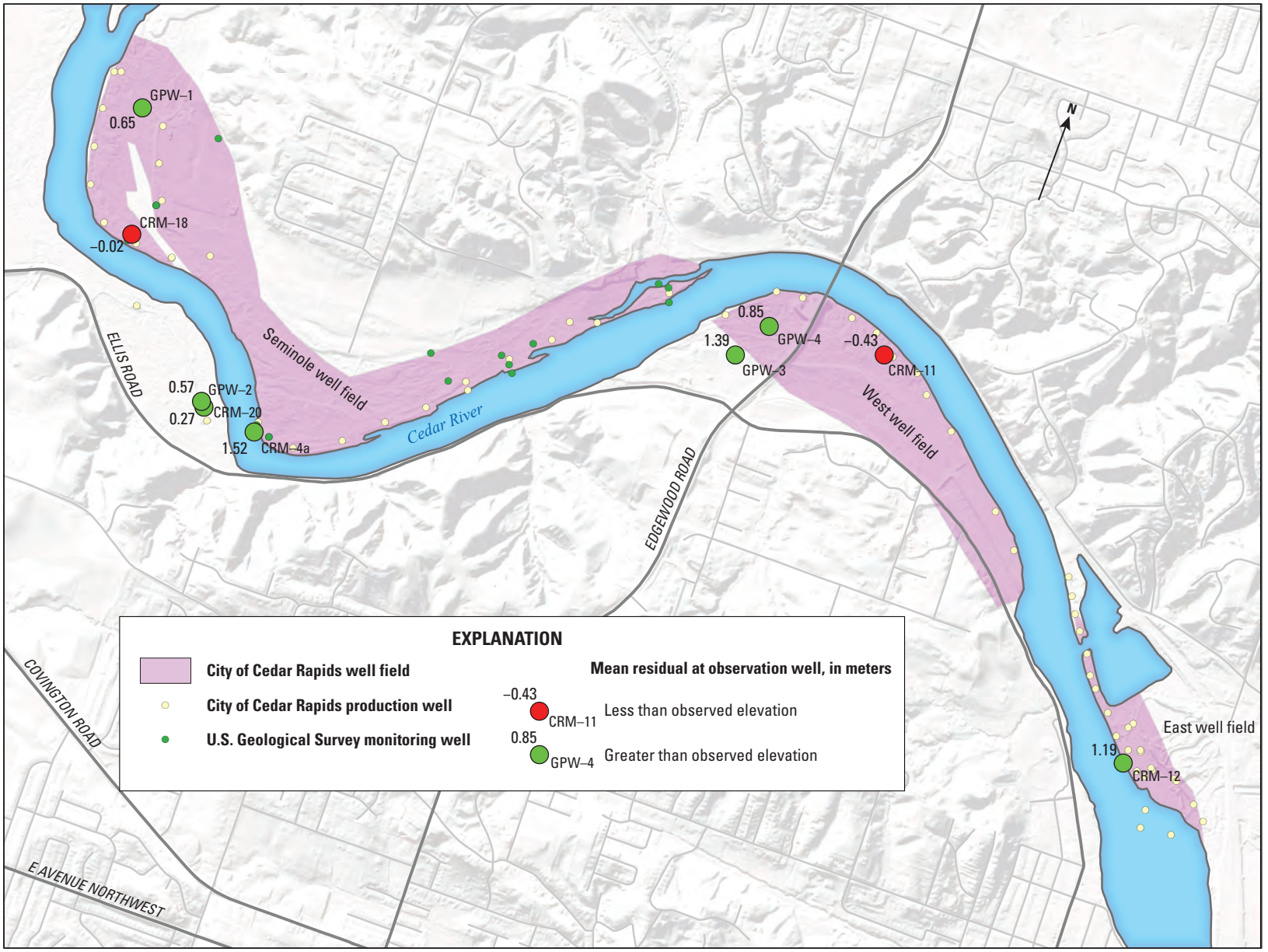

Figure 20. Spatial distribution of mean residuals for model-simulated water level values at calibration targets for the calibration period, from October 1, 2016, to August 31, 2018.

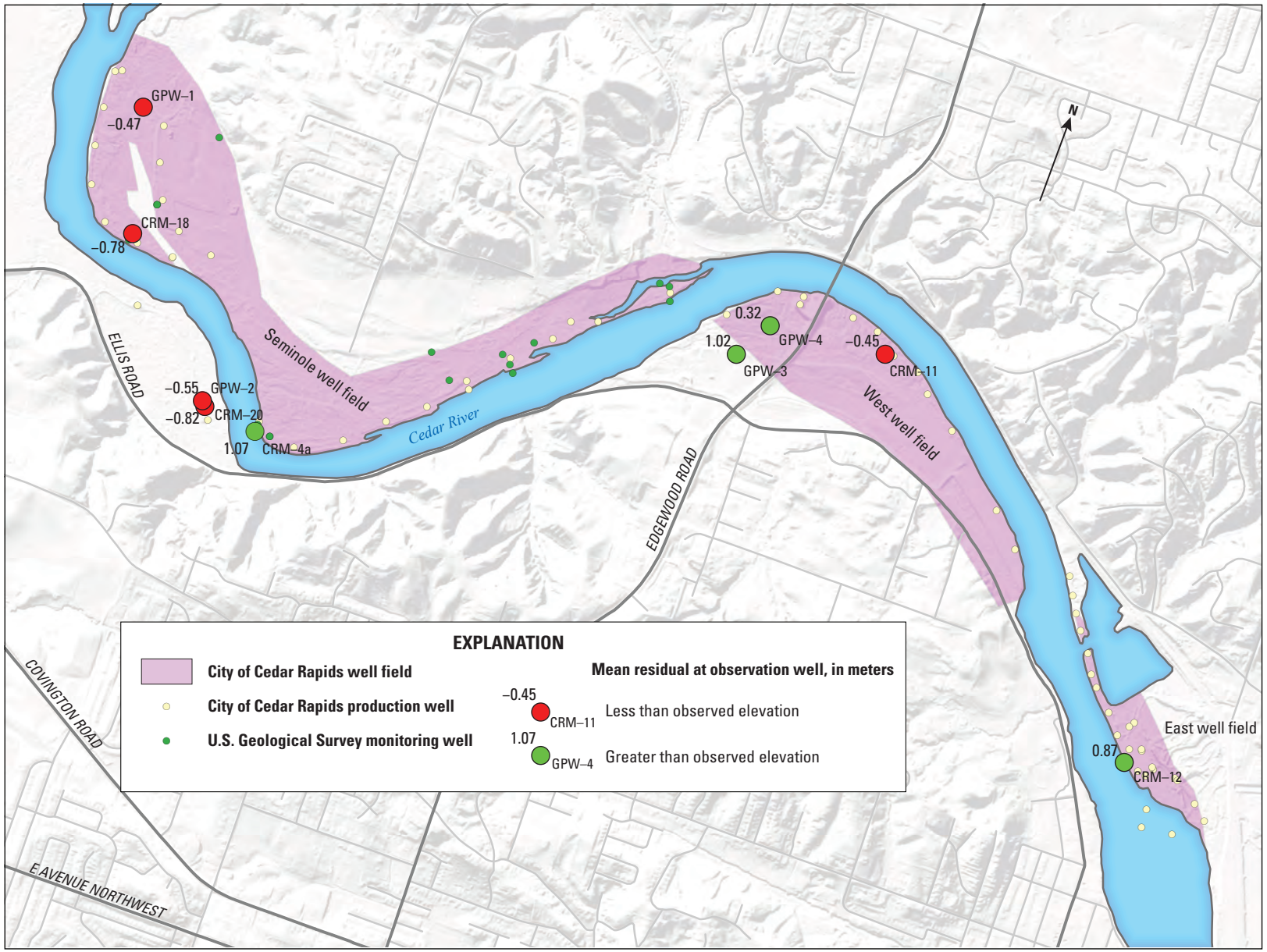

Figure 21. Spatial distribution of mean residuals for model-simulated water level values at calibrated target locations from October 19, 2017, to February 28, 2018.

between each zone, groundwater withdrawals, recharge, evapotranspiration, and inflow from and outflow to storage and stream channel seepage. Zone budgets were calculated for the steady-state model and for all stress periods of the transient model and are available in an accompanying data release (Ha and Haj, 2021). The zone budget for the steady-state model and six selected stress periods of the transient model were used to create a groundwater budget for hydrogeologic units, hereafter referred to as "groundwater budget." The six selected transient stress periods represented periods of high aquifer stress having low water levels in monitoring wells and sustained pumping stresses (B. Jacobs, City of Cedar Rapids, written commun., 2019).

Several factors were considered when evaluating the groundwater budget. The general assumption was that the alluvial sediment unit is analogous to the Cedar River alluvial aquifer. Although most of the Cedar River alluvial aquifer is composed of model cells that were assigned a unit value of alluvial sediment, some areas of the aquifer include model cells that were assigned other unit values. For example, in areas of the model where eolian sediment overlies alluvial sediment, cells in layer 1 of the model were given a unit value of eolian sediment. Alternatively, in parts of the model area, alluvial sediment was deposited in tributary valleys far from the Cedar River valley. In those areas, cells in layer 1 of the model were given a unit value of alluvial sediment but overlie cells with unit values of weathered glacial till, unweathered glacial till, or weathered bedrock. Although these factors may have affected groundwater budget values to a small degree, the assumption that the alluvial sediment unit is analogous to the Cedar River alluvial aquifer is useful for general evaluation of the groundwater budget.

The simulated transient groundwater budget for stress period 101 (September 26 to October 2, 2017) occurred during a time of consistent low stage (or low-flow conditions) of the Cedar River, and indicated that about 151,120 m^3/d, or about 39.9 million gallons per day, was pumped from the aquifer for municipal use (fig. 22). During the time, no recharge occurred, and the aquifer lost 14,063 m^3/d because of evapotranspiration. The Cedar River is generally a gaining stream in the model area (Turco and Buchmiller, 2004), and groundwater from adjacent and underlying units flows into the aquifer as well, with contributions from eolian sediment (inflow = 2,475 m^3/d), unweathered glacial till (inflow = 17,836 m^3/d), and weathered bedrock (inflow = 114,216 m^3/d) units. In contrast, the groundwater budget indicated that the Cedar River contributes 40,040 m^3/d to the aquifer during this time, likely from induced recharge (or stream capture) from pumping wells near the stream channel. Also, storage depletion in the aquifer was 18,446 m^3/d. The remaining two outflows from the alluvial sediment unit were 2,688 m^3/d to weathered glacial till and 25,139 m^3/d to drains, which likely occurred in parts of the model area where alluvial sediment in tributary valleys overlies weathered glacial till. The water budget for stress period 101 indicates that groundwater-surface-water interaction was altered near the Cedar Rapids well fields because of pumping stresses, but this relation is better demonstrated in a comparison of groundwater budgets from multiple stress periods.

The groundwater budgets for the steady-state model and six transient stress periods (stress periods 4, 34, 79, 101, 153, and 161) were compared using the contribution of inflow to the alluvial sediment zone (table 8). These stress periods all occurred during, and were preceded by, a time of prolonged low flow (stage) on the Cedar River, had variable pumping stresses from the municipal aquifer, and were distributed throughout the length of the calibration period. These data indicated that when pumping rate increased, there was a direct and proportional increase in stream seepage into the alluvial aquifer. This relation was more apparent when groundwater budget fluxes were evaluated as a percentage of total inflow to the alluvial aquifer (table 9) and then compared to pumping rates, also as a percentage of inflow (fig. 23). As shown in figure 23, as pumping rate increased, river seepage into the alluvial aquifer increased proportionally, whereas other fluxes decreased. The increased river seepage is interpreted as increased seepage from the river near the municipal well fields (stream capture) because of increased pumping stress.

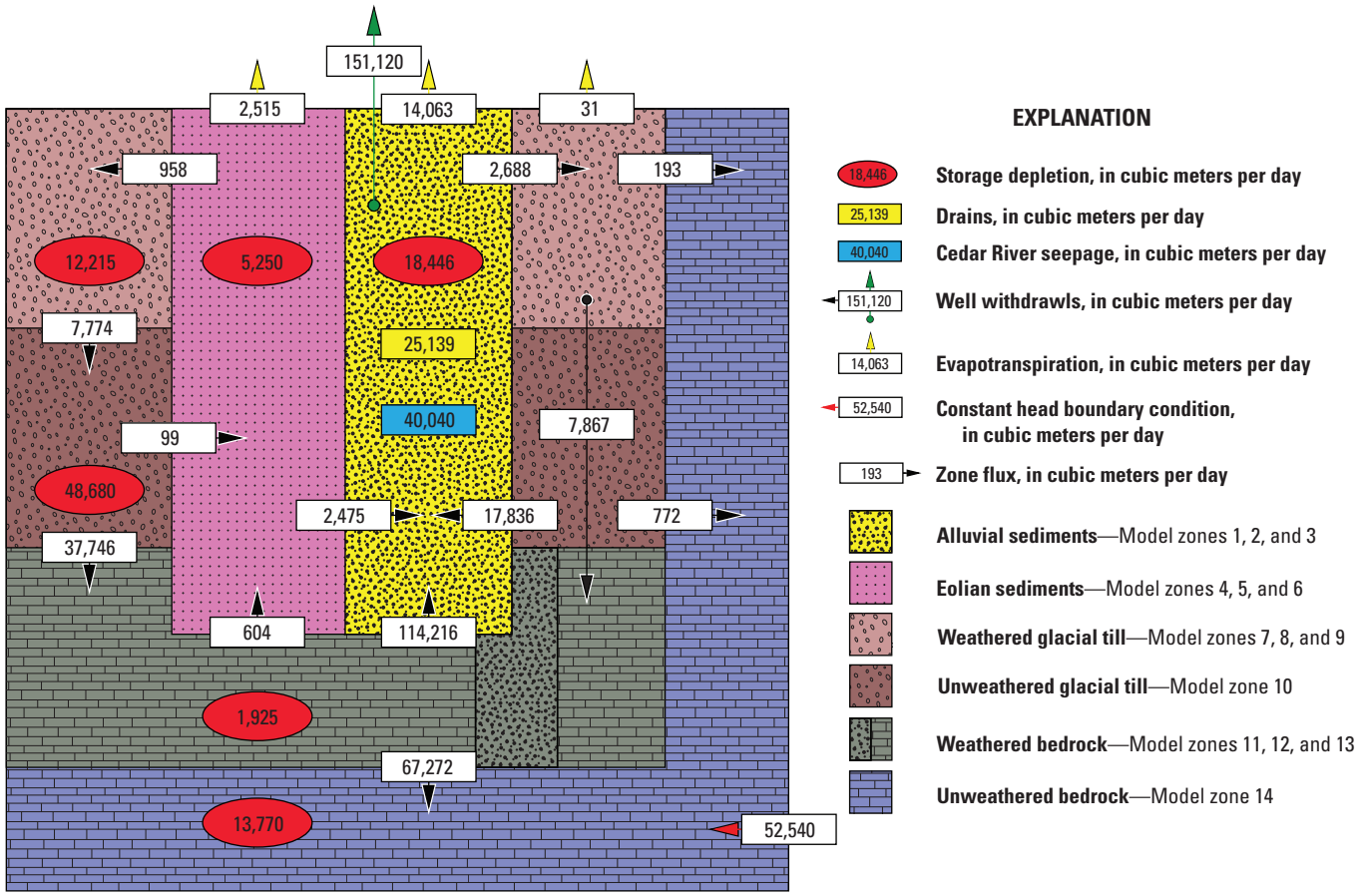

Figure 22. Groundwater budget for transient simulation stress period 101 (September 26 to October 2, 2017).

Table 8. Groundwater budget fluxes for steady state and six selected stress periods.

[m^3/d, cubic meter per day; SP4, stress period 4; SP34, stress period 34; SP79, stress period 79; SP101, stress period 101; SP153, stress period 153; SP161, stress period 161; --, no data; const., constant; ET, evapotranspiration]

Component	Steady-state model, m^3/d	Transient model stress period					
		SP4	SP34	SP79	SP101	SP153	SP161
		Contribution of inflow to alluvium zone, m^3/d					
Zone flux							
Eolian	22,458	13,133	5,559	3,715	2,475	1,513	269
Weathered till	2,585	−1,792	−2,609	−2,561	−2,688	−2,796	−2,783
Unweathered till	30,639	33,348	24,821	20,563	17,836	15,140	14,188
Weathered rock	208,242	208,741	155,661	130,478	114,216	100,001	93,488
Unweathered rock	0	0	0	0	0	0	0
Inflow							
Storage	--	63,513	46,508	39,877	23,631	20,704	15,741
Const. head inflow	0	0	0	0	0	0	0
River seepage (gain)	104,060	101,550	112,440	155,030	151,500	174,310	178,570
Recharge	57,542	0	0	0	0	0	0
Outflow							
Storage	--	8,431	1,409	6,067	5,185	2,167	7,412
Const. head	0	0	0	0	0	0	0
Wells	133,240	136,720	132,740	175,540	151,120	178,060	165,460
Drains	99,827	68,906	50,235	32,370	25,139	16,506	15,300
River seepage (loss)	148,650	188,250	142,590	118,810	111460	98,812	98,000
ET	43,816	16,173	15,407	14,319	14,,063	13,335	13,296
Inflow total	425,526	418,493	342,380	347,102	306,970	308,872	299,473

Table 9. Groundwater budget fluxes for steady state and six selected stress periods as percentages of alluvial sediment unit inflow.

[SP4, stress period 4; SP34, stress period 34; SP79, stress period 79; SP101, stress period 101; SP153, stress period 153; SP161, stress period 161; --, no data; const., constant; ET, evapotranspiration]

Component	Steady-state model	Transient model stress period					
		SP4	SP34	SP79	SP101	SP153	SP161
	Contribution to alluvium zone, percent of total inflow						
Zone flux							
Eolian	5	3	2	1	1	0	0
Weathered till	1	0	−1	−1	−1	−1	−1
Unweathered till	7	8	7	6	6	5	5
Weathered rock	49	50	45	38	37	32	31
Unweathered rock	0	0	0	0	0	0	0
Inflow							
Storage	--	15	14	11	8	7	5
Const. head inflow	0	0	0	0	0	0	0
River seepage (gain)	24	24	33	45	49	56	60
Recharge	14	0	0	0	0	0	0
Outflow							
Storage	--	2	0	2	2	1	2
Const. head	0	0	0	0	0	0	0
Wells	31	33	39	51	49	58	55
Drains	23	16	15	9	8	5	5
River seepage (loss)	35	45	42	34	36	32	33
ET	10	4	4	4	5	4	4

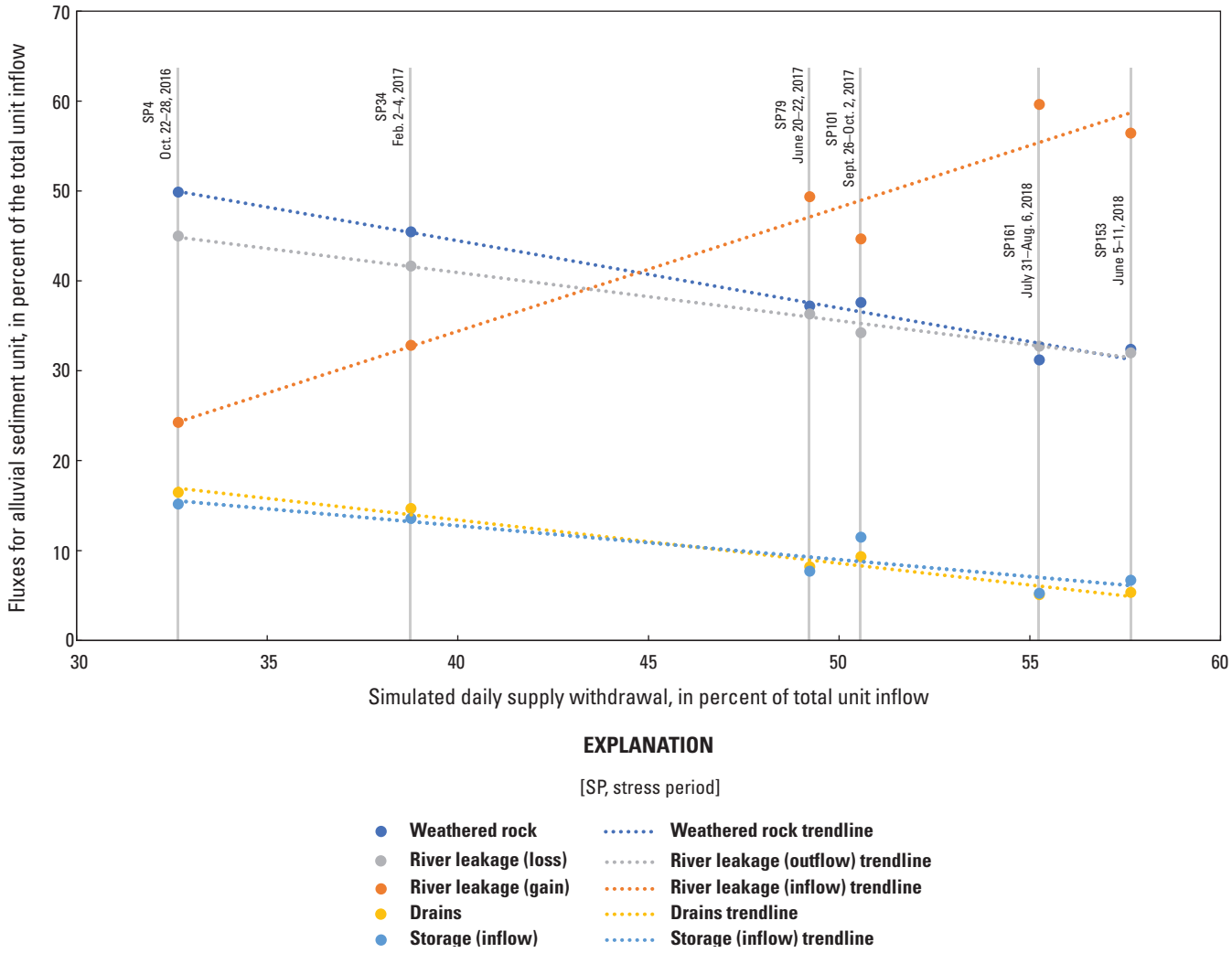

Figure 23. Graphical comparison of groundwater budget fluxes for six selected stress periods as percentages of alluvial sediment unit inflow.

Groundwater Flow Results for the 2012 Drought Period

The groundwater model was primarily assessed by its ability to replicate the low water levels observed in the HCWs and monitoring wells during the 2012 drought period. Additionally, groundwater flow directions and hydraulic gradients interpreted from potentiometric surfaces were interpreted in context of the conceptual model. Although few water level observations exist from this period, measurements at two observations wells, CRM–3a and CRM–4a, were available for multiple model-simulated stress periods (table 10), and measurements from multiple monitoring wells and production wells were available for one stress period (table 11) and allowed for the comparison and evaluation of the transient model over a time series.

Comparison of Simulated Potentiometric Surfaces

Measurements of water level were made at six monitoring wells from December 3 to December 5, 2012 (stress period 58), a time during the 2012 drought when extremely low water levels were observed in the HCWs (tables 10 and 11, fig. 2).The simulated water table surface for the Cedar River alluvial aquifer (model layer 2) for December 5, 2012 (end of stress period 58), was mapped from simulated elevation values for each cell in layer 2 (fig. 24). The simulated water table surface indicates a depression near the HCWs of 1 to 2 m and near the vertical well fields, and groundwater flows from the aquifer and river toward the municipal wells (fig. 24). The simulated water levels at the monitoring well and HCW locations were generally overestimated compared to measured values (TR_simA and wl_obs, table 11).

Table 10. Comparison of simulated water level to available water table measurements made during the 2012 drought.

[TR_simA, transient model simulation A; TR_simB, transient model simulation B; wl_obs, water level observations; SP3, stress period 3; SP14, stress period 14; SP29, stress period 29; SP34, stress period 34; SP44, stress period 44; SP58, stress period 58; SP60, stress period 60; SP70, stress period 70; --, no data]

Monitoring wells	Stress period number with beginning and ending dates, water level values in meters shown are TR_simA/TR_simB/wl_obs							
	SP3	SP14	SP29	SP34	SP44	SP58	SP60	SP70
	Oct. 29–Nov. 7, 2011	Mar. 13–15, 2012	June 14–16, 2012	July 9–11, 2012	Sept. 3–5, 2012	Dec. 3–5, 2012	Dec. 11–13, 2012	Apr. 7–9, 2013
CRM–10	--	--	--	--	--	218.76/ 213.55/ 217.92	--	--
CRM–18	--	--	--	--	--	218.20/ 212.73/ 214.33	218.18/ 212.47/ 214.33	--
CRM–20	--	--	--	--	--	215.02/ 212.83/ 208.26	--	219.25/ 213.97/ 219.12
CRM–26	--	--	--	--	--	218.00/ 211.61/ 215.80	--	--
CRM–3a	218.64/ 216.90/ 218.62	218.13/ 214.35/ 217.92	--	--	--	218.51/ 213.13/ 212.08	--	--
CRM–4a	--	--	218.01/ 213.52/ 219.27	217.97/ 213.35/ 218.94	218.02/ 212.56/ 216.68	218.51/ 213.13/ 212.35	--	--
CRM–6a	--	--	--	--	--	218.96/ 214.19/ 212.56	--	219.13/ 214.27/ 218.98

Table 11. Comparison of simulated water levels to observed water levels in monitoring and production wells for one model stress period.

[Well map_ID, well map identification; TR_simA, transient model simulation A; TR_simB, transient model simulation B; wl_obs, water level observations]

Well map_ID	Water table elevations in meters for stress period 58 (December 3–5, 2012)		
	TR_simA	TR_simB	wl_obs
CRM–10	218.76	213.55	217.92
CRM–18	218.20	212.73	214.33
CRM–20	215.02	212.83	208.26
CRM–26	218.00	211.61	215.80
CRM–3a	218.51	213.13	212.08
CRM–4a	218.51	213.13	212.35
CRM–6a	218.96	214.19	212.56
HCW1	215.02	212.83	205.58
HCW2	218.82	213.23	210.38
HCW3	215.18	208.40	210.89
HCW4	215.01	206.85	208.30

Modifications of the Numerical Model for Improved Groundwater and Surface-Water Interactions

Seepage is defined as the rate that water exchanges between surface waters and a hydraulically connected aquifer. Seepage rates depend on the hydraulic gradient between the surface water and the aquifer, and the hydraulic conductivity of the geologic materials between the surface water and aquifer, or the streambed materials (Barlow and Leake, 2012). The Cedar River in the model area is characterized as a gaining stream and receives as much as 80 percent of its annual discharge from groundwater contributions (Squillace and others, 1993) Near pumping wells, the elevation of the water table may fall below the elevation of the river because of pumping and create a local reversal of flow direction. In those areas, water moves from the river to the aquifer, referred to as "induced recharge" (or stream capture). Recent studies related to stream capture have indicated that more than 90 percent of seepage occurs within 12 m of the shoreline closest to a pumping well (Rosenberry and Healy, 2012), and low seepage rates are generally associated with low river stage because of low-head gradients (Barlow and Leake, 2012).

During drought conditions in 2012, the Cedar River had low flows and a low stream stage. When low-flow conditions are concurrent with high pumping rates, clogging mechanisms in the streambed, such as fine-grained sediments or biological veneers, cause a decreased seepage rate that can lower the aquifer water level and create an unsaturated zone beneath the streambed (Ulrich and others, 2015). The occurrence of unsaturated conditions beneath the streambed leads to a further decrease in infiltration (seepage) from the river and a lack of recharge to the aquifer. Water level observations from stress period 58 indicate that this phenomenon may have occurred during the 2012 drought and is supported by unpublished seepage data collected in 2014 (G. Littin and D. Rosenberry, U.S. Geological Survey, written commun., 2014).

The transient numerical groundwater flow model was modified to account for a decrease in seepage rate caused by low flow in the Cedar River and increased production. Seepage rates for RIV cells were reduced by a factor of 25 by decreasing hydraulic conductivity of the RIV cells until the conductance value was 25 times less than the initial value. This value is a value recommended by the Rosenberry and Healy (2012) study for settings where a thin, fine-sediment veneer may exert greater effect on seepage rates—although it is noted that larger reductions have been reported in laboratory and natural settings. Streambed sediments are less mobile in the model area, as evidenced by an established riparian corridor. Low-flow conditions exist for long periods of time when the streambed sediments are less mobile, allowing for the deposition of finer grained sediment on the streambed. Also, Cedar Rapids well fields are near an area of the river where flows are affected by the downstream Five in One Dam located beneath the Interstate 380 bridge (fig. 1: Rosenberry and Healy, 2012). The Five in One Dam also creates less turbulent flow conditions where the streambed materials are less mobile. These factors indicate a potential for elevated amounts of fine-grained sediments on the streambed compared to natural systems and that the selected factor of reduction in the seepage rate is a conservative estimate.

A simulation was completed for the 2012 drought using the numerical model with a modified seepage rate, referred to as "transient model simulation B" (TR_simB). The simulated water table surface for the Cedar River alluvial aquifer for December 5, 2012 (end of stress period 58), was created from simulated elevation values for each cell in layer 2 (fig. 25). As with the prior simulation (TR_simA), the water level results

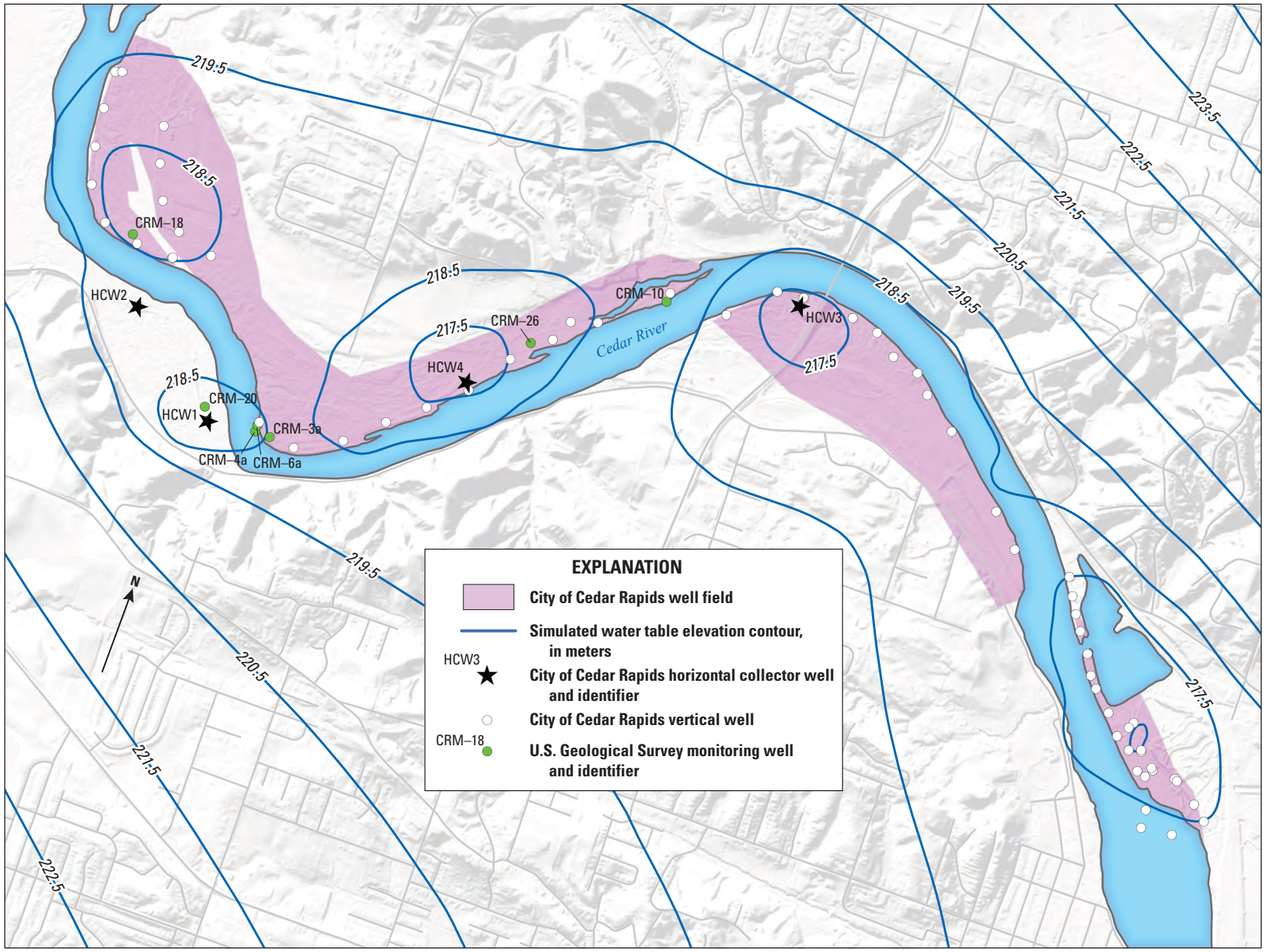

Figure 24. Simulated water level contours for the Cedar River alluvial aquifer.

indicated a depression in the water table near the HCWs of about 2–4 m and a depression of 1–2 m near the vertical well fields. Groundwater flowed from the aquifer and river toward the production wells. The TR_simB simulated water levels for stress period 58 were closer to the observed values in the model area than the TR_simA simulated elevations (figs. 24 and 25; TR_simB and wl_obs, table 11). Results demonstrated the ability of the model to simulate observed water levels in the HCWs and monitoring wells during the 2012 drought when accounting for a decrease in infiltration from the Cedar River. Future model development plans include the creation of transient seepage parameters for the river cells that will allow for transient simulations to transition into and out of drought conditions and better forecast the dynamic effects of drought and increased HCW production in the Cedar River alluvial aquifer.

Model Parameter Sensitivity

Model parameter sensitivity is a measure of the effect that a change in model input, such as various model parameters, has on model outputs, such as observation targets (Doherty, 2004; Doherty and Hunt, 2010). During calibration, PEST modifies MODFLOW-NWT input files by slightly adjusting a single model parameter, then runs the model to generate output files, and compares the result to the model outputs based on the initial parameter dataset. During the calibration process, changes in parameters with the highest sensitivity have the greatest effect on model outputs. Specifically, high-sensitivity parameters have the greatest effect on the model results interpreted at calibration targets used during model calibration. For this study, model calibration was done for steady-state and transient models. During sensitivity analysis with PEST, one can choose the parameter sensitivity run per zone, run the sensitivity analysis, then compare parameter sensitivities (Doherty, 2004; Doherty and Hunt, 2010). Output from multiple sensitivity tests indicated that horizontal hydraulic conductivity for the x-axis and horizontal hydraulic conductivity for the y-axis for zone 3 (medium to coarse alluvial sand and gravel) and zone 14 (unweathered bedrock) and evapotranspiration rate were the most sensitive parameters of all the parameters in the steady-state and transient models. The horizontal hydraulic conductivity values for zones 1, 2, and 4–13 (table 6) and recharge rates were among the least sensitive parameters during the sensitivity analyses. Sensitivities were calculated by PEST for the calibrated model parameters and averaged by parameter group. Parameter values were updated based on the PEST results for those five most sensitive parameters as described previously (horizontal hydraulic conductivity for zones 3 and 14, respectively). The mean model parameter relative sensitivity by parameter group was used in model calibration. All model parameters that were considered not sensitive were not calibrated. All model sensitivity results are provided in Ha and Haj (2021).

Model Simplifications, Assumptions, and Limitations

Groundwater flow models are simplified representations of complex natural systems and are constructed with assumptions that lead to limitations in their use and uncertainty in model results. The inability to characterize processes, properties, and hydrologic outputs in complex numeric groundwater systems can result in a nonuniqueness of the calibration process (Leaf and others, 2013); therefore, different combinations of hydraulic properties that could result in an acceptable comparison of observations and model-simulated values can be applied to a model. The hydraulic properties determined through the model calibration process minimized the difference between observations and model results, and these properties were similar to estimates from previous publications. The final distribution of model parameters determined during model calibration and the resulting water levels were based on the spatial and temporal availability of hydrologic data. Hydrologic data were not available for use in model calibration for some parts of the model area; therefore, the results of the model as determined through the calibration process for those areas could be substantially different when compared to observations.

Model simplifications included spatial and temporal discretization, aquifer conceptualization, boundary condition representation, and calibration of aquifer hydraulic properties. Discretization of the model area into a uniform grid of 120-by-120-m square cells resulted in a simplified representation of land surface topography, geologic contacts, and aquifer properties and created inaccuracies in the total aquifer volume and the location of some aquifer boundaries represented in the model. Aquifer properties were averaged and uniform in each model cell where actual aquifer material could be highly variable. The spatial simplification of hydraulic properties could cause the model to misrepresent the aquifer response to localized stresses, such as additional demands for groundwater withdrawal.

The stream channel was simplified by using uniform 120-m square cells, which caused some inaccuracy in streambank placement and distance from production wells. Surface elevations and streambed elevations for RIV cells in the numerical model were constructed to ensure that a realistic channel depth and downstream and lowland landscape gradients were maintained. Mean stream widths and lengths for RIV cells in the model were interpolated from available imagery of the model area, and a mean value was applied to all cells. Additionally, stage and seepage rates for RIV cells were held constant for simulation of drought conditions, limiting the ability of the model to calibrate to and simulate water level changes caused by changes in stream stage. These stream simplifications caused inaccuracies in the ability of the model to calibrate to all climate scenarios such as abrupt changes in stream stage or flood events. An application of the model to predict absolute water levels for all conditions would require additional data to improve calibration.

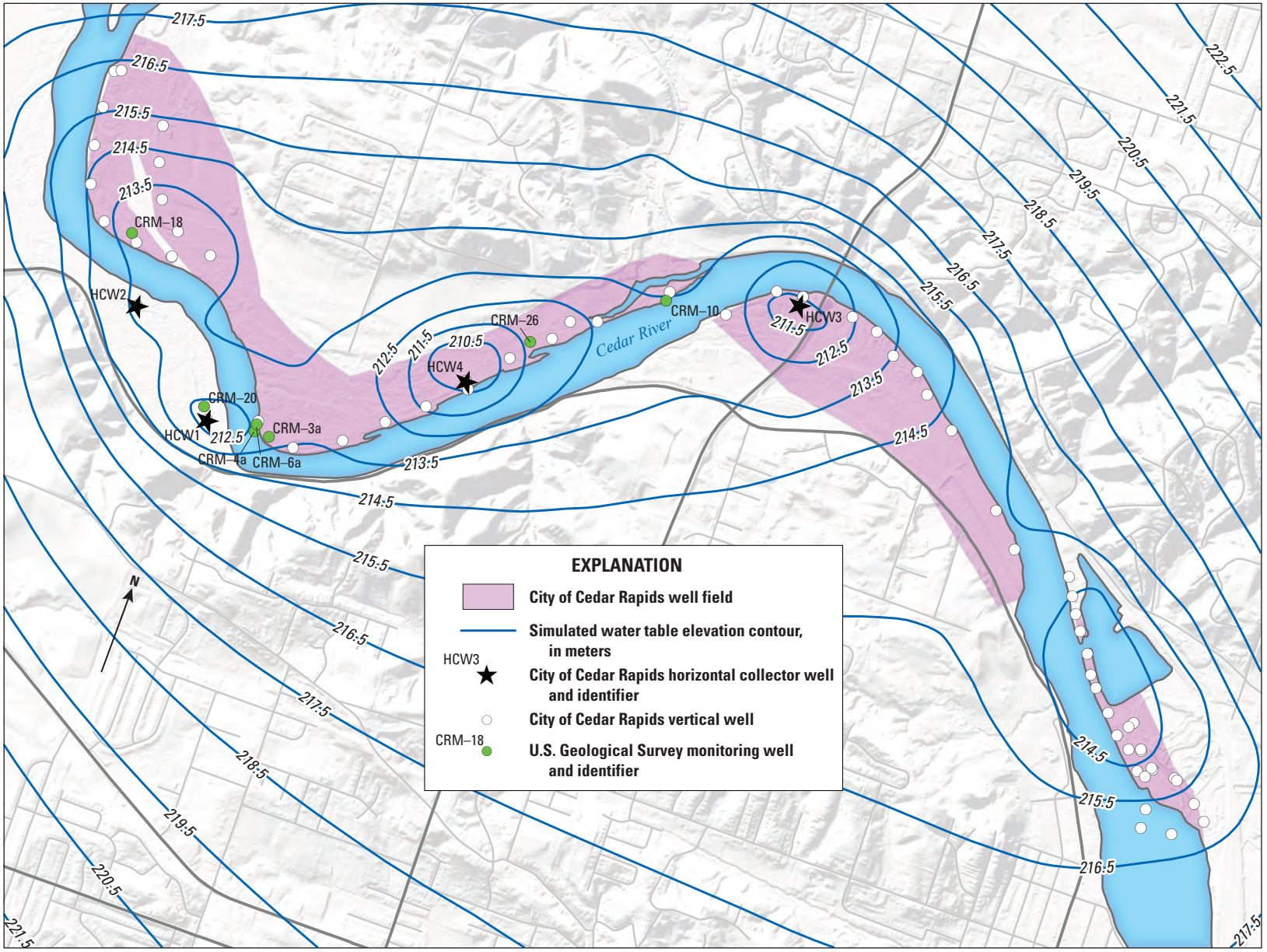

Figure 25. Simulated water level contours for the Cedar River alluvial aquifer with numerical model seepage rate modification.

Model calibration of hydraulic conductivity and storage parameters was simplified into zones to optimize the time required for calibration. Horizontal and vertical hydraulic conductivity are spatially variable in the model area and in each model zone; however, a uniform value for horizontal and vertical hydraulic conductivity was assigned to each zone. This simplification allowed for some heterogeneity in the aquifer materials, but abrupt localized changes in heterogeneity were not well represented. Similarly, uniform values for specific storage and specific yield were used for each zone. Spatially varied values were not used to reduce model calibration time because high-resolution data for specific storage were not available. Although spatial variation in aquifer storage values likely exists in the model area, the variations were assumed to have a minimal effect on model results because of the small model area and the fact that calibrated values were within a reasonable range of estimates from previous studies. Additionally, observations for the determination of calibration targets for drought periods were discontinuous, sparse, and localized, which affected the ability of the model to calibrate hydraulic properties in model layers during drought.

Summary

Between July 2011 and February 2013, the City of Cedar Rapids observed water level declines in their horizontal collector wells approaching 11 meters (36 feet). As a result, pumping from these production wells had to be halted, and questions were raised about the reliability of the alluvial aquifer under future drought conditions. The U.S. Geological Survey, in cooperation with the City of Cedar Rapids, completed a study to better understand the effects of drought stress on the Cedar River alluvial aquifer using a numerical groundwater flow model.

A simple conceptual model was developed for the model area and illustrates the hydrogeologic framework and sources and sinks of groundwater in the model area. In the model area, bedrock and surficial sediments were conceptualized as seven hydrogeologic units: alluvial sediment (including the Cedar River alluvial aquifer), eolian sediment (including windblown sands and silts), residual soils, weathered glacial till, unweathered glacial till, weathered bedrock, and unweathered bedrock. Sources of groundwater recharge include seepage from the stream channel and precipitation. Sources of groundwater loss include evapotranspiration, stream base flow, and withdrawals from vertical and horizontal collector wells.

A hydrogeologic framework (framework) for this study was a three-dimensional model of the hydrogeologic units and subunits for the groundwater flow system. The framework was developed using previously conceptualized hydrogeologic units, the lithostratigraphic model, airborne-electromagnetic survey data, detailed surficial geology and depth to bedrock maps, and hydraulic relations and characteristics published in U.S. Geological Survey reports. The hydrogeologic units included (1) weathered bedrock, (2) unweathered bedrock, (3) weathered glacial till, (4) unweathered glacial till, (5) alluvial sediment, (6) eolian sediment, and (7) residual soils. The framework was used to determine the number of layers, layer thicknesses, and hydrogeologic units and zones ascribed to each cell of the numerical groundwater flow model using MODFLOW-NWT.

Model calibration was completed using the software package PEST. A single model simulation using a user-defined set of model input parameters was completed, and model outputs were compared to calibration targets derived from daily water table measurements obtained from U.S. Geological Survey National Water Information System water level data. Parameters adjusted during model calibration were horizontal hydraulic conductivity for each model zone, vertical hydraulic conductivity for each model zone, a recharge multiplier, and an evapotranspiration multiplier. Calibration results for optimal parameter estimates of horizontal and vertical hydraulic conductivity, recharge, and evapotranspiration multipliers compared well with literature values. Optimal parameter estimates were evaluated by comparing model-simulated values to calibration targets of water level at six monitoring wells. Statistical tests were used to assess the numerical model during the model calibration period, and results varied from satisfactory to unsatisfactory, likely because of stage changes in the Cedar River and vertical well production rates near monitoring wells.

Simulated water levels during the 2012 drought indicated a depression near the horizontal collector wells, although simulated elevations at these locations and at monitoring wells were generally overestimated compared to measured values. The numerical groundwater flow model was modified to account for a decrease in seepage rate caused by low flow in the Cedar River and increased well production. With seepage rate modification, model results improved; the simulated water levels were similar to those observed in horizontal collector and monitoring wells. Results demonstrated the ability of the model to simulate water levels observed in the horizontal collector wells and monitoring wells during the 2012 drought when accounting for a decrease in infiltration from the Cedar River.

References Cited

Advanced Geosciences, Inc., 2009, Instruction manual for EarthImager 2D, versions 2.4.0 and 2.4.4—Resistivity and IP inversion software: Advanced Geosciences, Inc.,134 p., accessed April 2015 at https://www.agiusa.com/agi-earthimager-2d.

Allen, D., Flaum, C., Ramakrishnan, T.S., Bedford, J., Castelijns, K., Fairhurst, D., Gubelin, G., Heaton, N., Minh, C.C., Norville, M.A., Seim, M.R., Pritchard, T., and Ramamoorthy, R., 2000, Trends in NMR logging: Oilfield Review, v. 12, no. 3, art. OIREE70923–1730, 19 p., accessed July 3, 2018, at https://connect.slb.com/~/media/Files/resources/oilfield_review/ors00/aut00/p2_19.pdf.

Barlow, P.M., Cunningham, W.L., Zhai, T., and Gray, M., 2015, U.S. Geological Survey groundwater toolbox, a graphical and mapping interface for analysis of hydrologic data (version 1.0)—User guide for estimation of base flow, runoff, and groundwater recharge from streamflow data: U.S. Geological Survey Techniques and Methods, book 3, chap. B10, 27 p., accessed September 2, 2019, at https://doi.org/10.3133/tm3B10.

Barlow, P.M., and Leake, S.A., 2012, Streamflow depletion by wells—Understanding and managing the effects of groundwater pumping on streamflow: U.S. Geological Survey Circular 1376, 84 p. [Also available at https://doi.org/10.3133/cir1376.]

Behroozmand, A.A., Keating, K., and Auken, E., 2015, A review of the principles and applications of the NMR technique for near-surface characterization: Surveys in Geophysics, v. 36, no. 1, p. 27–85. [Also available at https://doi.org/10.1007/s10712-014-9304-0.]

Bettis, A.E., III, Tassier-Surine, S., and Haj, A., 2005, Overview of the Quaternary geology of Martin Marietta's Cedar Rapids Quarry, *in* Anderson, R.R., and Langel, R.J., eds., Quaternary and Silurian geology at the Martin Marietta Cedar Rapids Quarry, Linn County, Iowa: Geological Society of Iowa, Guidebook 77, p. 5–18. [Also available at https://www.iihr.uiowa.edu/igs/publications/uploads/GSI-077.pdf.]

Building Seismic Safety Council, 1994, NEHRP recommended provisions for seismic regulation for new buildings—Part1—Provisions: Washington, D.C., Building Seismic Safety Council for the Federal Emergency Management Agency, 290 p.

Chesapeake Technology, 2015, SonarWiz user guide, revision 6.01.0008: Mountain View, California, Chesapeake Technology, Inc., 783 p., accessed April 2015 at https://www.chesapeaketech.com/.

Day-Lewis, F.D., White, E.A., Johnson, C.D., Lane, J.W., Jr., and Belaval, M., 2006, Continuous resistivity profiling to delineate submarine groundwater discharge—Examples and limitations: The Leading Edge, v. 25, no. 6, p. 724–728. https://doi.org/10.1190/1.2210056.

Deszcz-Pan, M., Smith, D.V., Smith, B.D., Haj, A.E., and Johnson, M.R., 2018, Airborne electromagnetic and magnetic survey data and inverted resistivity models, Cedar Rapids, Iowa, May 2017: U.S. Geological Survey data release, accessed May 5, 2018, at https://doi.org/10.5066/P9BS882S.

Doherty, J., 2004, PEST—Model-independent parameter estimation user manual (5th ed.): Watermark Numerical Computing, variously paged, accessed March 30, 2018, at https://pesthomepage.org/.

Doherty, J., 2015, Calibration and uncertainty analysis for complex environmental models: Brisbane, Australia, Watermark Numerical Computing, 223 p.

Doherty, J.E., and Hunt, R.J., 2010, Approaches to highly parameterized inversion—A guide to using PEST for groundwater-model calibration: U.S. Geological Survey Scientific Investigations Report 2010–5169, 59 p., accessed June 28, 2010, at https://doi.org/10.3133/sir20105169.

Gannon, J.M., Witzke, B., and Langel, R., 2011, Groundwater availability modeling of the Silurian Aquifer in East-Central Iowa, 187 p., accessed July 1, 2018, at https://www.iihr.uiowa.edu/igs/publications/uploads/WRI-5.pdf.

Gassman, P.W., Reyes, M.R., Green, C.H., and Arnold, J.G., 2007, The Soil and Water Assessment Tool—Historical development, applications, and future research directions: Transactions of the ASABE, v. 50, no. 4, p. 1211–1250. [Also available at https://doi.org/10.13031/2013.23637.]

Gupta, H.V., Sorooshian, S., and Yapo, P.O., 1999, Status of automatic calibration for hydrologic models—Comparison with multilevel expert calibration: Journal of Hydrologic Engineering, v. 4, no. 2, p. 135–143. [Also available at https://doi.org/10.1061/(ASCE)1084-0699(1999)4:2(135).]

Ha, W.S., and Haj, A.E., 2021, MODFLOW-NWT model used to simulate groundwater levels in the Cedar River alluvial aquifer near Cedar Rapids, Iowa: U.S. Geological Survey data release, https://doi.org/10.5066/P96CF4L5.

Hallberg, G.R., 1980, Pleistocene stratigraphy in east-central Iowa: Iowa City, Iowa, Iowa Geological Survey Technical Information Series No. 10, 168 p. [Also available at https://ir.uiowa.edu/igs_tis/10.]

Hallberg, G.R., 1986, Pre-Wisconsin glacial stratigraphy of the central plains region in Iowa, Nebraska, Kansas, and Missouri: Quaternary Science Reviews, v. 5, p. 11–15. [Also available at https://www.sciencedirect.com/science/article/pii/0277379186901691.]

Harbaugh, A.W., 1990, A computer program for calculating subregional water budgets using results from the U.S. Geological Survey modular three-dimensional finite-difference ground-water flow model: U.S. Geological Survey Open-File Report 90–392, 46 p. [Also available at https://doi.org/10.3133/ofr90392.]

Harbaugh, A.W., 2005, MODFLOW-2005—The U.S. Geological Survey modular ground-water model—The ground-water flow process: U.S. Geological Survey Techniques and Methods, book 6, chap. A16, variously paged. [Also available at https://pubs.er.usgs.gov/publication/tm6A16.]

Harbaugh, A.W., Banta, E.R., Hill, M.C., and McDonald, M.G., 2000, MODFLOW–2000, the U.S. Geological Survey modular ground-water model—User guide to modularization concepts and the ground-water flow process: U.S. Geological Survey Open-File Report 2000–92, 121 p. [Also available at https://doi.org/10.3133/ofr200092.]

Hillaker, H.J., 2012, Historical report—The drought of 2012 in Iowa: Des Moines, Iowa, Iowa Department of Agriculture and Land Stewardship, Climatology Bureau, 6 p., accessed September 19, 2018, at https://www.iowaagriculture.gov/climatology/weatherSummaries/2012/DroughtIowa2012Revised.pdf.

Horick, P.J., 1984, Silurian-Devonian aquifer of Iowa: Iowa Geological Survey Miscellaneous Map Series 10, 4 sheets.

Hull, R.B., Johnson, C.D., Stone, B.D., LeBlanc, D.R., McCobb, T.D., Phillips, S.N., Pappas, K.L., and Lane, J.W., Jr., 2019, Lithostratigraphic, geophysical, and hydrogeologic observations from a boring drilled to bedrock in glacial sediments near Nantucket Sound in East Falmouth, Massachusetts: U.S. Geological Survey Scientific Investigations Report 2019–5042, 27 p., accessed June 5, 2018, at https://doi.org/10.3133/sir20195042.

Ibs-von Seht, M., and Wohlenberg, J., 1999, Microtremor measurements used to map thickness of soft sediments: Bulletin of the Seismological Society of America, v. 89, no. 1, p. 250–259. [Also available at https://doi.org/10.1785/BSSA0890010250.]

Iowa Department of Natural Resources, 1998a, Bedrock geology, Linn County, Iowa: Iowa Department of Natural Resources, Geological Survey Bureau Open File Map 98–3, scale 1:100,000, accessed October 29, 2018, at https://www.iihr.uiowa.edu/igs/publications/uploads/ofm-1998-3.pdf.

Iowa Department of Natural Resources, 1998b, Depth to bedrock—Linn County, Iowa: Iowa Department of Natural Resources, Geological Survey Bureau Open File Map 98–6, scale 1:100,000, accessed October 29, 2018, at https://www.iihr.uiowa.edu/igs/publications/uploads/ofm-1998-6.pdf.

Iowa Department of Natural Resources, 1998c, Surficial geologic materials of Linn County, Iowa: Iowa Department of Natural Resources, Geological Survey Bureau Open File Map Series 98–2, prepared by Quade, D.J., Bettis, E.A., III, Ludvigson, G.A., Giglierano, J.D., and Slaughter, M.K., scale 1:100,000, accessed August 6, 2018, at https://www.iihr.uiowa.edu/igs/publications/uploads/ofm-1998-2.pdf.

Iowa Geological and Water Survey, 2010, Bedrock geologic map of Iowa: Iowa Geological and Water Survey Map M–22, compilation by Witzke, B.J., Anderson, R.R. and Pope, J.P., scale 1:500,000, accessed October 29, 2018, at https://www.iihr.uiowa.edu/igs/publications/uploads/M-22.pdf.

Iowa Geological Survey, 2017a, Stratigraphic column of Iowa: Iowa City, Iowa University of Iowa, 1 p., accessed October 29, 2018, at https://www.iihr.uiowa.edu/igs/publications/uploads/2017-07-26_13-07-19_strat_column_2017.pdf.

Iowa Geological Survey, 2017b, Stratigraphic nomenclature of Iowa: University of Iowa Hydroscience & Engineering, accessed October 29, 2018, at https://www.iihr.uiowa.edu/igs/files/2015/09/Stratographic-nomeclature-of-Iowa.pdf.

Iowa Geological Survey, 2018, GeoSam lithologic database: Iowa Geological Survey web page, accessed August 6, 2018, at https://www.iihr.uiowa.edu/igs/geosam/home.

Iowa Geospatial Data, 2017, Three meter digital elevation model of Linn County, Iowa, derived from LiDAR: Iowa Geospatial Data, accessed September 15, 2018, at https://geodata.iowa.gov/dataset/three-meter-digital-elevation-model-iowa-derived-lidar.

Iowa Geospatial Data, 2020, One-meter shaded relief county downloads, Linn County, Iowa, derived from LiDAR: Iowa Geospatial Data, accessed June 1, 2020, at https://geodata.iowa.gov/pages/one-meter-hillshade-county-downloads.

Johnson, A.I., 1967, Specific yield-compilation of specific yields for various materials: U.S. Geological Survey Water Supply Paper 1662–D, 74 p. [Also available at https://doi.org/10.3133/wsp1662D.]

Johnson, C.D., Bristow, E.L., White, E.A., Gruhn, L.R., Pappas, K.L., Phillips, S.N., and Lane, J.W., Jr., 2020, Geophysical data collected in the Cedar River floodplain, Cedar Rapids, Iowa, 2015–2017: U.S. Geological Survey data release, https://doi.org/10.5066/P9YXJDHX.

Johnson, C.D., and Lane, J.W., Jr., 2016, Statistical comparison of methods for estimating sediment thickness from horizontal-to-vertical spectral ratio (HVSR) seismic methods—An example from Tylerville, Connecticut, USA, *in* Symposium on the Application of Geophysics to Engineering and Environmental Problems, Denver, Colorado, March 20–24, 2016, Proceedings: Denver, Colorado, Environmental and Engineering Geophysical Society, p. 317–323. [Also available at https://doi.org/10.4133/SAGEEP.29-057.]

Johnson, C.D., and White, E.A., 2007, Marine geophysical investigation of selected sites in Bridgeport Harbor, Connecticut, 2006: U.S. Geological Survey Scientific Investigations Report 2007–5119, 32 p., accessed April 25, 2019, at https://doi.org/10.3133/sir20075119.

Kalin, L., and Hantush, M.M., 2006, Hydrologic modeling of an eastern Pennsylvania watershed with NEXRAD and rain gauge data: Journal of Hydrologic Engineering, v. 11, no. 6, p. 555–569. [Also available at https://doi.org/10.1061/(ASCE)1084-0699(2006)11:6(555).]

Kenyon, W.E., Day, P.I., Straley, C., and Willemsen, J.F., 1988, A three-part study of NMR longitudinal relaxation properties of water-saturated sandstones: Society of Petroleum Engineers Formation Evaluation, v. 3, no. 3, SPE–15643–PA, 15 p., accessed July 3, 2018, at https://doi.org/10.2118/15643-PA.

Keys, W.S., 1990, Borehole geophysics applied to groundwater investigations: U.S. Geological Survey Techniques of Water-Resources Investigation, book 2, chap. E2, 150 p. [Also available at https://doi.org/10.3133/twri02E2.]

Koller, M.G., Chatelain, J.-L., Guillier, B., Duval, A.-M., Atakan, K., Lacave, C., and Bard, P.-Y., 2004, Practical user guidelines and software for the implementation of the H/V ratio technique—Measuring conditions, processing method and results interpretation: 13th World Conference on Earthquake Engineering, Vancouver, B.C., August 1–6, 2004, paper no. 3132, 10 p.

Lane, J.W., Jr., White, E.A., Steele, G.V., and Cannia, J.C., 2008, Estimation of bedrock depth using the horizontal-to-vertical (H/V) ambient-noise seismic method, *in* Symposium on the Application of Geophysics to Engineering and Environmental Problems, Philadelphia, Pennsylvania, April 6–10, 2008, Proceedings: Denver, Colorado, Environmental and Engineering Geophysical Society, 13 p. [Also available at https://doi.org/10.3997/2214-4609-pdb.177.170.]

Langevin, C.D., Hughes, J.D., Banta, E.R., and Niswonger, R.G., Panday, S., and Provost, A.M., 2017, Documentation for the MODFLOW 6 Groundwater Flow Model: U.S. Geological Survey Techniques and Methods, book 6, chap. A55, 197 p., accessed April 1, 2018, at https://doi.org/10.3133/tm6A55.

Leaf, A.T., Hunt, R.J., and Fienen, M.N., 2013, Teaching concepts of non-uniqueness and uncertainty in groundwater, *in* 125th Anniversary Annual Meeting and Expo, Denver, Colorado, October 27–30, 2013: Geological Society of America, v. 45, no. 7, session abstract no. 388, p. 860, accessed February 21, 2018, at https://gsa.confex.com/gsa/2013AM/webprogram/Paper233847.html.

Loke, M.H., 2018, Tutorial—2-D and 3-D electrical imaging surveys, revision date—May 4, 2018: accessed April 24, 2019, at ftp://geom.geometrics.com/pub/mag/G857_MagCD/OhmMapper/COURSENOTES.pdf.

McDonald, M.G., and Harbaugh, A.W., 1988, A modular three-dimensional finite-difference ground-water flow model: U.S. Geological Survey Techniques of Water-Resources Investigations, book 6, chap. A1, 586 p. [Also available at https://pubs.er.usgs.gov/publication/twri06A1.]

Micromed S.p.A., 2015, Grilla, version 6.1: Treviso, Italy, Micromed S.p.A., accessed May 2015 at https://moho.world/en/.

Moriasi, D.N., Arnold, J.G., Van Liew, M.W., Bingner, R.L., Harmel, R.D., and Veith, T.L., 2007, Model evaluation guidelines for systematic quantification of accuracy in watershed simulations: Transactions of the ASABE, v. 50, no. 3, p. 885–900. [Also available at https://doi.org/10.13031/2013.23153.]

Morriss, C., Rossini, D., Straley, C., Tutunjian, P., and Vinegar, H., 1997, Core analysis by low-field NMR: The Log Analyst, v. 38, no. 2, p. 84–94.

Nakamura, Y., 2000, Clear identification of fundamental idea of Nakamura's technique and its applications: Auckland, New Zealand, 12WCEE, paper no. 2656, 8 p.

Nash, J.E., and Sutcliffe, J.V., 1970, River flow forecasting through conceptual models, part I—A discussion of principles: Journal of Hydrology (Amsterdam), v. 10, no. 3, p. 282–290. [Also available at https://doi.org/10.1016/0022-1694(70)90255-6.]

National Centers for Environmental Information, 2019, Data tools—1981–2010 normals: National Oceanic and Atmospheric Administration web page, accessed April 25, 2019, at https://www.ncdc.noaa.gov/cdo-web/datatools/normals.

National Weather Service, 2019, NOWData—NOAA online weather data: National Oceanic and Atmospheric Administration web page, accessed June 14, 2019, at https://w2.weather.gov/climate/xmacis.php?wfo=dvn.

Niswonger, R.G., Panday, S., and Ibaraki, M., 2011, MODFLOW-NWT, a Newton formulation for MODFLOW-2005: U.S. Geological Survey Techniques and Methods, book 6, chap. A37, 44 p. [Also available at https://doi.org/10.3133/tm6A37.]

Prior, J.C., 1991, Landforms of Iowa: Iowa City, Iowa, University of Iowa Press, 153 p.

Rosenberry, D.O., and Healy, R.W., 2012, Influence of a thin veneer of low-hydraulic-conductivity sediment on modelled exchange between river water and groundwater in response to induced infiltration: Hydrological Processes, v. 26, no. 4, p. 544–557. [Also available at https://doi.org/10.1002/hyp.8153.]

Rutledge, A.T., 1998, Computer programs for describing the recession of ground-water discharge and for estimating mean ground-water recharge and discharge from streamflow records—Update: U.S. Geological Survey Water-Resources Investigations Report 98–4148, 43 p. [Also available at https://pubs.usgs.gov/wri/wri984148/.]

Schulmeyer, P.M., 1995, Effect of the Cedar River on the quality of the ground-water supply for Cedar Rapids, Iowa: U.S. Geological Survey Water-Resources Investigations Report 94–4211, 68 p. [Also available at https://doi.org/10.3133/wri944211.]

Schulmeyer, P.M., and Schnoebelen, D.J., 1998, Hydrogeology and water quality in the Cedar Rapids area, Iowa, 1992–96: U.S. Geological Survey Water-Resources Investigations Report 97–4261, 77 p. [Also available at https://doi.org/10.3133/wri974261.]

Schilling, K.E., and Tassier-Surine, S., 2006, Hydrogeology of pre-Illinoian till at the I380 rest stop site, Linn County, Iowa: Des Moines, Iowa, Iowa Department of Natural Resources, Technical Information Series, 51, 53 p. [Also available at https://ir.uiowa.edu/igs_tis/51.]

Singh, J., Knapp, H.V., and Demissie, M., 2004, Hydrologic modeling of the Iroquois River watershed using HSPF and SWAT: Illinois State Water Survey, 24 p.

Squillace, P.J., Liszewski, M.J., and Thurman, E.M., 1993, Agricultural chemical interchange between ground water and surface water, Cedar River Basin, Iowa and Minnesota—A study description: U.S. Geological Survey Open-File Report 92–85, 26 p. [Also available at https://doi.org/10.3133/ofr9285.]

Tucci, P., and McKay, R.M., 2006, Hydrogeology and simulation of ground-water flow in the Silurian-Devonian aquifer system, Johnson County, Iowa: U.S. Geological Survey Scientific Investigations Report 2005–5266, 78 p., accessed March 10, 2019, at https://doi.org/10.3133/sir20055266.

Turco, M.J., and Buchmiller, R.C., 2004, Simulation of ground-water flow in the Cedar River alluvial aquifer flow system, Cedar Rapids, Iowa: U.S. Geological Survey Scientific Investigations Report 2004–5130, 39 p. [Also available at https://doi.org/10.3133/sir20045130.]

Ulrich, C., Hubbard, S.S., Florsheim, J., Rosenberry, D., Borglin, S., Trotta, M., and Seymour, D., 2015, Riverbed clogging associated with a California riverbank filtration system—An assessment of mechanisms and monitoring approaches: Journal of Hydrology (Amsterdam), v. 529, p. 1740–1753. [Also available at https://doi.org/10.1016/j.jhydrol.2015.08.012.]

U.S. Census Bureau, 2018, Cedar Rapids Iowa 2010 demographic profile, total population: U.S. Census Bureau web page, accessed October 23, 2018, at https://www.census.gov/quickfacts/cedarrapidscityiowa.

U.S. Geological Survey, 2018, USGS water data for the Nation: U.S. Geological Survey National Water Information System database, accessed September 17, 2018, at https://doi.org/10.5066/F7P55KJN.

Valder, J.F., Haj, A.E., Bristow, E.L., and Valseth, K.J., 2019, Delineation of selected lithologic units using airborne electromagnetic data near Cedar Rapids, Iowa (ver. 1.1, February 2019): U.S. Geological Survey Scientific Investigations Map 3423, 2 sheets, 9-p. pamphlet, accessed January 10, 2020, at https://doi.org/10.3133/sim3423.

Vigil, J.F., Pike, R.J., and Howell, D.G., 2000, A tapestry of time and terrain: U.S. Geological Survey Geologic Investigations Series I–2720, 1 sheet, 32-p. pamphlet. [Also available at https://doi.org/10.3133/i2720.]

Walsh, D., Turner, P., Grunewald, E., Zhang, H., Butler, J.J., Jr., Reboulet, E., Knobbe, S., Christy, T., Lane, J.W., Jr., Johnson, C.D., Munday, T., and Fitzpatrick, A., 2013, A small-diameter NMR logging tool for groundwater investigations: Ground Water, v. 51, no. 6, p. 914–926. [Also available at https://doi.org/10.1111/gwat.12024.]

Walter, I.A., Allen, R.G., Elliott, R., Jensen, M.E., Itenfisu, D., Howell, T.A., Snyder, R., Brown, P., and Echings, S., 2001, The ASCE Standardized Reference Evapotranspiration Equation: Final report of the Task Committee on Standardization of Reference Evapotranspiration, 6 p.

Wang, W., Wang, Y., Sun, Q., Zhang, M., Qiang, Y., and Liu, M., 2018, Spatial variation of saturated hydraulic conductivity of a loess slope in the South Jingyang Plateau, China: Engineering Geology, v. 236, p. 70–78. [Also available at https://doi.org/10.1016/j.enggeo.2017.08.002.]

Ward, S.H., 1990, Resistivity and induced polarization methods, *in* Ward, S., ed., Investigations in Geophysics: Tulsa, Okla., Society of Exploration Geophysicists, p. 147–190.

Winston, R.B., 2018, Online guide to MODFLOW-2005: U.S. Geological Survey web page, accessed March 6, 2020, at https://water.usgs.gov/ogw/modflow/MODFLOW-2005-Guide/.

Appendix

Land-based and waterborne geophysical survey methods were used to characterize the extent and geophysical properties of floodplain and streambed sediments. Land-based methods included passive seismic horizontal-to-vertical spectral ratio (HVSR) and electrical resistivity tomography (ERT); waterborne methods included continuous resistivity profiling (CRP) and continuous seismic profiling (CSP). The locations of survey lines presented in this appendix are illustrated in figure 4 in the main report. Geophysical survey data were used to improve conceptual understanding of surface water, alluvial aquifer, and bedrock aquifer interaction in the Cedar River valley, Iowa (modified from Haj and others, 2016 [available for download at https://doi.org/10.3133/sir20215065]).

Reference Cited

Haj, A.E., Jr., White, E.A., Gruhn, L.R., Linhart, S.M., and Lane, J.W., Jr., 2016, Geophysical methods used to better characterized surface water, alluvial aquifer, and bedrock aquifer interaction in the Cedar River Valley, Iowa, *in* U.S. Geological Survey National Groundwater Workshop, Reno, Nevada, August 29–September 2, 2016, [Poster]: Reno, Nevada, U.S. Geological Survey.

For more information about this publication, contact:
Director, USGS Central Midwest Water Science Center
400 South Clinton Street, Suite 269
Iowa City, IA 52240
319–337–4191

For additional information, visit: https://www.usgs.gov/centers/cm-water

Publishing support provided by the
Lafayette and Rolla Publishing Service Centers

ISSN 2328-0328 (online)
https://doi.org/10.3133/sir20215065